Master Thesis in Geosciences

Development and sedimentology of the Lower Eocene deep marine gravity flow deposits in the eastern part of the Ainsa Basin, the Pyrenees, Spain

Roger Flåt

UNIVERSITY OF OSLO
FACULTY OF MATHEMATICS AND NATURAL SCIENCES

Development and sedimentology of the Lower Eocene deep marine gravity flow deposits in the eastern part of the Ainsa Basin, the Pyrenees, Spain

Roger Flåt

Master Thesis in Geosciences

Discipline: Petroleum Geology and Geophysics

Department of Geosciences

Faculty of Mathematics and Natural Sciences

UNIVERSITY OF OSLO

02.06.2008

Tutor(s): Johan Petter Nystuen

This work is published digitally through DUO – Digitale Utgivelser ved UiO

http://www.duo.uio.no

It is also catalogued in BIBSYS (http://www.bibsys.no/english)

Acknowledgements

I would like to thank my supervisor, Johan Petter Nystuen, for his guidance in the field and his comments and feed-back during the writing of the master thesis. A special thanks to my co-supervisor, Roy H. Gabrielsen, for helpful guidance during fieldwork in Ainsa.

Also, I would thank Odd Nilsen for helping with the photography of the thin-sections. Marit Sørlie and Kristin Rangnes at the library, thanks for helping with finding literature. Thanks to all fellow students that have made studying Geoscience at the university a pleasure, especially the guys at rom 217 at Zeb.

I would also thank my family and friends for their support through the study. I would never accomplish a master degree without you!

Abstract

The Eocene Ainsa Basin is situated in the central south Pyrenees formed by collision of the Iberian plate with the Eurasien plate during Late Cretaceous to early Miocene times. The basin was formed due to movements of the central southern Pyrenean thrust system in a piggy-back fashion. The depositional system was controlled by the Mediano growth fold and the Faradada tear fault system. The climate was a secondary factor controlling the sea-level variations (Milancovich cycles). These controlling factors have been reflected in the recorded data gathered in the Arro and Charo areas (Arro sandstone body. The succession can be divided into 4 distinct units; a basal mass transport complex, an inter-channel dominating succession, a turbidite channel succession, and a channel-levee dominated succession. This may reflect a system that has been triggered by tectonism and subsequently formed instabilities on the ramp of the basin. The relative sea-level may have been influenced by movement of the structures described above, and subsequently gradients in the depositional system from the source area in the Pyrenean axial zone to the deep marine Ainsa Basin. This is reflected in the progradation of the Montanana delta and the San Eseban fandelta. Palaeo-current trends give a NNW direction of the deep marine depositional ramp system.

Contents

1 Introduction

Deep marine turbidite sandstone deposits are exploration targets in basins around the world today. In the period 1950-1970 oberservations of deep-sea processes and facies gave knowledge and insight into theses systems (Pickering et al., 1989). Post-1970 published work is comprehensive and diverse regarding terminology of the depositional processes of gravity flows and interpretations of depositional environment and style in the deep marine realm.

The aim of this study was to look into the development of the deep marine succession in the Arro and Charo areas of the eastern Ainsa Basin belonging to the southern Pyrenean Eocene foreland basins. Sedimentological data were gathered from three localities to be further analysed as regards lithofacies, facies associations, and petrography in order to make an interpretation of the depositional environment and processes of sediment transport and sedimentation.

The stratigraphic nomenclature of the sedimentary successions in the Ainsa Basin is complicated and inconsistence, and by this reason a challenge to grasp. The systematics of Mutti's work (1985) and Mutti *et al*. (1988) have been used with some minor modifications. In addition to the complexity of the stratigraphic nomenclature, the work has also been hampered by the fact that there do not exist any published regular geological maps of the area. The study area is highly deformed by faulting of the splay faults from the Cotiella thrust. This made logging the area somewhat complicated, especially in northern part of locality 1.

The main object of the study is various types of gravity flow deposits within the so called Arro sandstone body in the eastern part of the Ainsa Basin, one of several piggy-back basins together forming the Southern Pyrenean Foreland Basin. The Arro sandstone body belongs to the deep marine Eocene Hecho Group (Mutti, 1985b) of the Ainsa Basin. The Arro

sedimentary system was sourced by the fluvial Montanana delta from the east/southeast and the San Esteban fandelta from the north (Nijman, 1998). The initiation of the movements along the detachment of the Mediano anticline (Mutti et al., 1988) has probably triggered a massive mass transport complex that contains a piece of the incised ramp (slump sheet). The scar on the ramp floor has further been eroded by gravity flows, which gradually scoured into the shallow marine ramp and formed the Charo canyon. The canyon funnelled the fluvial and the shallow marine sediments into the deep marine ramp through a gully systems during the upper part of the Montanana complex and the lower part of the Santa Liestra complex.

This main framework of the study object and its basinal setting is very similar to many other deep-marine basins of the World hosting turbidite sandstone deposits and other related gravity flow deposits. Being today important targets for petroleum exploration and production, stratigraphic, sedimentological and morphological properties of these types of reservoir rocks are of particular interest for the international petroleum industry. Facies variation, architectural style, volume, geometry and stacking pattern of sandstone bodies in these depostional settings of submarine canyons, gullies, channels, levees and fan systems are of crucial importance for the petroleum industry to model these reservoir rocks. In addition, processes of sediment intitiation and transportational and depositional mechanisms are of basic scientific interest. The present study has been carried out by the ambition to supply data and knowledge to some of these aspects.

2 Method

2.1 Introduction

To make a geological interpretation of the deep marine depositional systems in the eastern part of the Ainsa Basin (Arro and Charo area) field data was collected from the period 10.07.2007 - 04.08.2007. The data have been interpreted by lithofacies, facies associations, depositional environment, and petrography.

2.2 Fieldwork data

The data was collected by logging of three localities, measurements of palaeo-current directions, and gathering 10 rock samples of interest. 16 logs were made in scales of 1:20, 1:50, 1:100, and 1:200. Most of the logs are logged in 1:50, log 1 and log 5 in the scale of 1:200, log 15 was logged in the scale of 1:100, and log 7(2) in the scale of 1:20. A Garmin GPS was used to make note of the UTM coordinates of the different logs. The reference geoid used was Euref 79. For the palaeo-current measurements a Silva compass was used with a dip meter. 10 rock samples were taken from inter-channel sandstones (chapter 7), mainly, with one sample taken from a chaotic mass complex (chapter 7). The locality 1 deposits are logged on the back-limb of an eroded anticlinal structure and the locality 2 deposits are logged on the overturned fore-limb of the same structure. The locality 3 deposits represent also the fore-limb of the same structure, but these beds are not overturned.

2.3 Rock sample analysis

Polished thin-section was made for each of the rock samples. These thin-sections were analyzed in a light emitting microscope, with non-polarized light and polarized light to recognize the mineral composition of the rock samples. Then the thin sections were point-counted to establish a statistical analysis of the mineral composition of samples.

3 Geological framework

3.1 Introduction

The evolution of the Pyrenean orogeny is described in the next sections, and focus on the central south Pyrenean units (upper cover thrusts and the influence of the axial zone). Detailed field work has been carried out in the eastern part of the Ainsa Basin (10 kilometres east of the village of Ainsa, in the Arro/Charo area (figure 3.1 A B). The basin is located between the Mediano and Boltaña anticlines (the Buil syncline) (figure 3.1 C).

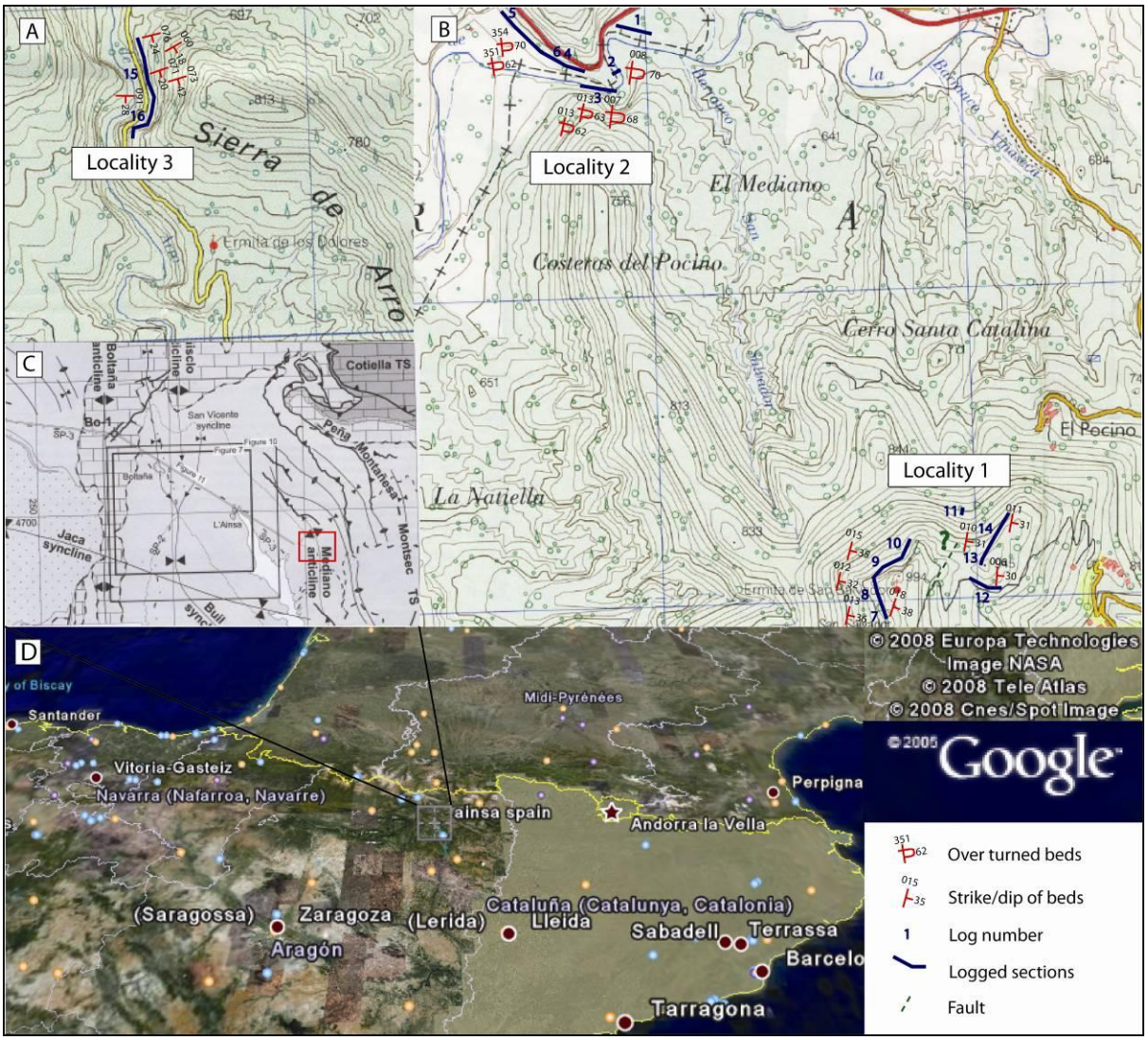

Figure 3.1: A) Logged section in locality 3. B) Logged sections in localities 1 and 2. C) The Ainsa Basin (red square represent the study area) from the Mediano anticline in the east to the Boltaña anticline in the west (modified from Fernandez, 2004). D) Regional overview of the study area.

3.2 Evolution of the Pyrenean orogeny and the south Pyrenean fold and thrust belt

The orogenesis that created the Pyrenees is characterized by low grade metamorphism (greenshist facies) and no volcanic activity. The northern part of the Iberian plate was located at latitudes of about 35 ° N, and the climatic conditions were tropical to subtropical as recorded by palynoflora and microfaunal data (Pickering and Corregidor, 2005)

The formation of the Pyrenean orogen is related to the collision between the Iberian plate and the Eurasian plate from Campanian to Early Miocene, where the Iberian plate subducted underneath the Eurasian plate. The anticlockwise rotation of the Iberian plate with the Eurasian plate gave rise to both a N-S and an E-W shortening. The structural evolution of the thrust and fold belt started with transpression in the Late stages of Cretaceous and through the Paleocene and Eocene Epoch. At the end of the Eocene and beginning of the Oligocene there was a period of translation of the thrust sheets before pure compressional forces acted on the foreland (Nijman, 1989) and infilling of the Ebro foredeep (Figure 3.2). The left stepping en-echlon style of the Faradada tear fault had a dextral movement (Nijman, 1989), due to rotation of the Iberian plate and the stress that was built up. Totally, the shortening of the orogen is 147 kilometres (Muñoz, 1992).

The evolution and progression of the south Pyrenean thrust sheets is controlled by the thick-skinned deformation in the axial zone of the orogen by the imbricate stacking of crystalline thrust sheets and creation of antiformal stack (Puigdefabregas et al., 1992 and Pickering and Corregidor, 2005). The axial zone thrust sheets (Nougueres antiformal stack) comprises the Nogueres zone, the Orri thrust sheet and the Rialp tectonic window. At the same time the break-back thrusting of the foreland evolved due to the stacking of the basement thrust sheets. The Pyrenean basin geometry are formed by loading on the lithosphere and of subcrustal forces of the Iberian slab (Puigdefabregas et al., 1992). Vertically the Pyrenean thrust

geometry is V-shaped, where the detachment level is located in the upper-middle crustal rocks (Muñoz, 1992).

The eastern part of the foreland basin is controlled by the lower Cadi thrust sheets (basement rocks) and the upper Pedraforca thrust sheet and the western part (central Pyrenees) is controlled by the upper (Boixol, Montsec, and Sierras Marginales) thrust sheets unconformely above the basement rocks of pre-Triassic period. The Pedraforca and the Boixol thrust sheets are structural equivalent (Dinares et al., 1992). The termination of the western thrust sheets is the oblique Segre thrust zone (Mutti, 1985b; Vergés et al., 1992). The focus of this study is the development of the south central Pyrenean units and the western thrust sheets. The western termination of the antiformal stack of the axial zone is where the Gavarine thrust sheets are situated, which controlled the megaturbidite sequences in the Jaca Basin (Seguret, 1984, Teixell, 1996). The emplacement of the Gavarine thrust was a fault-bend-folding type of deformation and translation of the western most units (Teixell, 1996).

During synorogenic development of the Pyrenees development of a thrust and foldbelt was created by in-sequence piggyback tectonic sequences in Lower to Middle Eocene. The onset of detachment is more or less initiated with compression tectonics in the Late Cretaceous (Nijman, 1989). The detachment zone is situated in the Triassic evaporates (Puigdefabregas et al., 1992). There are 4 main structural features recorded in the orogen: 1. the cover upper thrust sheets (southern Pyrenees); 2. The basement involved lower thrust sheets; 3. The North Pyrenean fault zone, and 4. the North Pyrenean thrust sheets (Muñoz, 1992). The cover upper thrust sheets developed in Late Cretaceous and in Paleocene-Eocene and created the piggyback basins, and finally to evolve as a foreland basin during the Oligocene-Miocene (Ebro foreland Basin) (Nijman, 1998). The foreland subsidence was controlled by the position of the thrust sheet front of the axial zone (Puigdefabregas et al., 1992).

During the Campanian a transpessional wrench basin configuration took place and the north-eastern parts of the Pyrenees were uplifted and became a source of erosion of clastics. A transitional period to a foreland basin occurred in the Paleocene epoch, with a non marine

sedimentation from the east and a deep weathering of the basement. In the western part a shallow carbonate shelf was formed in a starved sedimentary regime. Further, the migration of the foreland Basin createed a thrust and foldbelt (piggyback basins) (Puigdefabregas and Souquet, 1986). The South Pyrenean Central Unit (Mesozoic and Paleogene deposits) consists of 3 thrust sheets known as "The cover upper thrust sheets" (Muñoz, 1992), which are the Serres Marginales, Montsec and the Boixols imbricate thrust sheets (figure 3.2 B).

The upper cover thrust sheets developed progressively in a break back sequence (figure 3.2 C). The Boixols thrust sheet was the first thrust sheet that developed on older extensional faults of the Early Cretaceous Epoch. The Montsec thrust sheet was emplaced during the Ypresian stage, and the Serres Marginales was emplaced between the Early and the Late Eocene and later deformed in Late Eocene – Oligocene (Muñoz, 1992). The Serres Marginales is the southern boarder of the South Pyrenean Unit, which separates the thrust-top basins from the Ebro foreland Basin.

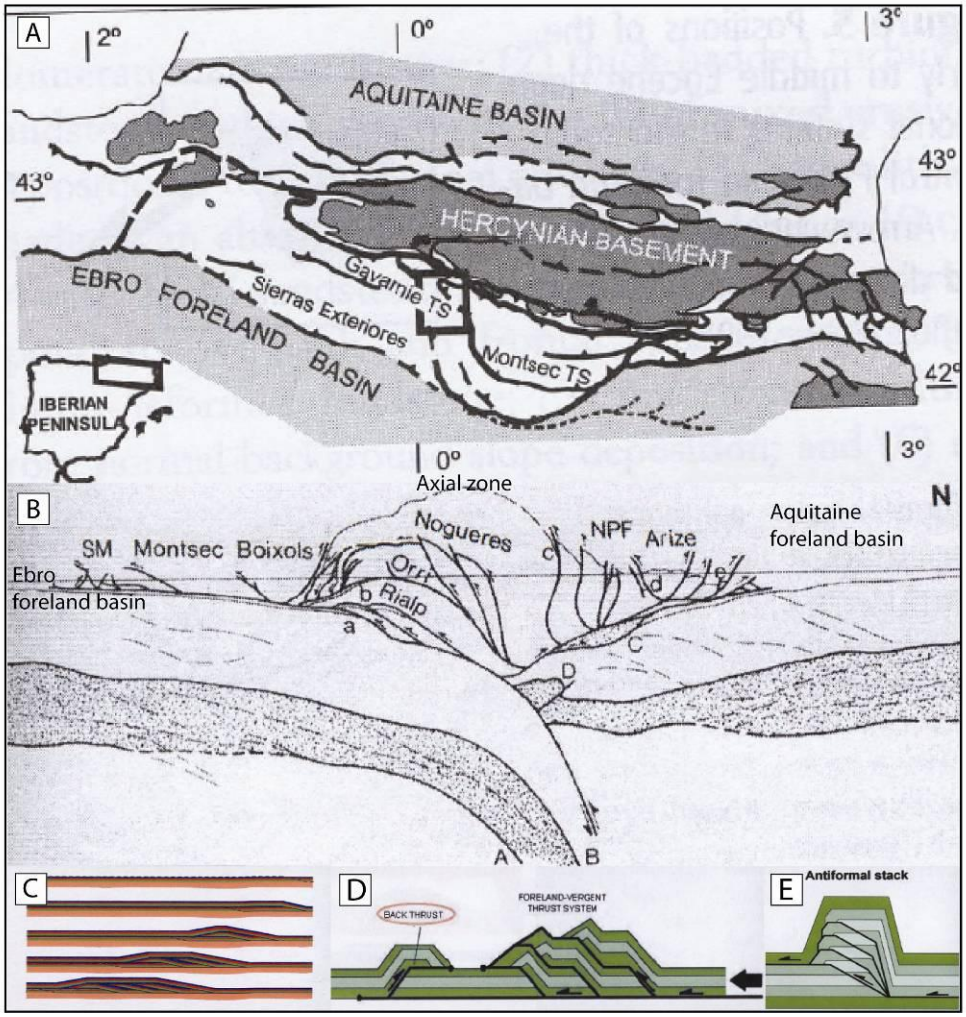

Figure 3.2: A) The Pyrenean foreland basins and the axial zone (Fernandez, 2004). B) The V-shaped geometry of the orogen (Muñoz, 1991). C) Evolution of the break-back imbricate thrust sheets from Andresen (2005) (written com.). D) Figure illustrates the back thrusting (Morreres thrust) of the northern part of the central south Pyrenean thrust sheets, which also represent as a passive roof thrust of the antiformal stacked basement thrust sheets (Muñoz, 1991) from Andresen (2005) (written com.). E) Illustrates the Nogueres antiformal stack from Andresen (2005) (written com.).

3.3 The Ainsa Basin

3.3.1 Sequence stratigraphic relations of the Hecho Group

The organization of one specific nomenclature in the Ainsa Basin has not been developed jet. There exists a lot of confusion around the Formation and Group names of the Ainsa Basin, which is sometimes mixed with the fluvial formation names. This study will use the nomenclature from Mutti *et al*. (1985, 1988), Mutti and Normark (1987) and Kane *et al*. (2007), where Hecho Group is used for the Eocene deep marine deposits that comprises 4 depositional complexes (Figols Group, Montanana Group, Santa Liestra Group, and Campodarbe Group) seen in figure 3.3. Even if the nomenclature is far of track regarding conventional stratigraphical nomenclature used is that from Mutti (1985) and Mutti *et al*.(1988) with modifications. The Castissent Group that is being referred to in the work by Mutti *et al*. (1988) may lead to confusion because the Castissent Group, which is the uppermost part of the Montanana Group, is a fluvial formation (Castissent Formation) (Nijman, 1998) (figure 3.6). The uppermost Campodarbe Group is shallowing upwards to shallow-marine sediments (Cronin et al., 1998). The Montanana Group and the Santa Liestra Group comprises channel-levee systems (Fosada, Arro, Banaston, Ainsa, Morillo, Gauso) (figure 3.3A) (Mutti, 1985b). The lowermost Figols Group is referred to as shelfal and slope mudstones by Mutti *et al*. (1988).

Classification systems of sedimentary deposits aim to relate the sedimentary rocks into genetic related strata in time and space. The Exxon group (Van Wagoner *et al*., 1988) made a sequence stratigraphic framework, where sequences are bounded by unconformities and their correlative conformities. The Arro sandbody can be related to a sequence by the basal correlative conformity (mass transport complex) in log1 at 93 metres. The correlative conformity may be related to the Exxon group model as a type 2 sequence boundary, with Basinal progradation due to a relative drop in sea-level. This relation can not be confirmed because the recorded units show no direct unconformities, but correlative conformities at 93

metres in log1 and at 62 metres in log15. The constraints of this interpretation lie in that there is no control of the shoreline. The sequence can be subdivided into systems tracts, which can be related to the depositional system of Mutti (1985). The system tracts is related

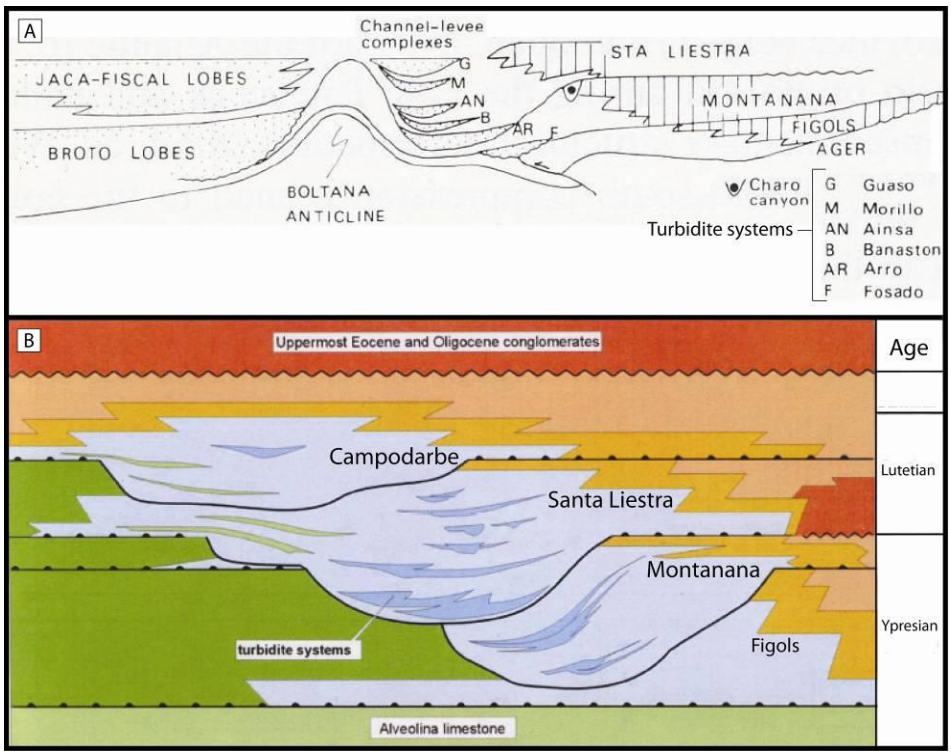

Figure 3.3: A) The 6 sequences represent the Hecho Group deposits in the Ainsa Basin from Mutti (1985) and the correlative prograding fluvio-deltaic sequences of the Montanana Group. B) The same sequences as in A, with sequence boundaries (modified from Fernandez, 2004). The basal Alveolina limestone was deposited during the Maastrichtian transgression.

to the eustatic sea-level curve by the lowstand fan, slope fan, lowstand wedge, transgressive systems tract and the highstand systems tract. In the eastern part of the Ainsa Basin the sea-level is sub-ordinate the tectonic imprint, where major movement of the thrust sheets is supposed to the major factor for formation of unconformities and their correlative unconformities sequences in the basin may be divided into tectono-stratigrahic relationships in the same manner as with the eustatic sea-level curve from Van Wagoner *et al*. (1988).

3.3.2 Tectono-stratigraphic relations

The Ainsa Basin is situated between the Mediano Anticline in the east and the Boltaña Anticline to the west, and to the northeast by the Peña Montañesa thrust in the south central Pyrenees. East of the basin is the contemporary Tremp-Ager Basin (also called Tremp-Graus Basin), and to the west is the contemporary Jaca Basin (figure 3.4). The basal turbidite deposits in the Jaca and Ainsa Basins are not affected by the movement of the two anticlines, due to that they had not started to evolve. The Fosado and Arro turbidites are deposited prior to movement of the Boltaña anticline in a single Jaca/Ainsa Basin (figure 3.4) (Mutti, 1985b). The movement of the Mediano detachment fold commenced between 47.2 and 51 Ma (Poblet et al., 1998) and the Boltaña anticline was out of phase with respect to development of the Mediano anticline, but commenced on a later time.

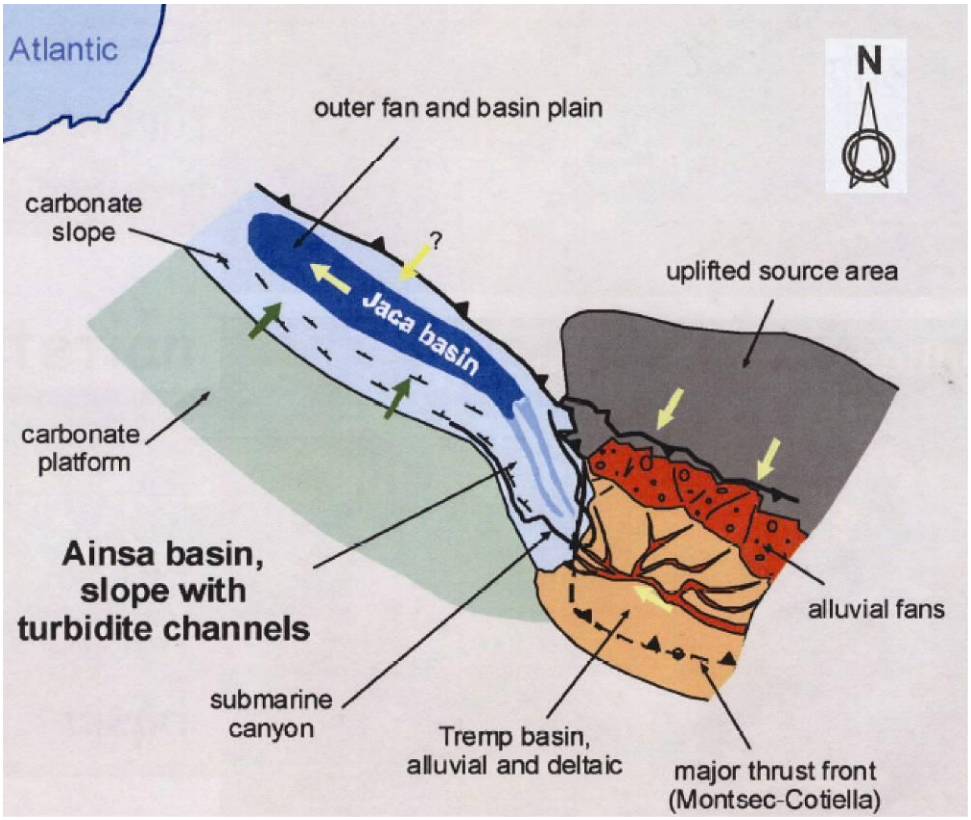

Figure 3.4: The central south Pyrenean Basin and the western Ainsa and Jaca boundary Basins. The pale-yellow arrows indicate the palaeocurrent direction in the different Basins. The green arrows indicate the source for the collapse breccia found in the Jaca Basin (modified from Fernandez, 2004).

The Ainsa and Jaca Basins are structally controlled narrow elongated basins (figure 3.4) formed during the syn-tectonic activity in the lower and middle Eocene epoch. The growth of the Boltaña anticline separated the western foredeep into to parts. The Ainsa Basin was mainly controlled by the Nogueres antiformal stack in the central axial zone and the Jaca Basin by the Gavarnie thrust. These basins are referred to as syn-sedimentary piggyback basins on the western side of the central south Pyrenean unit, with source for sedimentation in the eastern and northern parts. The basins are from east towards west: terrestrial, shallow marine and deep marine basins during deposition of the Hecho group, respectively. Later infilling is related to uplift of the axial zone (Trave et al., 1998) and the deltaic Sorbrabe Formation, the fluvial Escanilla and the uppermost alluvial Collegats Formation was formed stratigraphically above each other.

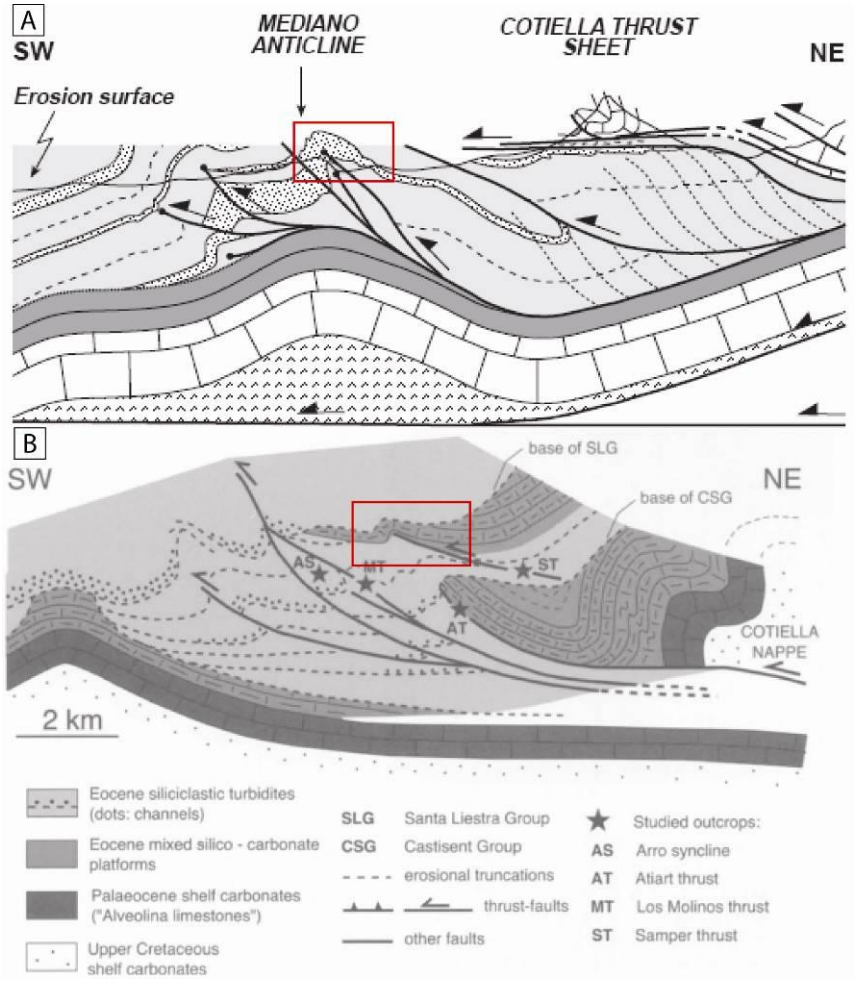

Figure 3.5: The cotellia thrust sheet and the related splay faults (Study area in red square) A) A cross section through the eastern part of the Ainsa Basin (Poblet *et al*., 1998). B) A close up of the splay thrusts in the Charo/Arro area (Trave *et al.*, 1998).

The Hecho Group, which comprises the deep marine turbidite deposits of the Ainsa and Jaca Basins is lower Ilerdian to Upper Lutetian in age. These deposits have been divided into 6 systems (Fosado, Arro, Banaston, Ainsa, Morillo, and Gauso) seen in figure 3.3 A (Mutti, 1985b). The Hecho Group is deposited contemporarily with the Montañana Group of the Tremp-Ager Basin (figure 3.6). Sedimentation was

controlled by emplacement of the thrust sheets.

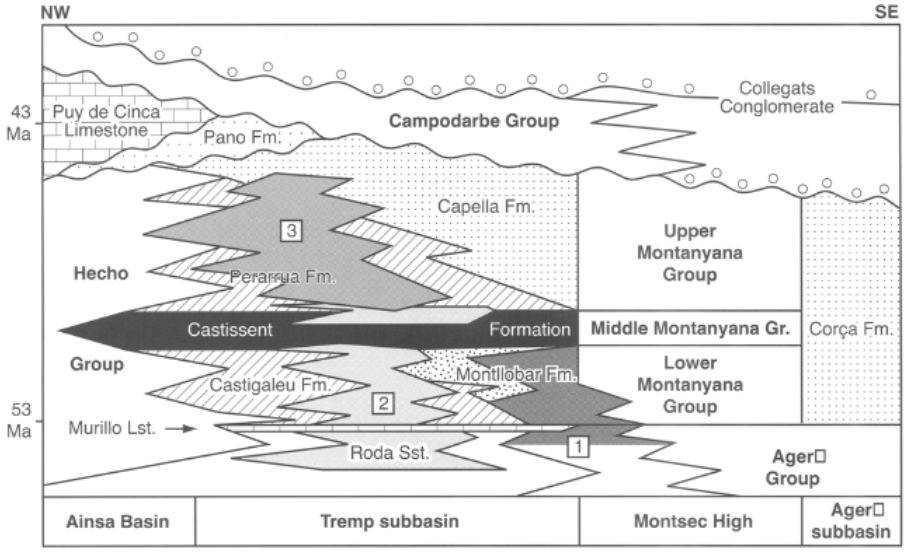

Figure 3.6: The correlative depositional Groups, Hecho and Montanana, which belongs to the Ainsa and Tremp-Ager Basins, respectively. Deposition occurred during Early and Middle Eocene epoch (Nijman, 1998).

Deposition of the Campdevanol Group and Castissent complexes (Castissent Group) took place during Late Ypresian (Puigdefabregas and Souquet, 1986) and a more progressive phase of deposition by slumping and sliding due to increase in gradient of the slope by movement of the N-S trending Mediano and Boltaña detachment folds. This movement may be related to the emplacement of the Montsec and the Cotiella thrust sheets, which are connected along the Mediano blind thrust (Dinares et al., 1992). The main movement of the Cotiella nappe was during Ypresian and the frontal thrust system was active up through the middle Eocene. From the north the Cotiella thrust splayed out into the Atiart thrust, samper thrust and the Los Molinos thrust (figure 3.5). The Samper thrust is out-of-sequence with the other thrusts. Movement along the Samper thrust zone can be related to the basal unconformity of the Castisent complex, and the Los Molinos thrust is an extention of the Atiart trust and is pre-Ypresian (figure 3.5B) (Trave et al., 1998).

The Boltaña structure may be related to movement along the Gavarnie-Serres Marginales thrust sheets seen in figure 3.2. Contemporarily there was a eustatic sea-level fall (50.4 Ma)

and a drop in the relative base level and incision of the shelf edge and formation of the Charo canyon and the correlative Fosado and Arro channel-levee complexes in the Ainsa Basin (Mutti, 1983/1984; Mutti, 1985b). Mutti (1985) suggested that the sea-level variations controlled the sedimentation and formed 3 different depositional systems, but the controlling factor is movement of the two colliding plates (Fernandez et al., 2004). The 6 systems seen in figure 3.3A may be related to periods of tectonic activity during deposition.

The fluvio-deltaic Montañana Group is fed by the southwards prograding Esteban alluvial fan and the westerly drained Castissent fluvial system. These deposits represent the sediment source for the turbidite deposits (Hecho Group) of the Ainsa and Jaca Basins (Nijman, 1989; Nijman, 1998). The Basin axis is parallel to the ramp axis that plunges to the NW (Montañana delta), which is also the main current direction in the Basin (figure 3.7).

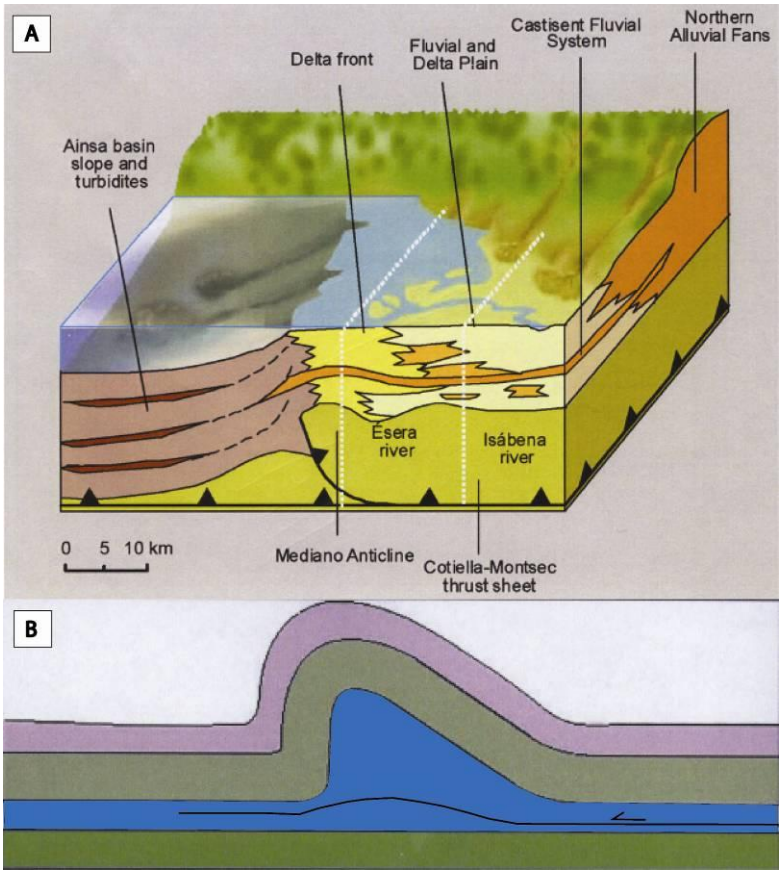

Figure 3.7: The depositional environment controlled by the Cotiella-Montsec thrust sheet. A) The northern alluvial fans and the westerly fluvial drainage system and the shallow marine environment, which is sourcing the deep marine Ainsa Basin (modified from Nijman, 1998; Puigdefabregas *et al*, 1991). B) The Mediano fold (modified from Andresen, 2005 written com.).

4 Processes of gravity flows

4.1 Introduction

Throughout the last 50-60 years a lot of proposals have been made for describing deposits of gravity flows supposed to have acted as turbidity currents. The most widely used is the Bouma classification. This classification is made from outcrop studies in southern France (Bouma, 1962), and according to Shanmugam (2002) it includes several misinterpreted data. This has led to some confusion regarding the interpretation of transporting and depositional processes of gravity flow deposits observed in the field.

The sediment gravity flow processes can been described by sediment-support mechanism and rheology (Carter, 1975; Lowe, 1979; Lowe, 1982; Middleton and Hampton, 1973; Nardin et al., 1979; Postma, 1986). The sediment-support mechanism can be divided into a cohesive flow or a non-cohesive flow (frictional flow) (Mulder and Alexander, 2001), and the rheology to be a Newtonian fluid or a Bingham plastic (figure 4.2) (Shanmugam, 1997). Shanmugam (1997) described a turbidity current like this: *"A turbidity current is a sediment-gravity flow with fluidal (i.e., Newtonian) rheology and a turbulent state in which sediment is held in suspension by fluid turbulence."* Dasgupta, (2003) claimed that the rheology and not the sediment-support mechanism should characterise debris flows. There exists a lot of confusion regarding how to describe gravity flows by the usage of the terms sediment support mechanism and rheology. Since the concept of turbidity current is not the proper way of describing all kinds of gravity flows many different models and classifications have been made of subaqueous gravity flows. Interpretation of the gravity flow deposits has been examined subjectively by several authors thought time, and there have been equally many different descriptions. This can cause a lot of confusion when reading the literature.

The classification of gravity flows from Middleton and Hampton (1973) have been used as subheadings in the following sections of this chapter, and the different processes behind deposition of deep sea deposits (figure 4.1) have been discussed.

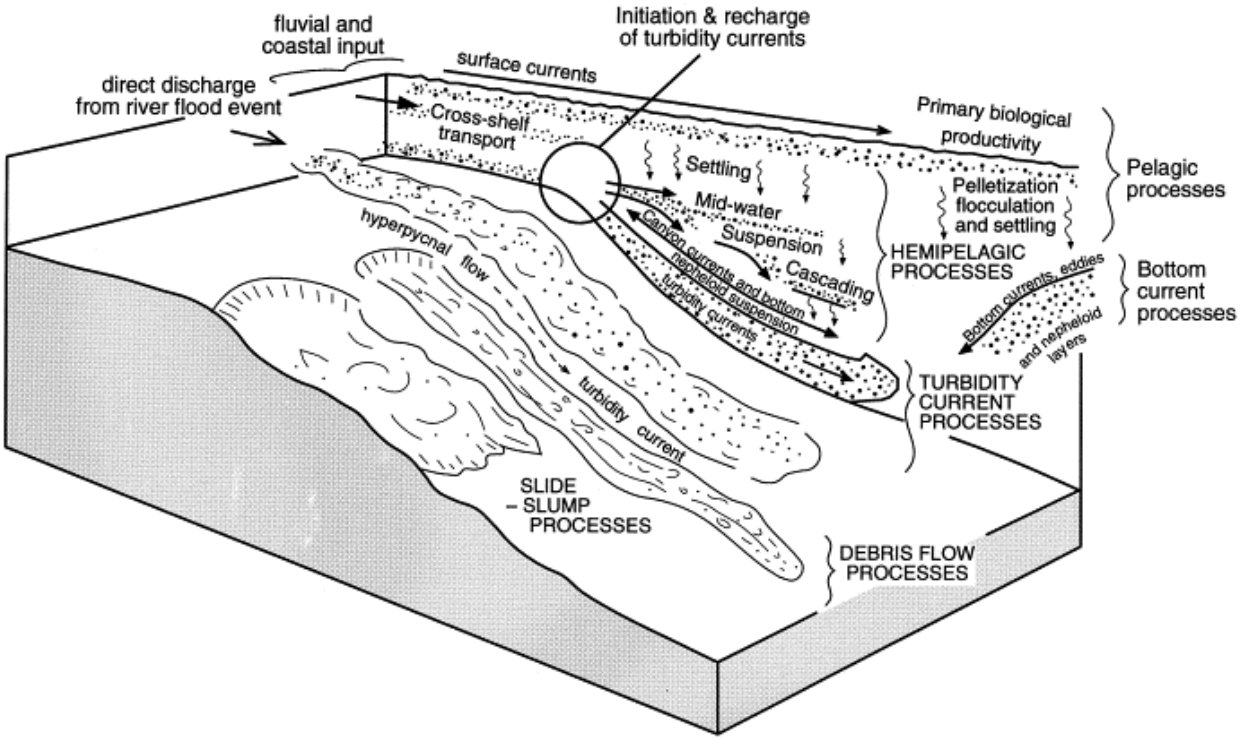

Figure 4.1: Processes behind deposition of subaqueous gravity flows from Stow and Mayall (2000).

4.2 Properties of gravity flows

Some of the terminology used for explaining sediment gravity flows is described in this section to get the fundamental concepts behind it clear. In the literature used to describe density flows, the concept behind rheology and the sediment-support mechanisms is very important to get the fundamental perceptions. Therefore, the properties of gravity flows are stated below. Figure 2 giving a visualisation of the properties of rheology, with graphs showing the Newtonian fluids, pseudoplasticity of fluids and the Bingham plastic. Definitions of some fundamental concepts are given below.

Viscosity is the internal friction in a fluid (on molecular level) (Young et al., 2004) or the resitance of a fluid to deformation (Robert, 2003). The viscosity of fluids is highly temperature dependent. The abbreviation is the Greek letter **μ**. The molecular (dynamic) viscosity is expressed by equation 4.1:

$$\tau = \mu * du/dy \quad \text{(eq. 4.1)}$$

where **τ** is the shear stress, **μ** is the dynamic viscosity, **du/dy** is the change of velocity over change in hight. The expression formulates that a greater dynamic viscosity, the smaller the deformation within the fluid (du/dy).

Viscosity can also be expressed as kinematic (eq. 4.2), and eddy viscosity (eq. 4.3):

$$\upsilon = \mu/\rho \qquad \text{(eq. 4.2)}$$

$$\tau = (\mu + \varepsilon)*du/dy \qquad \text{(eq.4.3)}$$

υ is the kinematic viscosity, ρ is the density of the fluid, and ε is the eddy viscosity coefficient. The kinematic viscosity stats that the ratio of molecular viscosity to the fluid density. The eddy viscosity (turbulent flows) expresses the vertical transfer of momentum, where a water package is transferred to regions of higher or lower flow (momentum) (Robert, 2003).

Plastic material is a permanently deformed material that has been subjected to an applied stress, which is irreversible (Young et al., 2004). Matter that is deformed pseudoplastically means that viscosity decrease or increase with increasing rate of shear, known as shear softening and shear hardening (figure 4.2).

Froude number: $Fr = U/\sqrt{gL}$ (eq. 4.4)

U is the mean velocity of the flow, **g** the acceleration of gravity, and **L** the height of the flow. The **U** represents the inertial forces of the flow and the **gL** represents the gravity force. The inertial force expresses the distance a part of the fluid travels before it comes to rest. The

Froude number expresses inertia/gravity forces, and if the number is below 1 the flow is sub-critical (giving rise to tractional structures T_b, T_c, and T_d of Bouma (1962)) and above 1 the flow is supercritical (giving rise to structureless units T_a of Bouma (1962)).

Densimetric Froude number: $\mathbf{Fr' = U/\sqrt{(\rho_d/\rho)*gh\cos\Theta}}$ (eq. 4.5)

U is the mean velocity, $\boldsymbol{\rho_d}$ is the density of the flow, **ρ** is the density of the ambient fluid, **g** acceleration of gravity, **h** is the height of the flow, and **Θ** is the angle of the bedding. This parameter is used because there exist a difference between the density of the flowing mass and the surrounding water (Kneller and Buckee, 2000) and a gradient on the slopes.

Dynamic pressure: $\mathbf{1/2*\rho v^2}$ (eq.4.6)

Regarding fluid dynamics dynamic pressure represents the kinetic energy in a fluid particle, where the **ρ** is the density of the fluid and **v** is the velocity of the fluid flow (eq.4.6) (Young et al., 2004).

Reynolds number: $\mathbf{Re = UL/\upsilon}$ (inertial forces/viscous forces) (eq.4.7)

U is the mean velocity of a flow, **L** is some length, and **υ** is the kinematic viscosity. Reynolds number (eq. 4.4) is unitless and used to describe a flow as turbulent or as laminar (uniform). When Re is lower than 500 the flow is defined as laminar, and when it is above 2000 it is defined as turbulent (Shanmugam, 1997).

Traction carpet. According to Lowe (1982) the traction carpet is a non-turbulent layer supported by grain collisions creating an inversely graded part, with structures like plane lamination and cross-stratification (see paragraph 4.7).

Kinematic sieving includes the phenomenon of smaller grains percolating through openings between larger grains (Le Roux, 2003). Middleton (1970) described the sorting of grains in grain flows as larger grains having the tendency to drift towards the free surface , in flows where there is a range of grain sizes of the particles.

Rheology is deformation due to an applied stress between two materials. Distinctions between Newtonian and non-Newtonian fluids are made by that a Newtonian fluid is lacking a yield stress **κ**.

μ is viscosity and du/dy is rate of shear strain illustrated in figure 2 below, and **n** is a positive number.

Newtonian fluid: (eq.4.8)

A Newtonian fluid (molecular viscosity) is a fluid with a constant viscosity μ and subsequently the deformation is linear (figure 4.2).

Bingham plastic is described as a Newtonian fluid above the yield strength **k** of a material (Postma, 1986) (figure 4.2):

$\tau = k + \mu^* du/dy$, where $k = C + \tau^* \tan\varphi$ (eq.4.9)

C is cohesion and tanφ is the friction. If C is the dominant component the flow is a cohesive debris flow, and if tanφ is the dominant component the flow will be frictional. In a grainflow the cohesive part will be zero (eq.4.9) (Bagnold, 1956; Lowe, 1979; Lowe, 1982; Nemec and Steel, 1984).

The Coulomb-viscous model (eq.1.4) was described by Johnson (1970):

$\sigma_s = C + \sigma_n * \tan\varphi + \eta\varepsilon_s$ (eq.3.7)

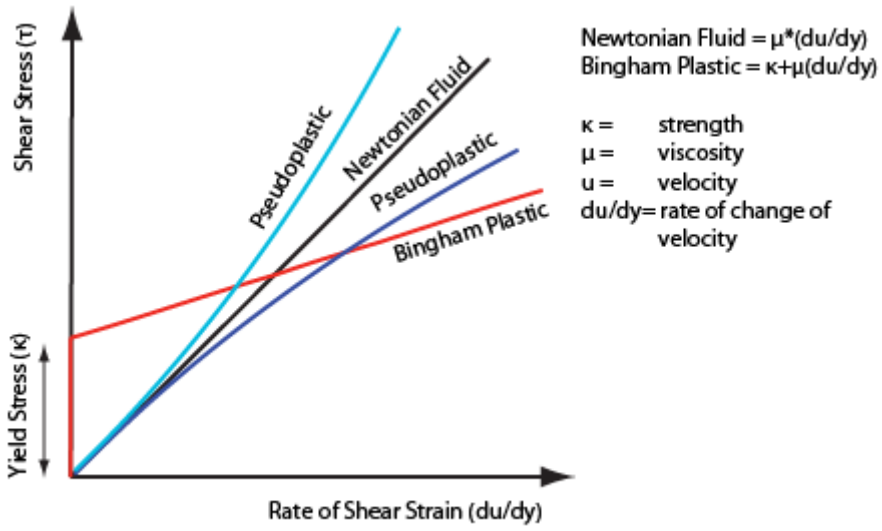

Figure 4.2: modified rheological diagram from Shanmugam (1997).

4.3 Turbidity current

Throughout the 20th century and up to today there have been a lot of proposals for the different mechanisms of turbidity currents. Most scientists agree on that turbidity currents are a type of sediment-gravity flow with Newtonian rheology and the upward component of fluid turbulence is the sediment support mechanism (Lowe, 1982; Middleton and Hampton, 1973; Sanders, 1965; Shanmugam, 2000a; Stow et al., 1996).

The turbidity current can be divided into distinctive zones seen (figure 4.3), with a head, body and tail, from Allan (1991). The different parts of the classical turbidity current deposit have been divided into five zones by Bouma (1962), the first turbidite facies model created (Shanmugam, 2002). The sediments within a turbidity current are thought to be supported by the upward component of fluid turbulence (Mulder and Alexander, 2001) with the limit of 9 % by volume concentration of sediments, according to mechanisms described by Bagnold (1962). Many authors have used much higher sediment concentrations for turbidity currents than those of the 'Bagnold limit'. Such dense flows will not be regarded as turbidity currents in this context;the classification proposed by Mulder and Alexander (2001) are applied for such flows and related deposits (figure 4.4). Mulder and Alexander (2001) made a distinction between the cohesive and the frictional component of a flow. Frictional flows are divided into hyperconcentrated flows, concentrated flows and turbidity flows. Lowe (1982) and many others described these types of flows as high-density turbidity currents and low-density turbidity currents.

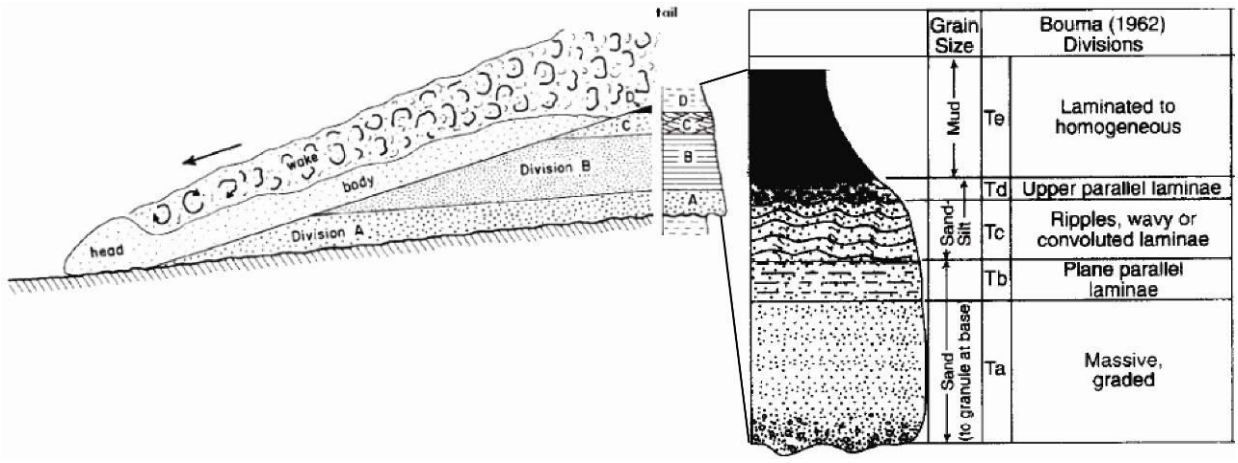

Figure 4.3: cross section through a turbidity current with Allen divisions of the turbidite deposits and the Bouma sequence, modified from Allan (1991).

Turbidity flows can be subdivided on the basis of their flow behaviour; surge flows, surge-like turbidity flows and quasi-steady turbidity currents. These flow types are distinguished by duration of sediment supply, if it is sustained flow or a short duration like a surge type of flow. The surge-like turbidity flows are probably mostly generated from other flow types of higher concentrations or collapse of suspension clouds (Postma, 1969; Wilson and Roberts, 1995). Surge flows are an uncommon phenomenon stated by Mulder and Alexander (2001). These two flow types alone are mainly depositional and not erosional, and normally contain not larger grain sizes than the sand fraction (Mulder and Alexander, 2001).

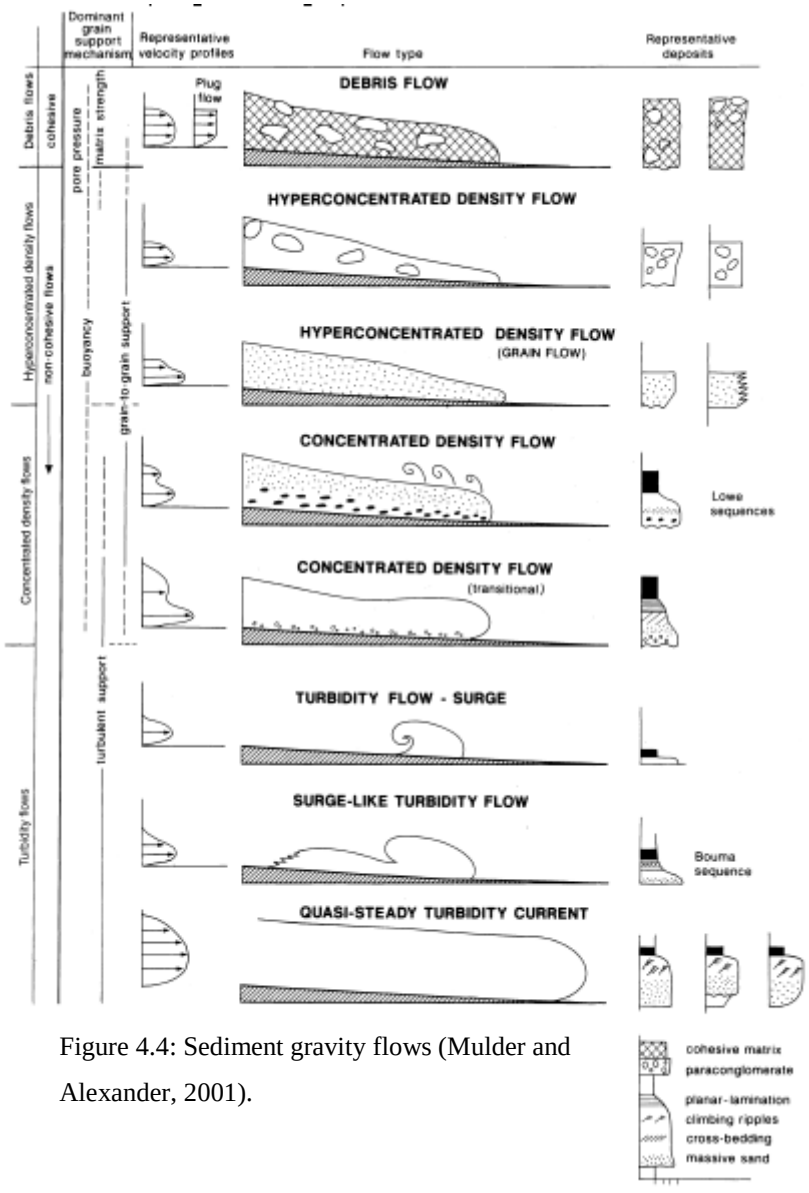

Figure 4.4: Sediment gravity flows (Mulder and Alexander, 2001).

Deposits of turbidity flows show normal grading due to fall out of the heavier sediment fraction from the suspension. Likewise, debris flows may give rise to normal grading, but these deposits may have floating clasts, which the turbidity current is lacking. The Bouma sequence is interpreted to be deposited by one single event in time. This has never been observed in laboratory experiments or observed in nature (Kuenen, 1966; Middleton, 1967).

4.4 Debris Flow

Wheras the turbidity current is a two-phase flow consisting of water and solid (Coussot and Meunier, 1996) a debris flow is considered to be a one phase flow where the flowing mass is an entity (Shanmugam, 1997). Debris flows have the sediment support mechanism of a cohesive flow, as stated by Lowe (1979, 1982) and Nemec and Steel (1984), and the rheological behaviour of a Bingham plastic (Johnson, 1970). When the shear stress of a debris flow is less than the shear strength k, the flow will freeze *en masse* (figure 4.5).

If the frictional resistance is the dominating component in the Coulomb-viscosity model the flow can be seen as a cohesionless debris flow, and if the cohesive material that is present in the system dominates it is identified only by the shear resistance and is defined as a cohesive debris flow (Dasgupta, 2003).He also state that due to the wide spectrum of cohesive flows with varied flow character the debris flow should only be defined by rheology.

Cohesive density flows can, according to Mulder and Alexander (2001), be divided into two types of flows; namely mud flows and debris flows due to sediment size sorting. The distinction between these two types is based on the volume fraction of gravel within flow. This fraction is set to less than 5% for mud flow and more than 5% for debris flow (Mulder and Alexander, 2001). Debris flow has the characteristic of poorly sorting and little or no signs of internal structures because of the rigid plug and *en masse* deposition. Large particles may show preferred orientation caused by pulsed shearing of the flowing mass (Leigh and Hartley, 1992). The debris flow consists of two parts, which is the laminar flow part and the plug flow part (Johnson, 1970). The plug is a part of the flow with no deformation because the shear stress is lower than the yield stress of the flow.

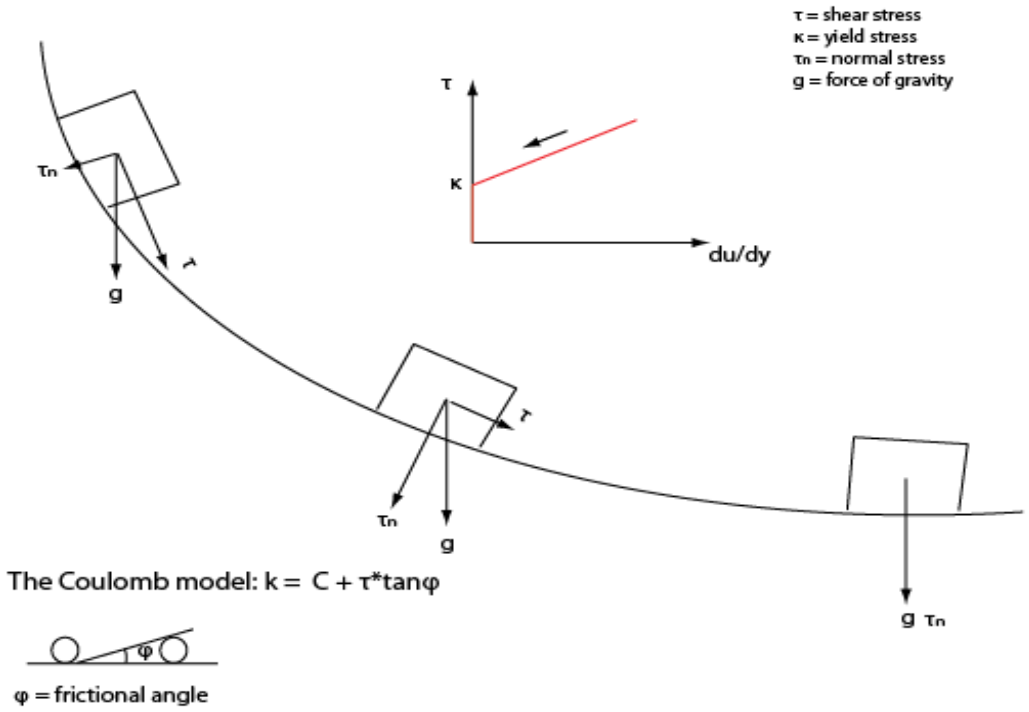

Figure 4.5: A debris flow stop flowing when the shear stress equals the yield stress (modified from Johnson, 1970 p.455).

Debris flows have been observed to flow up to several hundred kilometres on slopes of less than 1° (Aksu and Hiscott, 1992; Elverhøi et al., 1997; Embley, 1982; Laberg and Vorren, 1995; Masson et al., 1993; Shor and Piper, 1989). For subaqueous debris flows to be able to be displaced with that amount of distance it has to be lubricated on its base. This phenomenon is referred to as hydroplaning (Mohrig et al., 1998). If the debris flow is able to have this property it must be impermeable for load-supporting pressures to build up and be sustained in the thin layer of water penetrating underneath the debris. A gravity flow may start as a debris flow and end up as a turbidity current by infiltration of water into the flowing mass. This will not be the case for a large consolidated block of rock gliding down a slope. For water to be able to function as a lubricating layer underneath the flow, the water layer has to be exposed to a dynamic pressure by the load from the block. By estimations from experiments (Mohrig et al., 1998) the densimetric Froude number must be greater than 0.4 for this to happen.

4.5 Fluidized Flow

A flow becomes fluidized when the sediment is only supported by the upward moving fluid escaping (Lowe, 1979). This process occurs only in loosely packed sand or when there is generated an excess pore pressure (Middleton and Hampton, 1973). Evidence of fluidization can be seen in outcrops as dish and pillar structures or ball and pillow structures. Fluidized flows both decelerate and transform to liquefied flows or it accelerates to become turbulent (Lowe, 1982).

4.6 Grain Flow

Grain flow has been described by many authors (e.g. Bagnold, 1954; Middleton and Hampton, 1973; Lowe 1982), but Bagnold (1954) is a pioneer regarding this type of flow. Through theoretical and experimental work he described that the dispersive pressure of colliding grains is proportional to the shear stress transmitted between the grains, which counteracts the grain settling. Mulder and Alexander (2001) categorized grain flows as frictional in character and that will be entrained by water due to their non-cohesive property during settling. They classified the grain flow by its concentration to hyperconcentrated flows, concentrated flow, and turbidity flows (figure 4.4).

The hyperconcentrated flows and concentrated flows can be compared with the sandy debris flow by Shanmugam (1996). In this type of flow the frictional strength of the colliding grains are higher than the applied tangential component of gravity (Lowe, 1979), also known as dispersive pressure. Lowe (1979) classified this type of flow as a high-density turbidity current. The bagnold limit for a turbulent suspension is used to classify a flow as a turbidity flow from a concentrated flow (Mulder and Alexander, 2001).

Deposition from hyperconcentrated flows and concentrated flows often develop a basal tractional carpet. In the hyperconcentrated flow the traction carpet is a consequence of both an

upward velocity gradient within the flow and a laminar regime and behaves rheologically like a pseudoplastic with a yield stress. In the concentrated flows the traction carpet may also be present if the basal part of the flow has a high concentration. This type of flow may show normal grading, which is an indication of a waning flow. The boundary between these two flows may be near the transition from non-Newtonian to Newtonian (Mulder and Alexander, 2001).

4.7 The tractional carpet

Sohn (1997) divided the tractional carpet into a collisional zone and a basal frictional zone with 80% volume concentration of the packed bed, and no grain segregation. The collisional region has a volume concentration between 15% and 80% of the pakced bed (figure 4.6). The inverse grading is a product of large gradients of the particle concentration in the collisional zone (Sohn, 1997). Postma *et al*. (1988) described the tractional carpet as an inertia flow layer in the base of a flow, which is inversely graded and may contain outsized clasts in the upper part of the flow in a flume experiment. The basal interia flow layer has an increasing velocity gradient and a slightly decreasing concentration gradient. Where these 2 gradients have an abrupt increase and decrease, respectively (rheological boundary), the vertical transformation from laminar to turbulent flow occur at this level. The boundary between these 2 layers that contain outsized clasts is important when distinction between amalgamated beds and inertia flow layers is made in the field observations. The tractional carpet concept described by Lowe (1979), where the dispersive pressure was suggested giving rise to inversely graded beds has proven to be wrong by Legros (2002). What may cause the inverse grading may be a contribution of compaction and kinematic squeezing in the frictional zone (finest grains) and expansion, low particle concentration, kinematic sieving, and large grain sizes in the collisional zone (Le Roux, 2003).

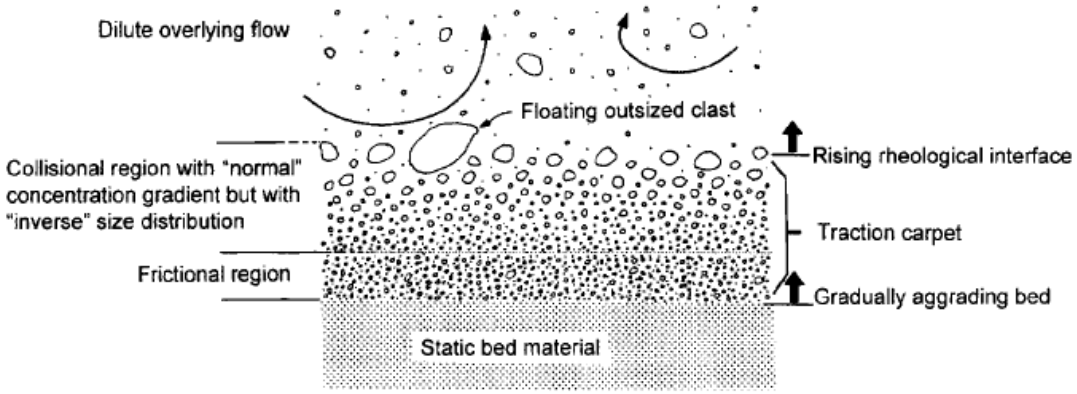

Figure 4.6: The traction carpet from Sohn (1997), with a frictional zone and a collisional zone.

The term “traction carpet” is as widely used as the term turbidity flows or turbidite deposits; however, according to (Legros, 2002), the traction carpet concept has been misinterpreted in many descriptions of gravity flow deposits. The word turbidite is heavily worked into the sedimentological terminology through time, and no other terms to describe the subaqueous gravity flows and the resulting deposits have gained the same success. Mutti (1977) is using the term turbidite for all deposits of subaqueous gravity flows, even though the deposits are debrites, slump deposits, or turbidite deposits.

5 Petrography

5.1 Introduction

The petrographic analysis of the thin sections aims to describe the textural and mineralogical composition of the samples selected from the study area, which will be interpreted for source area(s), environment of deposition, and to classify the rocks by using a classification scheme by NGU (Gjelle and Sigmond, 1995).

10 thin sections have been made from the 3 localities. The thin-sections RF8, RF9, and RF11 is from locality1, the thin sections; RF1, RF2, RF3, RF4, and RF6 are from locality2, and the RF10 and RF12 are from locality3 (table 4.1). These thin-sections have been prepared from sandstones from facies associations FA2.1 (sub-marine canyon floor) and FA3.1 (turbidite channel) with facies and characteristic descriptions seen in table 7.1.

Samples	RF1-102.0	RF2-19.6	RF3-19.8	RF4-89.75	RF6-30.5	RF8-7.7	RF9-10.3	RF10-64.4	RF11-3.2	RF12-9.0
Point counts	400	400	326	400	400	402	401	402	401	400
Minerals:										
Carbon-ate	22.3%	29.0%	20.5%	19.0%	19.5%	26.4%	27.4%	31.3%	35.4%	22.7%
Monocrys taline Qz	36.7%	38.0%	21.5%	45.2%	31.5%	15.2%	26.7%	24.1%	23.7%	31.2%
Polycrys-taline Qz	10.0%	7.0%	1.5%	4.0%	5.8%	0.7%	2.8%	2.7%	3.5%	3.8%
Chert	0.5%	0.7%	0.0%	0.7%	1.2%	0.5%	0.5%	0.0%	0.0%	0.8%
Feldspar	1.0%	1.0%	2.2%	1.8%	1.0%	1.0%	2.0%	0.0%	0.0%	7.7%
Num-mulites	0.0%	0.0%	14.7%	0.3%	0.0%	1.0%	0.0%	0.3%	0.0%	0.0%
Mica	0.5%	0.3%	0.3%	1.0%	1.0%	1.7%	0.0%	1.2%	2.0%	2.5%
Matrix	24.0%	21.3%	34.1%	26.5%	31.0%	46.3%	30.4%	26.4%	30.7%	25.0%
Plant/wo od debris	5.0%	2.7%	4.3%	1.5%	9.0%	7.2%	10.2%	13.5%	4.7%	5.7%
Pyroxene	0.0%	0.0%	0.0%	0.0%	0.0%	0.0%	0.0%	0.0%	0.0%	0.3%
Un-known	0.0%	0.0%	0.9%	0.0%	0.0%	0.0%	0.0%	0.5%	0.0%	0.3%

Table 5.1: The mineral composition of the 10 thin sections made of rock samples from the eastern part of Ainsa basin.

The mineral composition of the thin-sections is divided into 11 groups: carbonate, monocrystaline quartz, polycrystline quartz, Chert, feldspar, *nummulites*, mica, matrix, plant fragments/wood debris, Pyroxene, and unknown. Each sample has been point counted with approximately 400 counts for every sample, except sample number RF11, which has only 326 counts. The low number of counts is due to the grain size of the *nummulites*, and to avoid counting the same *nummelite* twice the interval of the point counter was increased. This may give a wrong description of the sample, which is dominated by *nummulites*. The composition of the samples is seen in table 5.1 and figure 5.1.

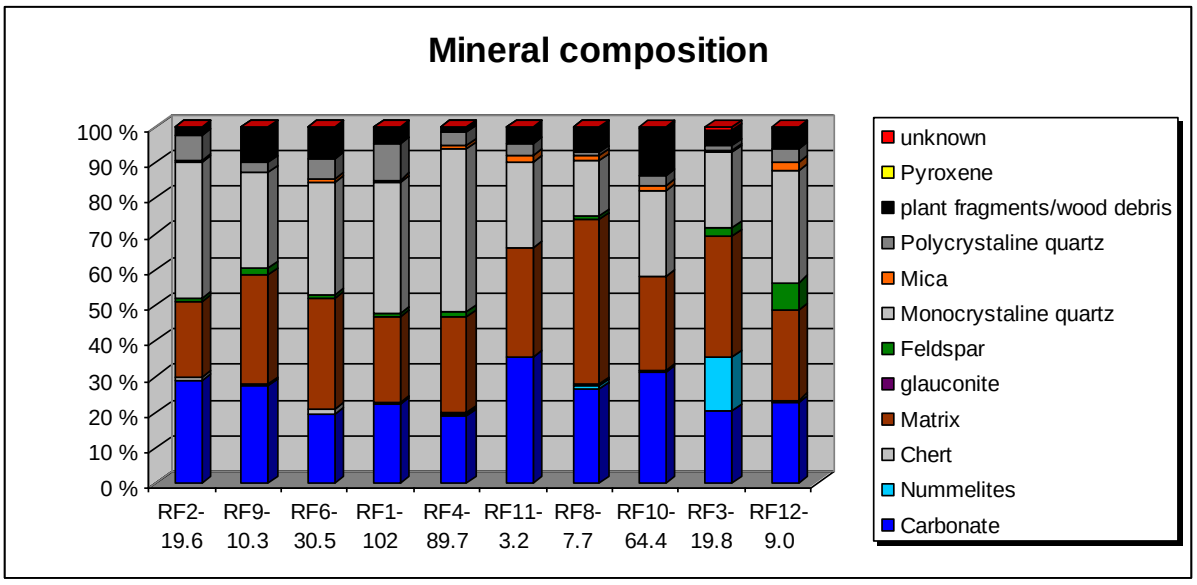

Figure 5.1: The mineral distribution of the rock samples.

The grains is from very poorly sorted to well sorted, with poorly/moderate as the most common sorting of the samples. The shape of the grains is commonly sub-angular to angular with one sample that was sub-rounded to angular in shape. The porosity is close to zero or zero in all the samples. The recognition of porosity is seen by the blue epoxy, which is not been observed in the thin sections.

5.2 Mineral composition

Quarz

Quartz minerals have been divided into monocrystaline quartz, polycrystalline quartz and chert (figure 5.2). These minerals belong to the tectosislicate group. The most common quartz mineral is monocrystaline quartz that has an average value for all the thin-sections of approximately 29.4%. The polycrystalline quartz has an average value of about 4.2%, and the chert has an average value of about 0.5%. Some of the quartz grains are corroded along the edges or "eaten" by the carbonate surrounding the grains, and some of the quartz grains are fractured.

Quartz is present in igneous rocks, metamorphic rocks, sedimentary rocks, and in hydrothermal and metal-bearing veins (Klein, 2002). The quartz belongs to the tectosilicate mineral group.

The quartz minerals in the samples are mostly strained quartz, which is recognized by an undulating extinction when you rotate the stage in cross-polarized light. In plane-polarized light quartz have a colourless appearance. There is also unstrained quartz present in the same samples, where undulating extinction is not present. The polycrystalline quartz is differentiated from monocrystalline quartz by the appearance of sutured quartz grains, and has a metamorphic origin. The different quartz grains (except the chert grains) derive from the axial zone of the hinterland (the Hercynian basement).

The chert is probably formed as nodular chert in a carbonate platform environment by silicious organisms (sponges, radiolarians, or diatoms) and later been shed into the deep marine realm. Probably, during early burial (diagenesis) the porewater may have been supersaturated with respect to silica from dissolved biogenic organisms and precipitated as chert (chertification). The formation of chert may have a marine or a non-marine origin

(Maliva and Siever, 1989). The most probable environment of chert formation in this study would be shallow marine origin. A study done by Gimènez-Montsant *et al* (1999) of the Lower Eocene chert of the Corones platform of the Spanish Pyrenees may be the source for the chert observed in the thin sections, and not an *in situ* process.

Feldspar

Feldspar is very common rock forming mineral with occurrences from various environments. The feldspar group can be divided into K-feldspar ((K, Na) $AlSi_3O_8$) and plagioclase feldspar ((Na,Ca) $AlSi_3O_8$) and belongs to the tectosilicate group. The K-feldspars are common in granites, syenites, granodiorites, and extrusive rocks as rhyolites and trachytes. The plagioclase feldspar series are more abundant than the K-feldspars and is found in igneous rocks, metamorphic rocks, and rarely in sedimentary rocks (Klein, 2002).

Feldspar clasts consists both of minerals with albite twinning, carlsbader twinning and pertithe structures, but the albite twinning is by far the most frequently registered and belongs to the plagioclase feldspars. This is what differentiates feldspar from quartz in the transmitted-light microscope. These different types of feldspar clasts are put in to one common group, due to the focus of maturity of the sandstones. The average content of feldspar in the samples is 1.76 %. Some of the feldspar is corroded by the high pH from the carbonate minerals and carbonate matrix, and therefore sometimes hard to distinguish from the calcite clasts, which may have twinning.

Mica

These minerals belong to the phylloscillicate group and have a monoclinic crystallography. The mica minerals observed in the thin sections are muscovite ($KAl_2(AlSi_3O_{10})(OH)_2$) and biotite ($K(Mg,Fe)_3(AlSi_3O_{10})(OH)_2$). The muscovite's show high order of birefringence (figure 5.2) and is not pleochroic. The biotite is brownish with cross-polarized light and it is pleochroic showing a pale brown to brown colour in plane-parallel light (figure 5.2).

Muscovite occurs in granites, granite pegmatites, and in certain mica schists (intermediate metamorphic grade rocks). The average content of mica in the thin-sections is about 1 %. The mica is derived from the hinterland. The biotite minerals are formed in many different environments as granite pegmatites, granites, diorites, gabbros, peridotites, felsic lavas, porphyries, and in a wide range of temperature and pressure conditions (metamorphic) (Klein, 2002).

Carbonate minerals:

These minerals have very high birefringence (pink to greenish high order colours) and are not pleochromatic (figure 5.2). Sometimes the crystallographic structures are visible; the calcite minerals ($CaCO_3$) have a rhombohedra structure, and multiple twinning is present in some of the clasts. The carbonate clasts constitutes for about 25.4 % on average of the mineral assemblage in all the samples.

The carbonate minerals are of either authigenic or allochgenic origin. The authigenic carbonate minerals are formed in the "carbonate factory", where the right temperature, salinity, and light intensity conditions for carbonate-producing organisms are found. The allochgenic carbonate is probably detrial clasts from the Mesozoic deposits of the thrust-sheets and/or Paleogene carbonate deposits. Homogenous limestone is very resistant in dry regions. When exposed in air a carstification of the landscape takes place. If the river transporting sediment has a high pH value, it would favour for transportation and deposition of limestone deposits (Nichols, 1999).

The allochgenic carbonate is transported by river currents and shelfal currents on the platform. Distinction between authigenic carbonate and allochenic carbonate is not carried out in the samples.

Matrix

The matrix is dominantly composed of micritic carbonate, which is brownish in cross-polarized light and colourless to brownish in plane-parallel light. The matrix is most likely derived from biogenic carbonate from the platform area and it has been transformed during an early stage of burial. Chemical processes of carbonates are much more important at low temperatures than for siliciclastic deposits (Bjørlykke et al., 1992).

Matrix composes of 29.5 % on average of the composition of the samples.

Nummulites

Nummulites are singled celled macro-foraminifera composed of calcite. They lived as benthic organisms between fair-weather wave base and storm wave base from Paleocene up to Oligocene (Jorry et al., 2005). They represent 1.6% on average of the thin sections, and are present in 4 of the 10 thin sections. The percentage of *nummulites* in these samples range from 0.25% up to 14.72%. Some of the *nummulites* show signs of abrasion. This may be due to storm derived currents, tidal currents and/or turbidity currents.

The *nummulites* consist of walled chambers, which represent porosity. These pores are either filled with reprecipitated calcite (sparite calcite) or organic matter, where the organic matter is opaque in both PPL and CPL. The *nummulites* are potential reservoir for accumulation of oil, if the right criterions are met.

Miscellaneous minerals:

Pyroxene

The pyroxenes crystallize at high temperatures, either early in a cooling igneous melt or in high temperature metamorphic rocks rich in Mg and Fe. Pyroxenes belong to the single chain inosilicate group (Klein, 2002). The mineral was violet, blue to black in XPL, with an extinction of the light at approximately 90° of rotation, and colorless in PPL (figure 5.2). There is only registered one pyroxene mineral in sample RF12.

Glauconite

The glauconite mineral have the same composition of elements as biotite, and is a member of the phyllosilicate group. The glauconite is emerald green in XPL and has a light green colour in PPL (Figure 5.x). It is observed in samples RF4 and RF12. The minerals are commonly formed on continental shelves in shallow marine environments with low sedimentation rate (sediment starvation). Amarosi (1997) has made a sequential relationship between glauconite and depositional sequences, where glauconite is transported from the shelf to slope or abyssal plain during transgressive systems tract or early highstand systems tract. The glauconite is formed contemporarily at the water/sediment interface and transported by currents (Amorosi, 1997).

Chlorite

There is observed a detrial chlorite grain in sample RF12. The mineral is black to white in XPL and light green in PPL (figure 5.2). Chlorite belongs to the phyllosilicates and is a clay mineral of the chlorite group. The chlorite are most likely a precipitation product formed during early burial from the porewaters filled with elements from decomposed dolomite, feldspar or biotite (Humphreys et al., 1989). The chlorite is light green to green in plane-polarized light and light brown to brown in plane-parallel light.

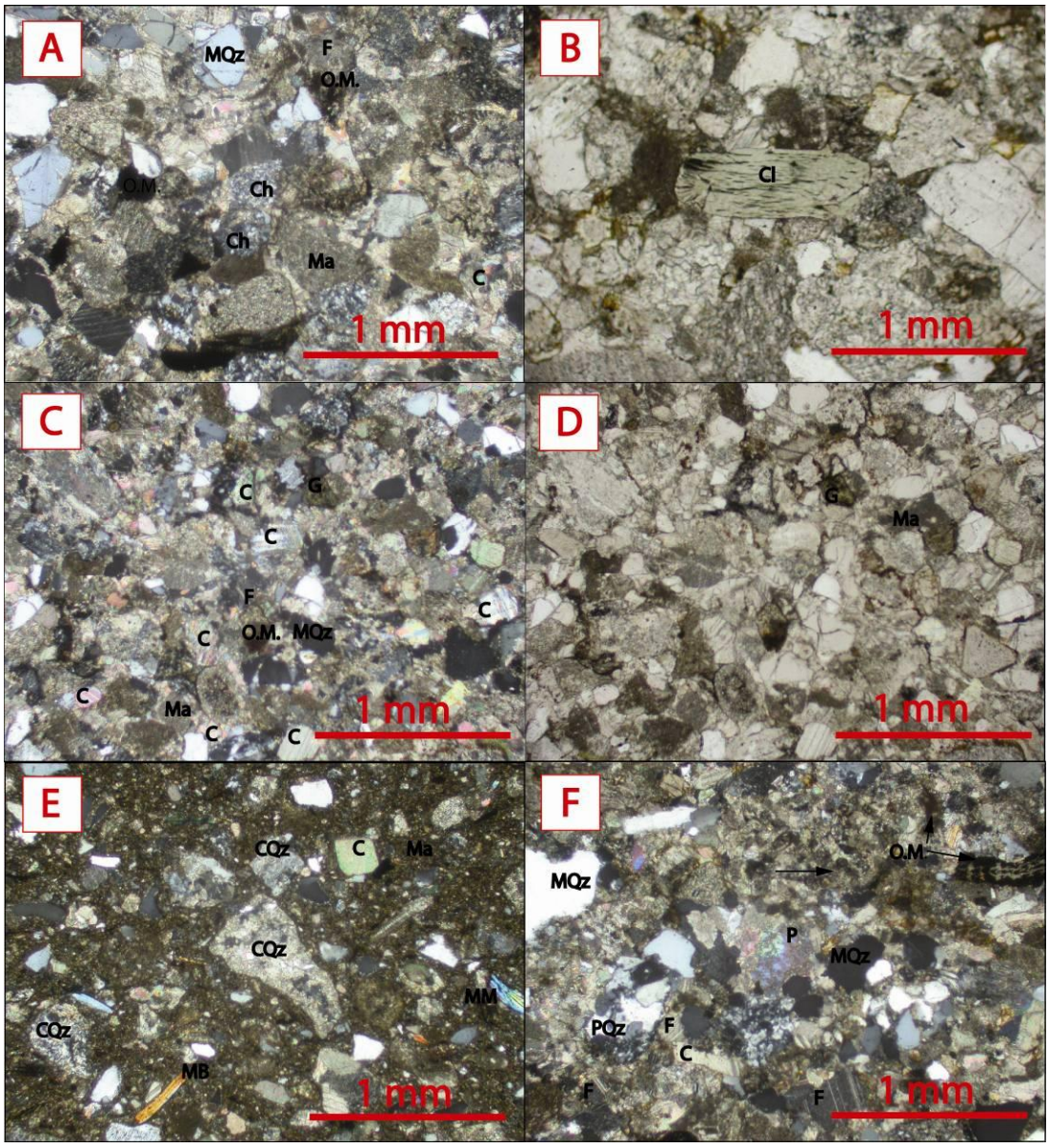

Figure 5.2: A) XPL of RF6: no porosity and angular to subangular grains, and the matrix is greyish to brownish. B) PPL of RF12: no porosity and angular to subangular grains, with a coarse detrial chlorite grain in the centre of the picture. C) XPL of RF2: no porosity and angular to subangular grains, and a detrial glauconite grain. D) PPL of RF2. E) XPL of RF6: no porosity and angulare grains, with corrosion of some quartz grains (matrix-supported fine grained calcareous sandstone). F) XPL of RF12: no porosity and angulare to subangular grains, with a pyroxene in the centre of the picture.

MQz – monocrystalline quartz **CQz** – corroded quartz **OM** – organic matter (plant/wood debris)

PQz – polycrystalline quartz **MM** – mica (muscovite) **MB** – mica (biotite)

Ch – chert **C** – carbonate **F** – feldspar

Ma - matrix **P** – pyroxene **G** – glauconite

Cl - chlorite

Plant fragments/wood debris

These deposits represent terrigenous deposits from the (Tremp-Graus basin) coastal areas east of the Ainsa basin, and are found in 6.4% of the samples on average. The organic matter is black to brown in appearance in both plane-parallel light and in cross-polarized light (figure 5.2).

5.3 Interpretation of sandstones

Source area(s)

The potassium feldspar is more chemically stable than calcium and sodium feldspar during weathering of the rock forming minerals. This would say that the amount of K-feldspar in the samples should be dominating, which is not the case. Then the explanation would be that the source is of metamorphic origin. Together with the polycrystalline quartz and the muscovite indicate a metamorphic source of intermediate metamorphic grade. Distinction of the carbonate grains is not made, but both allocthtonous and autochthonous grains may be present in the samples.

Environment of deposition

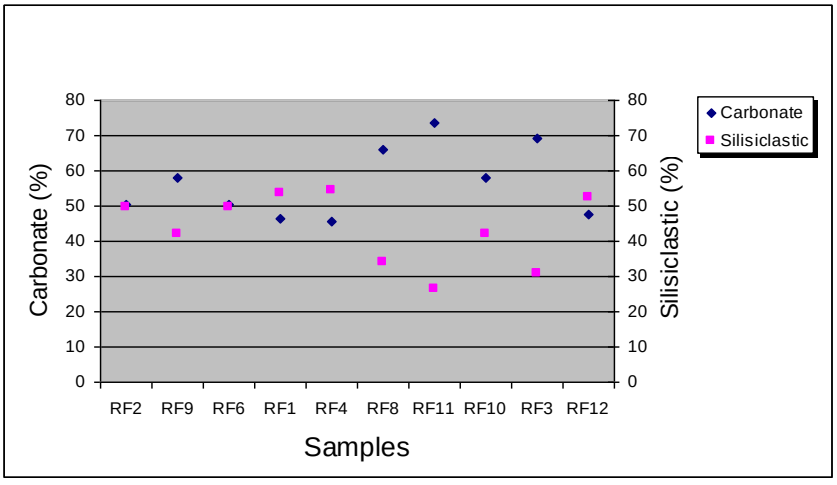

Figure 5.3: Carbonate minerals (autochthonous and allocthtonous grains) versus siliciclastic minerals.

The *Nummulites* lived at latitudes with tropical climate in shallow marine waters (below storm wave-base) (Beavington-Penney and Racey, 2004). Together with the high amount of detrial carbonate and carbonate

matrix in the samples (Figure 5.x) give evidence of tropical climate. The detrial carbonate may be derived from the thrust sheets that exposed the Mesozoic deposits. During rifting in the late Mesozoic era carbonate deposition took place (Caus et al., 1997). During The late Mesozoic and the early Cenozoic there was a period of global greenhouse conditions. This warm period can be related to the break-up of the supercontinent Pangaea (Ford and Golonka, 2003).

Classification of the turbidite sandstones

The classification of sandstones is made by looking at the textural and mineralogical composition in thin sections. The total amount of carbonate (including matrix) in average of the rock samples is 56.3% and the siliciclastic part counts for the remaining 43.7% (figure 5.3). If the matrix is not taken into consideration the carbonate content would be 26.7% on average. The classification scheme used for classifying the samples is from NGU (1995). The samples are plotted in the ternary diagram as calcerous sandstone (4 samples) or calcerous muddy sandstone (4 samples), and with 2 samples as calcerous mudstone (figure 5.4).

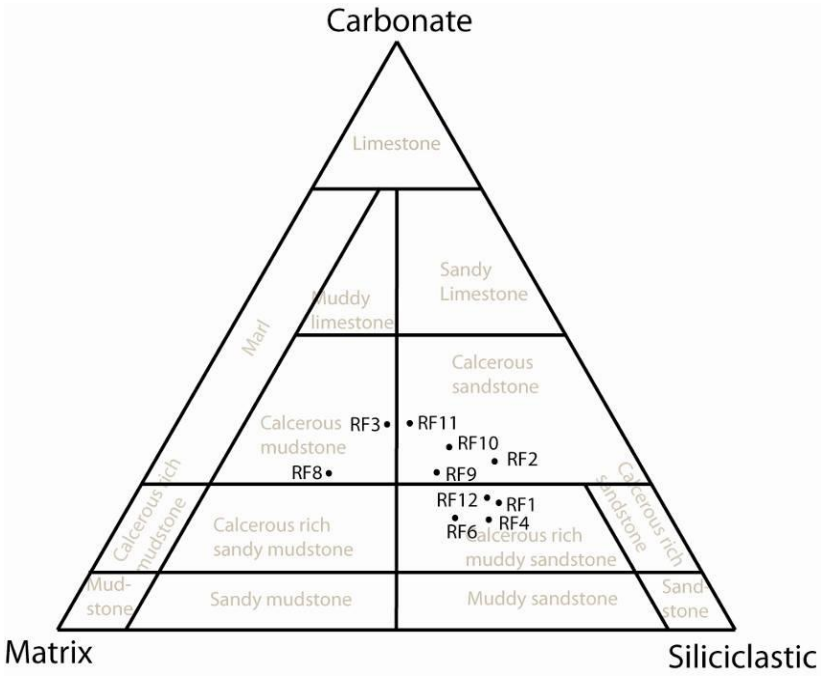

Figure 5.4: Mineralogical composition of samples from sub-marine canyon floor association, turbidite channel association, and debris flow association (modified from Gjelle and Sigmond (1995)).

6 Facies

6.1 Introduction

The word facies derives from the Latin word facia that means a general look of something or an overall external aspect of an object. This implies that it is an abstract term. In the facies descriptions and interpretations the facies is based on sedimentary features logged in the three localities east of Ainsa. In Table 6.1 all the facies are given a short description and interpretation according to lithology and structures.

There have been made 16 logs from 3 localities. Log1 and log5 have been logged in the scale of 1:200, log15 has been logged in the scale of 1:100, where log16 is a part of log15, and log7(2) has been logged in the scale of 1:20. Log7(2) is a part of log7 that is emphasising some load structures seen in figure 6.8, and log6 is a part of log4. Log6 is made due to folding and faulting of the succession between approximately 54 metres and 57.5 metres (log4).

Only the logs in the scale of 1:50 have detailed information of structures. The lithofacies are grouped into groups from A to E and the facies distribution of all the logs are seen in figure 6.1. The distribution of the sandstone facies that are logged in the scale of 1:50 are seen in figure 6.1 B. The aspect ratio (net/gross) for the logged successions of the Arro sequence in locality2 is 32.6%, the aspect ratio for locality3 is 47.4%, and the aspect ratio in locality1 is 33.2%. The value that is set for a system, which is classified as a mud-dominated delta fed system, is set to ≤ 0.3 (30%) by (Richards and Bowman, 1998).

Code		Facies	Description	Interpretation
A	A1	Mudstone - structureless	The mudstones are grey to dark grey with noe structures except sparsely with bioturbation traces and clasts.	Mud flow or background sedimentation.
	A2	Mudstone - laminated	The laminated mudstones are between 10 and 30 centimetres and greyish. No bioturbation traces seen in the beds.	Dysoxic environment and/or platy grains.
B	B1	Siltstone	Coarse silt layers with no strucutres, wavy bedding, lamianted or with ripples. Bde thickness is from 1- 40 centimetres.	Dilute turbidites.
C	C1	Ripple cross-laminated sandstone	The amplitude of the ripples are less than 5 centimetres and they are found in 43% of the logged sections in the scale of 1:50. Deposited in the lower flow regime.	Bouma T_c.
	C2	Cross-stratified sandstone	The amplitude of the dunes are more than more than 5 centimetres and they are either trough cross stratified or tabular in nature. These structures have been deposited in the lower flow regime.	Bouma T_c.
	C3	Plane parallel-laminated sandstone	The laminaes are less than 1 centimetres and the units are from 2 centimetres up to 10 centimetres. Deposition in both lower and upper flow regime.	Bouma T_b and Bouma T_d.
	C4	Plane parallel-stratified sandstone	The plane parallel bedding is thicker than 1 centimetres. The units are from 8 - 55 centimetres thick. These units have been deposited in the upper flow regime.	Bouma T_b.
	C5	Structureless sandstone	These units have no visible structures. Deposited rappidly and may have syn-sedimentary faulting in the basal part. Upper part of the upper flow regime.	Bouma T_a.
	C6	Normal graded sandstone	The grain size decreas from the basal part of the units and upwards, due to the waning stage of a subaqueous unidirectional current.	Deposited by a turbidity current as turbidites.
	C7	Inversely graded sandstone	The grain size increase from the basal part and upward. This indicates an increase in energy or kintic sieving.	Bouma T_a, Lowe S_2.
D	D1	Conglomerate - matrix-supported	The conglomerates are either monomictic, oligomictic or polymictic. Some of the clasts in the units have intraclasts in them.	Cohesive debris flow deposits.
E	E1	Sedimentary breccia	It have a sheet like geometry with internal bedding. Wrinkle marks and bioturbation traces giving evidence for a shelfal origin.	Slump sheet.
	E2	Chaotic mudstone and sandstone	Folded layers of silt or silt mud, and snowball structures of silt and mud in a muddy or sandy matrix.	Levee slumping and debris flow deposits.

Table 6.1: Facies in the logged sections of the Arro sandstone body.

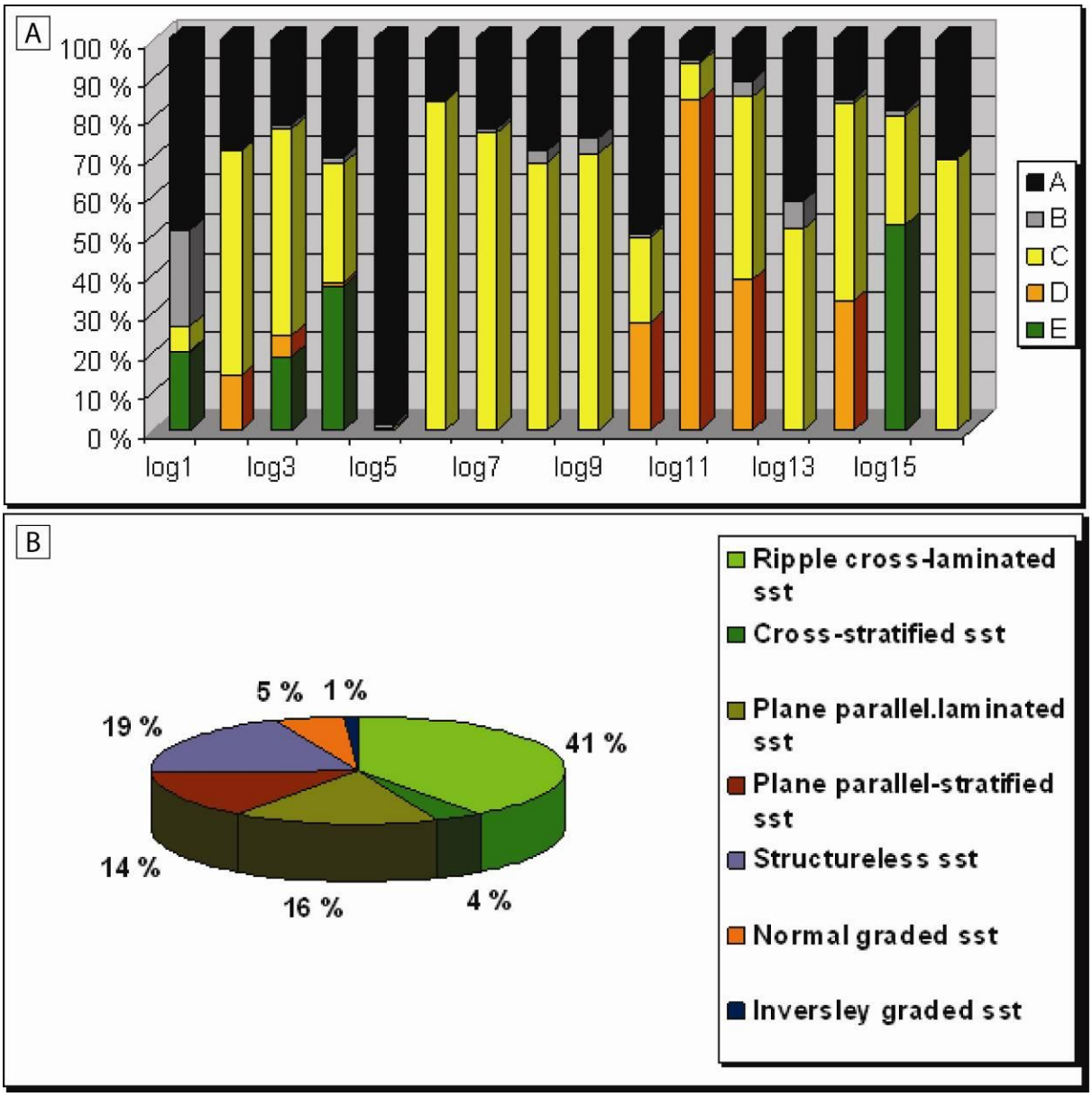

Figure 6.1 A) Facies distribution of the recorded Arro sandstone body. B) Facies distribution of the sandstones recorded in the logs in the scale of 1:50.

Trace fossils are good environmental indicators. In the logged sections there are recorded at least four ichnogenera; *Planolites*, *Thalassinoides*, *Nereites, and Skolithos*. These can be put into three ichnofacies that are recognized in the different logged sections, *Skolithos*, *Cruziana*, and *Nereites* ichnofacies. The *Skolithos* of the *Skolithos* ichnofacies is of high energy marine environmet, but can also be found in submarine canyons or deep marine fans. *Planolites* and

Thalassinoides belong to the *Cruziana* ichnogenus, which are characteristic of the offshore transitional zone and the offshore shelf. *Nereites* from the *Nereites* ichnofacies is of bathyal to abyssal plain environment (Pemberton et al., 1992), recorded in log 3 together with *Planolites* (Figure 6.2).

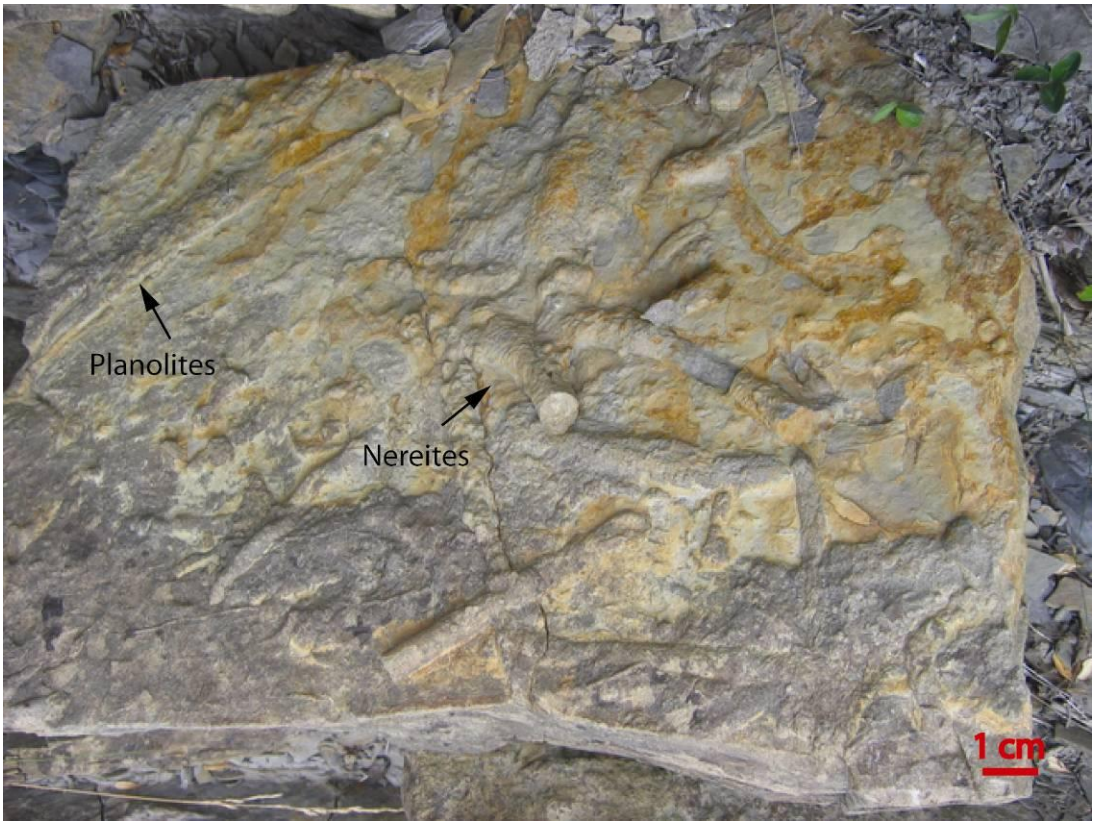

Figure 6.2: Trace fossils in base of bed at 21.7 metres in log 3.

6.2 Facies of the deep marine Ainsa Basin

A: Mudstone

The mudstone facies have been divided into two lithofacies: structureless mudstone (A1), and laminated mudstone (A2). The total thickness of beds with mudstone facies is about 158 metres, and 6.18 metres of the mudstones are laminated. The distribution of the lithofacies is seen in figure 6.1.

A1: Mudstone – structureless

Description

Structureless mudstones have no lamination, but a blocky appearance in the outcrops, and there can be traces of bioturbation or fossils in the sections logged. The mudstones can be divided into clay dominated mudstone and silt dominated mudstone. The distinction is made by either colour differences or by chewing the mudstone to feel if there are any silt grains in the mud. The boundaries are mostly sharp to over- or underlying sandstones or conglomerates, but also gradational boundaries are present, from clay dominated mudstone to silt dominated mudstone or the other way around. Coarse siltstone beds are found within the mudstone. These beds have a slightly lighter colour than the surrounding mudstone, which range from grey to dark grey in colour. The thickness variation of the different beds varies from 1 centimetre up to 11 metres with a mean of 10 to 20 centimetres. Bioturbation traces are only found in locality 3, logged in log 15 at 12.7 metres, which are both horizontal and vertical traces. There are also fossil gastropods in three beds at the same locality. These are spirally shaped and are from 4 centimetres to 10 centimetres long. The fossils have not been identified.

In log 11 and in log12 there are three beds sparsely with clasts and the grain size ranges from granules up to small cobbles. The shape of the clasts is sub-rounded to well-rounded, and some of the sandstone clasts have intraclasts of mudstone, Nummulites, and oyster fragments.

Interpretation

The structureless character of the beds may be due to either a very homogeneous and possibly rather rapid deposition or to a lack of platy grains. Bioturbation may also be the reason for the structureless character (Collinson and Thompson, 1989). The mudstone beds below 1.5 meters in thickness show no signs of processes other then deposition by hemipelagic

background sedimentation and probably reworked by bioturbation. Beds with clasts are interpreted as cohesive debris flows (Nemec and Steel, 1984). The direction of the clast a-axis is measured parallel to the flow, because this gives least shear resistance in a cohesive debris flow (Collinson and Thompson, 1989). The clasts that are scattered in the mudstone beds, recorded in log11 and log12, are intrabasinal clasts, with the same features as logged in stratigraphically lower layers and some bioclastic limestone clasts that may be of shallow-marine origin.

A2: Mudstone – laminated

Description

The laminated mudstones have a total thickness of 6.18 metres, and are mapped in all the localities. In log 7 at 17.3 metres there is a bed with laminated mudstone with increasing silt content upwards. No mica or other minerals are seen in the laminated intervals, no distinct colour differences, or in situ fossils are seen in the beds. Bioturbation traces are absent in these intervals, as well. All the laminated beds have a sharp upper and a lower boundary, with sandstone intervals that vary in grain size from very fine to medium. Pyrite has not been registered in any of the intervals recorded.

Interpretation

Clay minerals, chlorites and micas occur as platy grains that will have orientation when they are compacted. When the lamination is caused by grain size differences seen by, for example evidence of colour separations, the energy level must have been fluctuating. There are two processes that have to be taken into consideration: the first is sediment settling from suspension from the water column or a light turbid layer near the surface or the second alternative is that the coarser laminae is a product of weak dilute density currents and the finer laminaes are formed due to background sedimentation (Collinson and Thompson, 1989).

The intervals logged of this facies are probably deposited in an oxic envirnoment, with little or no bioturbation and organic content of the intervals. The absence of pyrite is an indication that the depositional environment is not dysoxic or anoxic (Rickards, 1997). The colour of the laminated mudstone is not very much darker than the structureless mudstone. This may indicate that the environment was not restricted regarding the oxygen conditions, with water circulation and contourite currents. There can be locally environments that may be somewhat restricted due to oxygen deficiency.

B: Coarse siltstone

Description

This lithofacies is present in all the localities. In the section logged with scale 1:20 (log7(2)) there have not been recorded any structures in the beds. The sections logged in the scale of 1:50, there are no structures like lamination or ripples in these intervals, but the bedding is often wavy. The total numbers of coarse siltstone intervals logged in the outcrops are 122. In log 7 at 2.5 meters there is shown an interval with disrupted coarse silt within mud (Figure 6.3). This resembles convolution structures.

The colour of the siltstone beds is greyish to yellowish, and the thicknesses are from 1- 40 centimtres. The majority of the beds are between 2 and 3 centimetres. The boundaries are sometimes hard to distinguish from the surrounding mud, but are both sharp and gradational. There may be a slight colour difference, or the beds are protruding out from the mud like thin ribs. In the section represented by log 4, between 16.1 metres and 18.5 metres, there are coarse silt layers “swimming” in the mudstone in the lowermost part, and rhythmically beds in the uppermost part of this section.

Figure 6.3: Silty layer (yellowish) with convolution structures in locality 1 log 7 at 2.5 metres.

Interpretation

These beds may have been deposited by several processes. The first process is deposition from diluted low density turbidity current, where the coarse silt is settled from suspension. An additional process may be that some of the siltstone beds can also be deposited by bottom ocean currents as contourites, but there is no clear evidence in the logged sections. There exists a lot of uncertainties when claiming deposits as contourites, but structures like inverse grading of laminae or beds, and bidirectional cross-lamination may be good indicators (Stow et al., 1998).

C: Sandstone

The sandstone facies has been divided into 7 lithofacies based on structures in 486 beds, which are: ripple cross-laminated sandstone (C1), cross-stratified sandstone (C2), plane parallel-laminated sandstone (C3), plane parallel-stratified sandstone (C4), structureless sandstone (C5), normal graded sandstone (C6), and inversely graded sandstone (C7). The dominating lithofacies are C1, C2, and C3. Some of the beds have scattered fragments of black oysters and *nummulites*, and less commonly, wood fragments, plant debris, and muscovite. Sole marks are very common throughout the sections, especially flute casts. The palaeo-current measurments of the flute marks are seen in Appendix I. The mean trending direction of the flute marks is NNW.

C1: Ripple cross-laminated sandstone

Description

The second most common facies throughout all the logged sections are current ripple cross-lamination, with 32% of the sandstones. The amplitude of the ripples is commonly 2-3 cm. This facies is present in all sections logged in the scale 1:50, except section represented by log 10. Climbing ripples are ripples with set boundaries that dip in the opposite direction to the dip of the general cross laminated layers. The angle of climb gives indications of the balance between the rates of upward bed growth and ripple migration (figure 6.4). Good examples of this structure are shown at 90.5 meters in log 4, where the climbing ripples have their lee side facing southerly direction.

The colour ranges from yellowish to greyish, and with interval thickness of sandstone structures ranging from 1 centimetre up to 7 centimetres. The lower boundary is most often gradational, usually with beds of facies C3 or C4 below. The upper boundary is sharp and always covered with mudstone. Where the lower boundary is sharp the rippled cross-laminated sandstone has mudstone both below and above. The grain size is between very fine

sand up to fine/medium sand. These rocks are siliciclastic in nature, and there are two places where plant fragments and wood debris are observed; at 7 metres in log 7 and at 16.25 metres in the section represented by log 9.

Figure 6.4: Climbing ripples with the angle of climb indicated by the drawing.

Interpretation

Ripples are defined by their size and shape, with wavelength less than 50 cm and amplitude seldom exceeding 3 cm (Collinson and Thompson, 1989). Their shape is either symmetrical or asymmetrical, generally symmetrical ripples are made by waves and asymmetrical ripples are made by currents. The ripples are triangular shaped with a stoss side and a lee side. The

stoss side is on the upstream side and the lee side on the downstream side. The asymmetrical ripples have a gentle upstream slope and a steep downstream slope, with a stoss side/lee side ratio above 3. These structures do not form where the grain size is larger than 0.6 millimetres, which corresponds to approximately medium/coarse sandstone (Collinson and Thompson, 1989). The ripples that are recorded in the logs are asymmetrical. This gives indication of that the ripples are made from unidirectional currents. Where the intervals are only 1 centimetre and consist of 1 bedset and have an underlying C3 interval may have been formed due to reworking of the underlying C3 interval (Walker, 1967). This facies can be compared to the Tc of a complete Bouma turbidite succession (Bouma, 1962). The grain size range, together with the structures, give information about the energy level of the flow and the grain sizes that

is available in the source area. These types of structures belong to the lower flow regime (Southard, 1971).

The plant- and wood fragments may be an indication of lowstand situation, where the shore line is moved closer to the deep marine system. From the article of Weber et al. (1997), claiming that fan systems are described as inactive during sea level rise and highstand, but not always the case.

C2: Cross-stratified sandstone

Description

The C2 facies comprises 3% of the facies logged in the scale of 1:50. The thicknesses of the C2 intervals are from 6 centimetres up to 12 centimetres, whereas the amplitude of the cross-stratification is between 6 and 10 centimetres. Both planar cross-stratified sandstones and trough cross-stratified sandstones are present in the logged localities, but the most common C2 structures are trough cross-stratified sandstones (Figure 6.5).

Figure 6.5: Trough-cross stratified sandstone with an intra-clast containing *nummulites*.

The beds have a greyish to yellowish colour in general, but the bed at 68 metres displayed in figure 6.5 is grey and red. The grain size distribution is from very fine sand up to coarse sand. The lower and upper boundaries are both gradational and sharp. Where this interval is present as isolated beds, both the upper and lower boundaries are sharp, bounded by mud. The cross-stratified sandstones are often seen together with the A2, C1, C3, and C4 facies.

Interpretation

The 3-D trough-cross stratified beds indicate higher mean flow velocities than the tabular 2-D dunes. The weaker flows give rise to grain flows that avalanche down the lee-side slope, forming angular forsets. A more powerful flow will give rise to flow separation and grain fall becomes the dominant process of dune formation, with formation of tangential foresets (Collinson and Thompson, 1989). The amplitude of this type of structures is more than 5 centimetres from maximum high to maxium low wave peak. In plan view, the different types of structures within C2 can be distinguished by the crests of the dunes by their morphology. They are either straight crested or have some degree of sinuosity. Cross-stratified sandstone can be divided into 2-D dunes and 3-D dunes. 2-D dunes have lower mean flow velocity compared to 3-D dunes, they are straight-crested and have tabular bed sets. 3-D dunes have a three-dimensional geometry that gives rise to trough-shaped transverse to the crest line and tabular bed sets in longitudinal cross sections (Collinson and Thompson, 1989). These structures are found in the lower flow regime, closer to the upper flow regime than the ripples (Southard, 1971). There is a general trend of larger grain size in these structures that also give indication of a higher energy environment than ripples. These structures can be compared with the Bouma Tc interval.

C3: Plane parallell-laminated sandstone

Description

Plane parallel-laminated sandstone occurs as flat bed sets that are parallel with each other. This type of sandstone is recognized in 13% of the sections that are logged in the scale 1:50. The thicknesses of the intervals are between 2 – 10 centimetres and the laminae are less than 1

centimetre, with the main distribution of co-sets around 5 centimetres. Beds of plane parallel-laminated sandstone have both sharp and gradational lower and upper boundaries, and the colour of the sandstone is greyish and yellowish. The main grain size distribution of 67 intervals (C3) recoded is very fine to fine, with two beds that are of medium grained sandstone. There is one bed at 16.25 meters in the section of log 9 with muscovite and plant fragments. The most frequent occurrence is C1 and C3 together, but C3 is also found isolated and together with C6. One bed includes facies C5, C4, C3, and C1 arranged vertically from base to top, *nummulites* and fragments of abraided oysters can occur, but is very rare.

Interpretation

Coarse silt and very fine sand may be transported by traction and by suspension in slow moving currents (Harms et al, 1982). Sand grains of fine to medium size deposited from a unidirectional current and creating parallel stratification or parallel lamination can indicate upper flow regime (Collinson and Thompson, 1989). In most of the beds with plan parallel-lamination the interval above is ripple cross-lamination and sometimes cross-stratified intervals.

Beds of C3 facies are deposited by relatively slow settling from suspension in the lower flow regime; with Froud number < 1 (Harms and Fahnestock, 1965), where the facies occurs as one single bed or the uppermost facies in a bed.

There are 9 intervals where the C3 facies occurs as a single T_d interval of a Bouma succession and no beds where C3 is logged above a Bouma T_c. The majority of the C3 intervals are found with an overlying C1. This indicates a waning flow from the upper flow regime to the lower flow regime, and therefore interpreted to be of the Bouma T_b interval. The intervals with nummulites and oyster fragments must have been transported with a fairly high level of energy and therefore, these beds would have been deposited in the upper flow regime, as depicted for the Bouma T_b according to (Collinson and Thompson, 1989).

The grains of muscovite seen in the outcrop must have been derived from a metmorphic or igneous rock from the hinterland.

C4: Plane parallell-stratified sandstone

Description

These intervals are sometimes wavy, when they are the basal structure overlying a muddy interval. Plane parallell-stratified sandstones have parallel bedding that is thicker than 1 centimetre. The parallel-stratified sandstones are present in 12% of the sandstone beds logged in the scale 1:50. The thickness of the C4 intervals is between 8 centimetres and 53 centimetres, with an average of approximate 16 centimeters. The colour is greyish and yellowish, and with grain size from very fine to medium. Both the upper and lower boundaries are gradational and sharp. Where the C4 interval represents a bed with mud below and above, the boundaries are sharp, and where it is gradational the C4 intervals is bordered by intervals of C1, C5 or C7. The most common structure seen together with C4 is C1.

Interpretation

In flat beds of parallel stratified sandstones of fine to medium in grain size, the flow velocity has been high and deposition from bedload transport (Simons et al, 1965) in the upper flow regime. The C4 (figure 6.6) intervals are results of sediment deposited in the upper flow regime (Harms et al., 1975), and can be compared with the Bouma T_b interval.

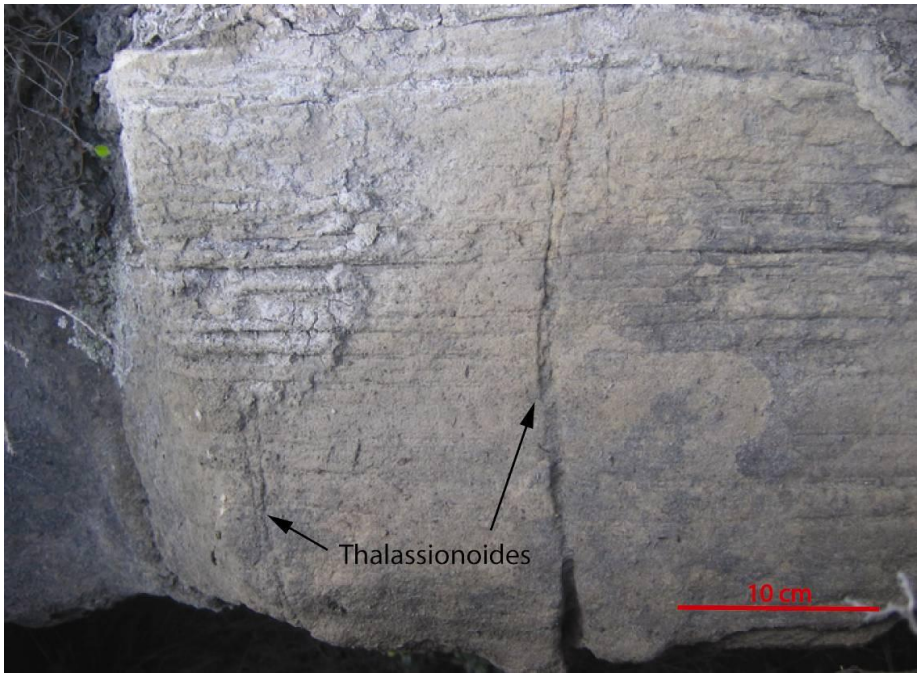

Figure 6.6: A T_b interval with *Thalassinoides* bioturbation thraces at locality 1.

C5: Structureless sandstone

Description

Structureless sandstones can have all ranges of grain sizes, but no tractional structures. There can be structures like disc and pillar structures or ball and pillow structures in this interval, but these structures have not been recorded in any of the logs.

The C5 facies is the most common sandstone facies, with 34% logged in the scale of 1:50. There are commonly *nummulites*, oyster fragments, and mud clasts scattered in this type of sandstone facies. The colour varies from greyish to yellowish and the grain size from very fine to very coarse. The base of the structureless sandstone beds is often sharp with the underlying mudstone. The upper boundary is gradational, generally with a decrease in grain size. It is most common together with C1 and C4, but it is found in beds with all the other sandstones, except C6. The basal part of the structureless sandstone seen in the Charo locality, have syn-sedimentary faulting. In log 7 at 18.5 metres and at 24 metres, there are syn-sedimentary faults with throw of about 60 centimetres in the lower most deformed area and about 15 centimetres throw at 24 metres (figure 6.7). Load cast structures are found in some of the beds in this lithofacies. In log 7(2) there are flame structures, and this log is mainly made to highlight these structures (figure 6.8).

Figure 6.7: Syn-sediemntary faulting at 19 metres in log 7 in locality 1.

Basal parts of some beds are very loose or uncemented. In these intervals there are always numerous detrital fragments like Nummulites, mudclasts, or oyster fragments. Structureless sandstone beds have an erosive base and often an uneven thickness.

Figure 6.8: Flame structures logged in log7(2) (seen in the square).

There are also 132 intervals, where there is lacking data of hydro-dynamically formed structures. These beds range in grain size from coarse silt/very fine sand to medium sand, and their thicknesses range from 1 centimetre up 140 centimetres. The most common thicknesses are between 2 – 10 centimetres.

Interpretation

Depositional intervals or beds of facies C5 are most likely deposited by a decelerating heavily sediment laden current with fast packing of the grains so that no specific bedform is created, and rapid suspension fall out from hyperconsentrated or concentrated flows (Mulder and Alexander, 2001). If there have been parallel layers present in sandstone, they may have been destroyed by bioturbation or by water escape structures (Collinson and Thompson, 1989). This was not seen in any of the logged sections.

Facies C5 represents sandstone deposited in the upper part of the upper flow regime and can be compared with the Bouma T_a interval. The uncemented parts of this facies may be indication of shallow burial.

Some C5 intervals were covered by lichens or some kind of fungus, which made it hard to distinguish this interval from other intervals. Occasionally, beds were totally covered and only grain size and bed thickness could be logged.

C6: Normal graded sandstone

Description

5% of sandstones logged in the scale 1:50 belongs to this facies. In the section represented by log 4, between 28.75 meters and 36 meters, there are 5 amalgamated beds with normal grading that are altogether 7.25 meters thick. The individual beds are distinguished by zones of mudclasts and by wavy contact between the beds. The grain size distribution ranges from fine/medium up to granular, and with a greyish colour. These beds have no clear visible structures to be classified according to structures, but there are wavy contact and mud clasts seen in the basal part of the lowermost bed in log 4. In the same bed there are also observed mud clasts in top of the bed. The bed at about 34 metres has *nummulites*, quartz grains, and oyster fragments in the lowermost 10 centimetres. The same features are seen a bed at 36.5 metres, except that there are no quartz grains.

Interpretation

Normal graded sandstone beds include beds in which the mean grain size is decreasing from the base of the interval and upwards. This is due to deceleration of a unidirectional current (Bogs, 2001). This facies is interpreted to be the product of the waning stage of turbidity current. Normal graded beds deposited in a sub-marine environment were first given a name by Arnold Bouma in his study of flysch deposits in the French Alps (Bouma, 1962).

There are mudclasts in both the upper parts and the lower parts of the amalgamated beds recorded in log 4. The mudclasts seen in the basal parts of the lowermost bed are due to erosion of the underlying mud during flow of a high density turbidity current. The turbidity currents are confined within a turbidite channel surrounded by mud, and during flow the currents dig out the base and side-walls of the channel, and some mud clasts may fall into the channel during or after the flow. The wavy contacts together with the mud clasts give evidence of episodically events of turbidity currents.

C7: Inversely graded sandstone

Description

This facies is not very common throughout the logged sections, only 1% of the sandstones in the scale of 1:50 have been recorded. There are zones of coarser sand grains that are very distinct in the outcrop. The basal boundary of these intervals is sharp, and the upper boundary is sharp. The basal parts are bordered by mud and the upper parts are bordered by sandstone with sand with smaller grain sizes. In the section of log 4 at 80 meters and at 82.3 meters there are beds that have inverse grading. The bed at 80 meters has three zones with inverse grading, and the grain size is from medium/coarse up to coarse/very coarse.

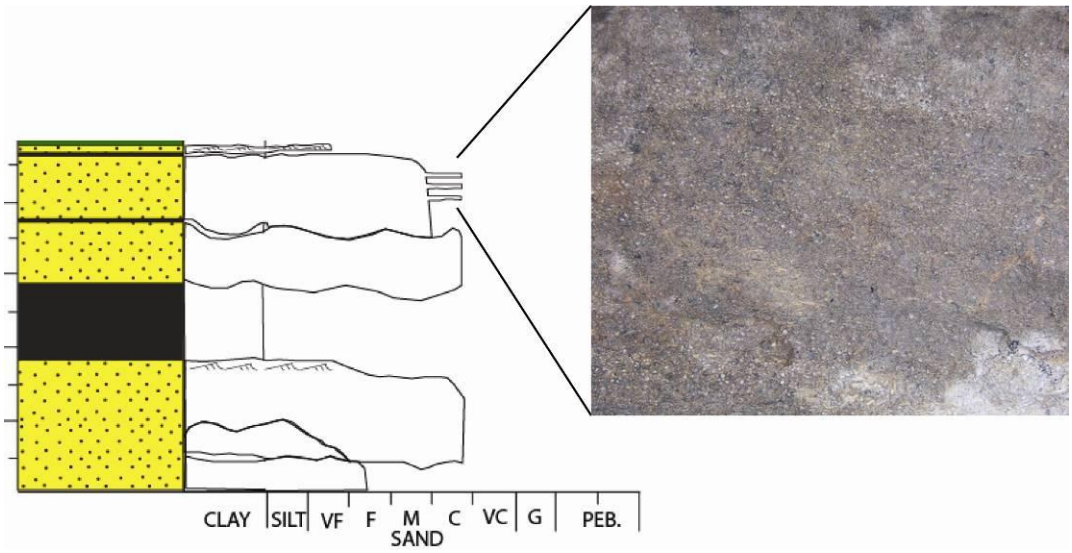

Figure 6.9: Inverse grading at 80.5 metres in log 4.

Interpretation

In the inversely graded beds the grain size is increasing from base of the sandstone and upwards. This type of sandstone is a product of inertia flow with medium sand or coarser particles are present (Sanders, 1965).

The sandstone bed at 80 meters in log 4 is interpreted as a traction carpet, as defined and described by Lowe (1982) as his S_2 interval. This interval has been deposited by grain to grain collisions, through the process called the dispersive pressure (Bagnold, 1956), or by kinetic sieving. Compared with Bouma´s classification, it would be classified as Bouma T_a and deposited in the upper flow regime.

D: Conglomerate

Collinson and Thompson (1989) suggested that intervals with 30 % clasts that are larger than two millimetres should be regarded as conglomerates and this definition is applied here.

The conglomerates are divided into two categories based on the type of mechanical support of large particles that the beds have. In clast-supported conglomerates the clasts are larger than two millimetres (gravel) and they are in contact with each other, and are referred to as clast-supported conglomerates. The matrix-supported conglomerates (D1) have a matrix that can consist of mud, silt or sand, where the clasts are not in contact with each other (Collinson and Thompson, 1989). The clast-supported conglomerates are not seen in any of the logged sections, and they are only logged in the river locality and the Charo locality.

D1: Conglomerate – Matrix-supported

Description

All the conglomerates have a matrix that is either mud or sand, where the mud is the most common. These beds have a total thickness of about 24 metres, and the range of the different depositional intervals is from 5 centimetres up to 6.6 metres. They are highly widespread in

the Charo locality, in the northern most logged turbidite successions. These conglomerates have clasts of sub-rounded to well rounded sandstones, and sandstones with intra-clasts of mud, quartz, *nummulites* and oyster fragments that have grain sizes from granules up to boulders. Both the upper and lower boundaries of the depositional intervals are erosive and sharp of different degrees.

The beds are monomictic, oligomictic, to polymictic, where the main clasts in the oligomictic beds are sandstone clasts that are yellowish and with intra-clasts off mud, nummulites and oyster fragments. Many of the boulder sized clasts show sedimentary structures like parallel lamination, and have a sub-rounded blocky appearance. *Nummulites* and oyster fragments are very common in the conglomerates, and well rounded quartz grains that are from granual up to pebble size, are the least recorded clasts. Within these beds there are made 38 palaeocurrent measurements parallel to the a-axis of the clasts shown in appendix 2, which gives a mean value of the direction of the flows to be WSW-ENE. In two of the beds in the Charo conglomerates imbrication of type a(p) b(i) occurs (figure 6.10). These beds are inverse graded and inverse- to normal graded beds (Nemec and Steel, 1984).

Conglomerates logged in the river section have a quiet different appearance than the conglomerates in the Charo locality. These intervals are much thinner (from 5 – 50 centimetres) and have a sandy matrix. The clasts in the beds are mainly *nummulites*, oyster fragments, and mud clasts. The mud clasts have grain sizes from 0.5 centimetres up to 5 centimetres. They have also erosive upper and lower boundaries like the Charo intervals. The matrix of these intervals is from coarse silt up to medium/coarse sand.

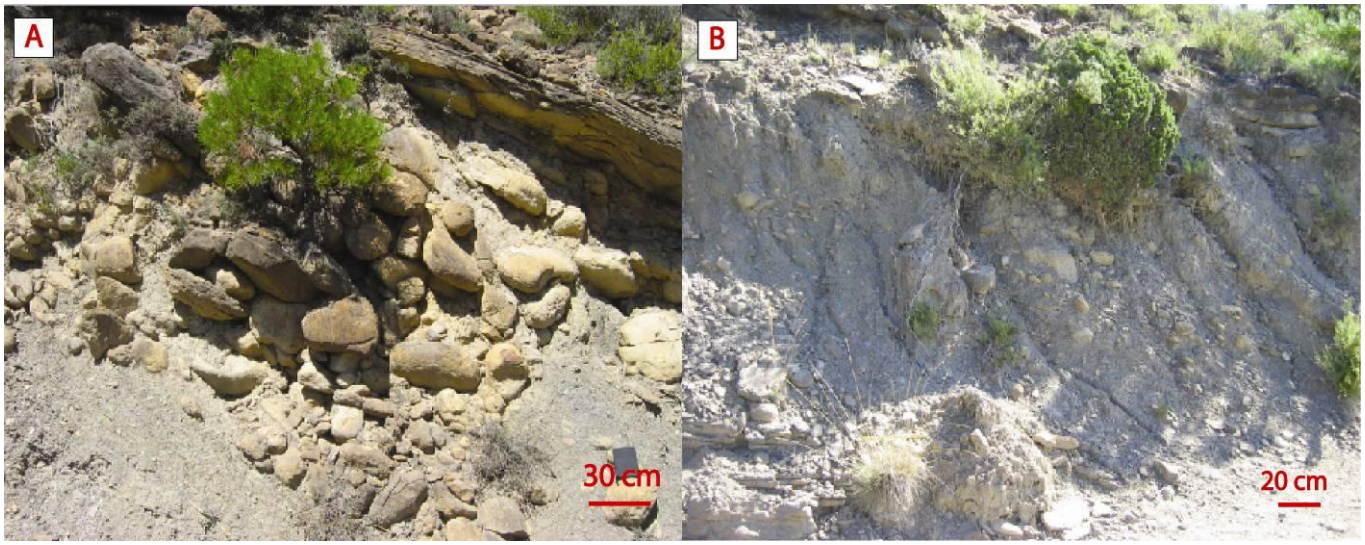

Figure 6.10: Matrix supported conglomerates at locality 1 in log 12. A) Inversley graded conglomerate with pebble to cobble sized clasts. B) Inverse to normal graded conglomerate.

Interpretation

Existence of schemes for conglomerates that can tell anything about the flow condition based on bedforms and grain size does not exist. The deposits can be associated with bed load transport or sediment gravity flows.

The Charo conglomerates are inferred to have been deposited from cohesive debris flows (Nemec and Steel, 1984). The clasts are mainly intra-basinal clasts, where the sandstone with *nummulites*, oyster fragments and mud clasts looks like beds logged further stratigraphically below. Some of the sandstone fragments may have originated from the platform, and also the abraided oyster fragments and the *nummulites* are indicative of shallow marine environment (foreshore/lower shoreface). The quartz grains are probably extra-basinal clasts from the hinterland. The D1 intervals by the river section are deposited by grain flows (Shanmugam, 2006).

E: Chaotic deposits

The E facies are divided into E1 (Sedimentary breccia) and E2 (chaotic mudstone and sandstone). These deposits have been deposited by slumping and cohesive debris flows. The intervals have a chaotic appearance in the outcrop, or structureless mudstone with "mudballs" and have isolated and uncommonly imbricated clasts. This facies is found log1, log 3, log4 and log 15 at locality 2 and locality 3. It consists of approximately 24% of the total facies in all the logs.

E1: Sedimentary Breccia

Description

Breccias are consisting of angular fragments, while conglomerates usually have more spherical clasts. This simple definition is her applied to differentiate between conglomerate and breccia. The breccia is a part of a mass transport complex at 93 metres to 119 metres in log1.

The sedimentary breccia is found in locality 2, by the river Rio Nata, at 105 meters in the section of log 1 (see chapter 7, figure 7.6). It is 1.5 – 2.4 meters thick and approximatly 60 meters in length. The internal bed configuration is of alternating mudstone and sandstone with wrinkle marks on top of the sandstone intervals. In the basal part of the breccia there are horizontal semi-relief bioturbation traces of the icnogenrea *Planolites* and *Thalassinoides*, which is up to about 1 centimetre in diameter. The wrinkle marks and bioturbation traces give indication that the breccia is lying "right-way up".

Interpretation

The breccia represents a slumped sheet from the shelf, with the wrinkle marks as evidence of this. Wrinkle marks are supposed structures made by microbial activity in shallow marine environments. The sub-environment has to be a harsh environment for other animals to live

on the sediments and destroy these structures (Hagadom and Bottjer, 1997). The environment is probably a platform ramp, with dysoxic or oxygenated conditions, which the *Thalassinoides* and the *Planolites* are evidence of.

During sliding, the sheet have not been flipped up side down or broken into small pieces. This may indicate a smooth sliding surface, with small topographic variations. In addition, there is a possibility that the sheet also had a basal water layer pressed underneath it (hydroplaning). Hydrodynamically the basal water layer may be a shearing basal layer (Mohrig et al., 1998) with a velocity gradient, and the sheet regarded as "the ridged plug" (see chapter 4) that has no internal deformation (Ilstad et al., 2004).

The triggering mechanism is probably due to liquefaction by an earthquake (Gee et al., 2005).

E2: Chaotic mudstone and sandstone

Description

There are 14 mudstone beds with distinct "mud-ball structures", folded silty layers, and clasts that range in grain size from granules up to cobbles. These intervals are from 1.5 metres up to 22 metres in thickness. The clasts are sandstone clasts, sometimes with intraclasts, bioclastic limestone clasts, with a lot of *nummulites*, mudstone clast with oyster fragments and *nummulites*, oyster fragments, and *nummulites* separately. The "mud-ball structures are laminated with dark grey to grey laminae and lighter shades of grey. This reflects probably a grain size difference between the different laminae (Collinson and Thompson, 1989). Some of the mud-balls have internal laminated or stratified zones that are reddish in colour. Morphologically they have an oval or elongated appearance in the outcrops, and with the longest axis, in a two-dimensional aspect, nearly parallel to bedding. No accurate measurement is made of the "mud-balls", but they range in size from about 5 centimetres to more than 1 metre in diameter (figure 6.9).

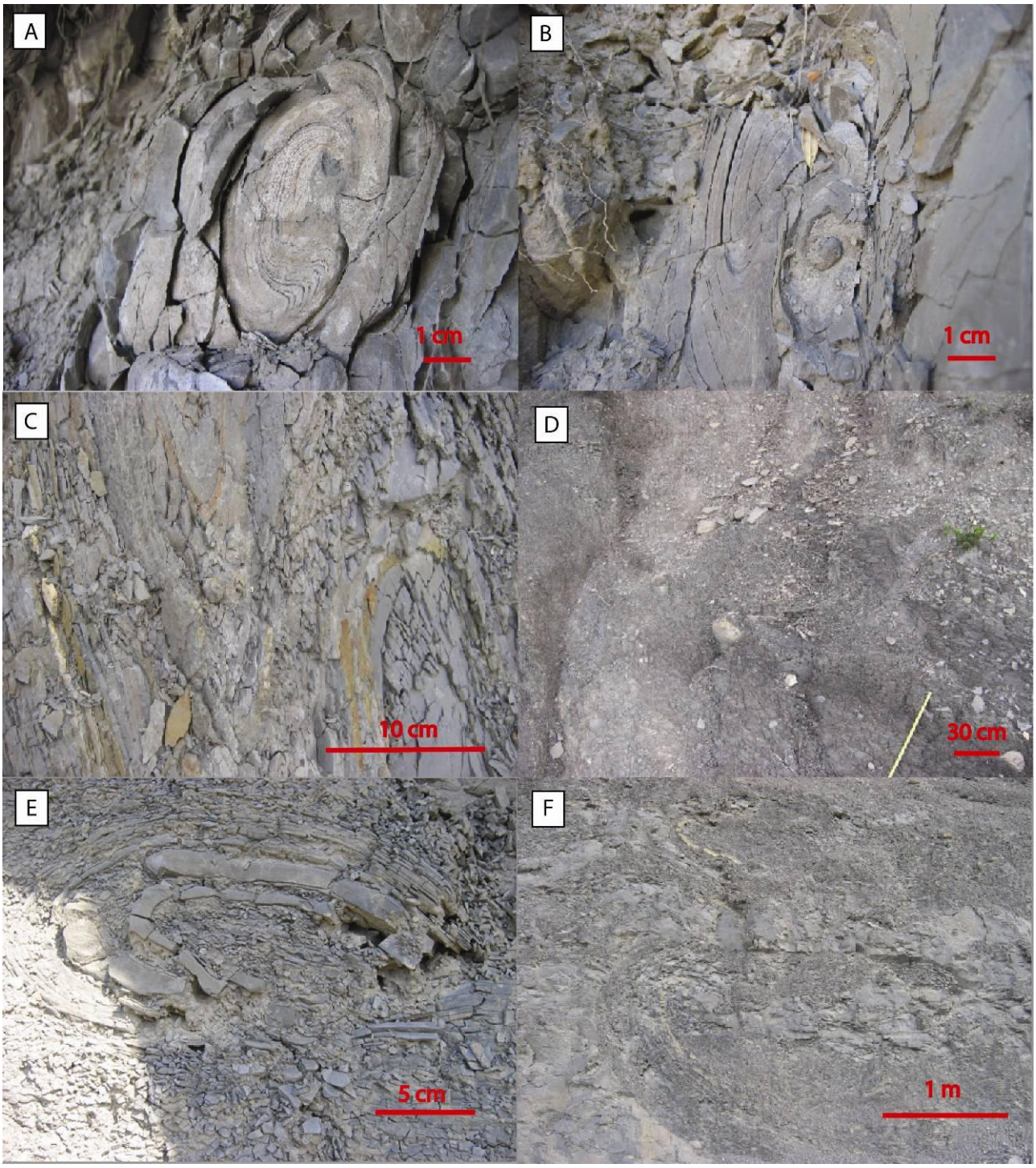

Figure 6.11: Different varieties of mud-ball structures observed in locality2 and locality3. A), B), and C) are mud-ball

Other types of slump structures like micro-folding, folded silt/very fine sand beds and a structure resembling kink folding are seen in the outcrop in locality 2 (figure 6.10A). In locality 3 there is an interval of 21.1 metres in log 15 with a matrix of very fine/fine in grain size. This interval have slumped mud-ball clast (figure 6.12) as intraclasts together with *nummulites*, oyster fragments and rounded quartz grains of granule size. There are also some bioclastic sandstone clasts and sandstone clasts, which are from pebbles to cobbles in size and are rounded to well-rounded.

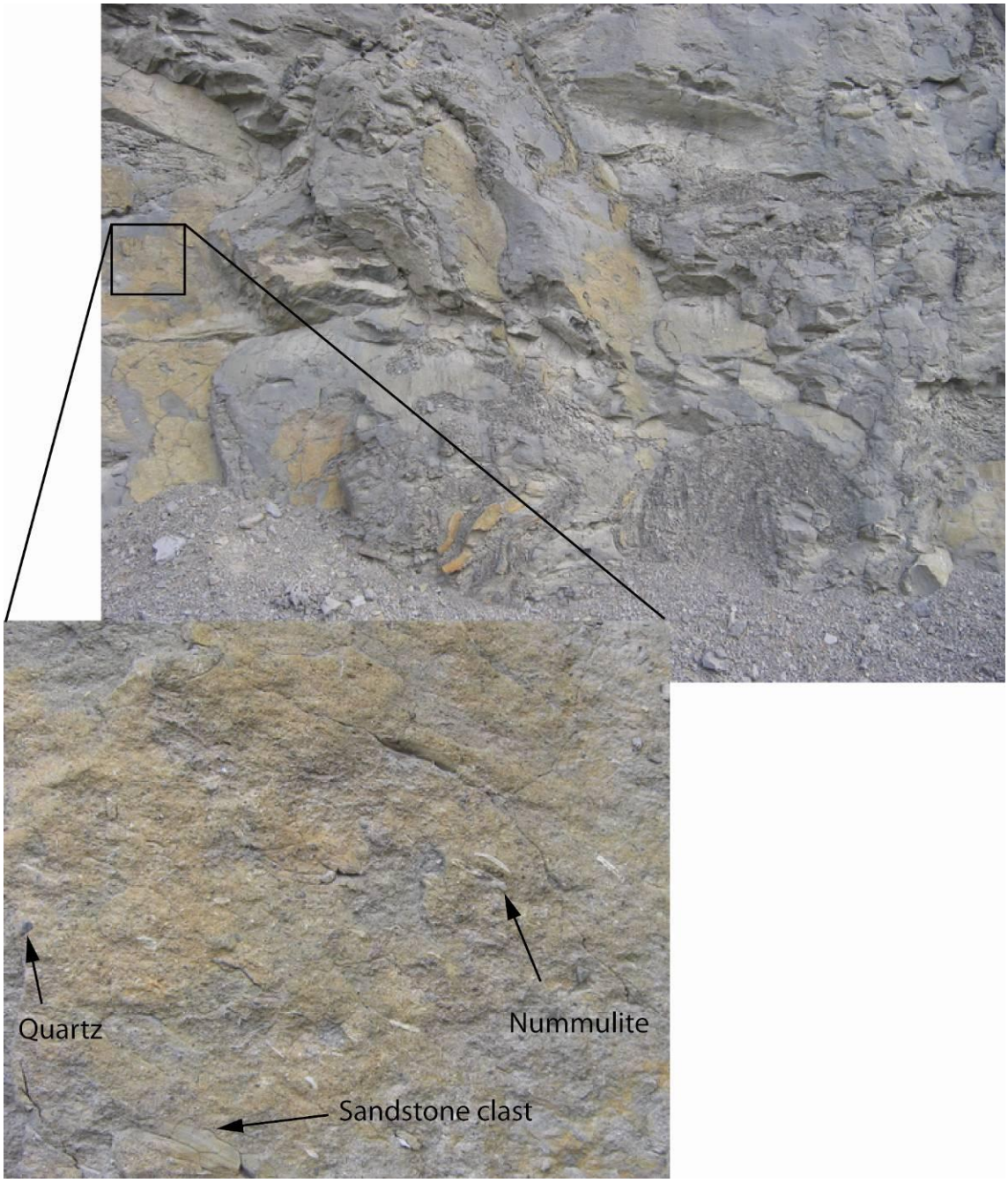

Figure 6.12: A chaotic bed between 69 metres and 90 metres in log 16. See text for details.

Interpretation

The “mud-ball structures” and the folded layers are most likely deformed levee in a channel-levee complex. These silty dominated layers are rolling and sliding along the sides of the turbidite channel. The levees are known to be unstable sediment that is confining the sub aqueous channels. The sliding of sediment down the sides of the channel may be triggered by an earthquake (Pickering et al., 1989) and a debris flow may have reached the valley slope and formed the levees into mud-balls. This can further be evidenced by the presence of clasts in these beds.

The mud-ball structures were for the first time described in detail by Kuenen (1948) in a Carboniferous outcrop in southern Wales. He interpreted these structures to be a product of slumping in a shallow marine environment. Figure 6.11 is presenting various types of mud-ball structures logged at locality 2 and locality 3. The different coloured laminations or stratifications in the mud balls are due to sediment with different grain sizes, and the reddish layers are due to oxidation of iron.

The elongated parallel, or sub-parallel, to bedding configuration of these structures may be a post-depositional feature due to loading during burial or syn-depositional. The most reasonable answer would be that it is a post depositional feature with σ_1 perpendicular to bedding and that the structures give information of how much the intervals have been compacted due to burial.

Bouma (1962) did not classify these types of deposits in his sedimentological study of “flysch” deposits, but this lithofacies can be compared with Mutti and Lucchi (1975) facies F.

7 Facies associations

7.1 Introduction

The facies are grouped into 6 facies associations, where the facies are genetically related based on the depositional processes and their spatial relation (proximal, medial or distal): FA1.1 (Basin slope), FA2.1 (Sub-marine canyon floor), FA3.1 (Turbidite channel), FA4.1 (Channel-levee), FA5.1 (Chaotic mass complex), and FA7.1 (Debris flow) seen in table 7.1. These relationships will be used to interpret the depositional environment in chapter 8.

Code		Facies Associations	Facies	Characteristics
FA 1	FA 1.1	Basin slope - thin bedded turbidites	A1, A2, B1, C3, C5, C7	Sheet sandstones
FA 2	FA 2.1	Sub-marine canyon floor - inter-channel and channel margin deposits	A1, A2, B1 C1, C2, C3, C4, C5, C5, C7	Fining upward and coarsening upward units
FA 3	FA 3.1	Turbidite channel	C6	Fining upward unit
FA 4	FA 4.1	Channel-levee	A1, B1, E2	Slide and slump deposits Cohesive debris flow deposits
FA 5	FA 5.1	Chaotic mass complex	A1, D1, E1, E2	Slump and debris flow deposits
FA 6	FA 6.1	Debris flow	D1	Cohesive and non-cohesive debris flow deposits

Table 7.1: facies grouped into 6 genetically related facies associations (architectural elements).

Log1 to log4 in locality 2 have recorded all the 6 facies associations from basin slope deposits to chaotic mass complex or mass transport complex (MTC_1) from Moscardelli and Wood (2008), with valley plain, channel-levee, and turbidite channel sequentially above each other. These logs comprise all the facies associations and have the main focus in this study, where log4 is giving a proximal to distal channel-levee trend upwards from the FA3.1 at 36 metres in the log. From locality1 to locality 3 the aspect ratio is decreasing, if the uppermost unit in locality3 is not taken into consideration. This unit represents an onset of a new sedimentation cycle and lateral shift of the channel-levee complex.

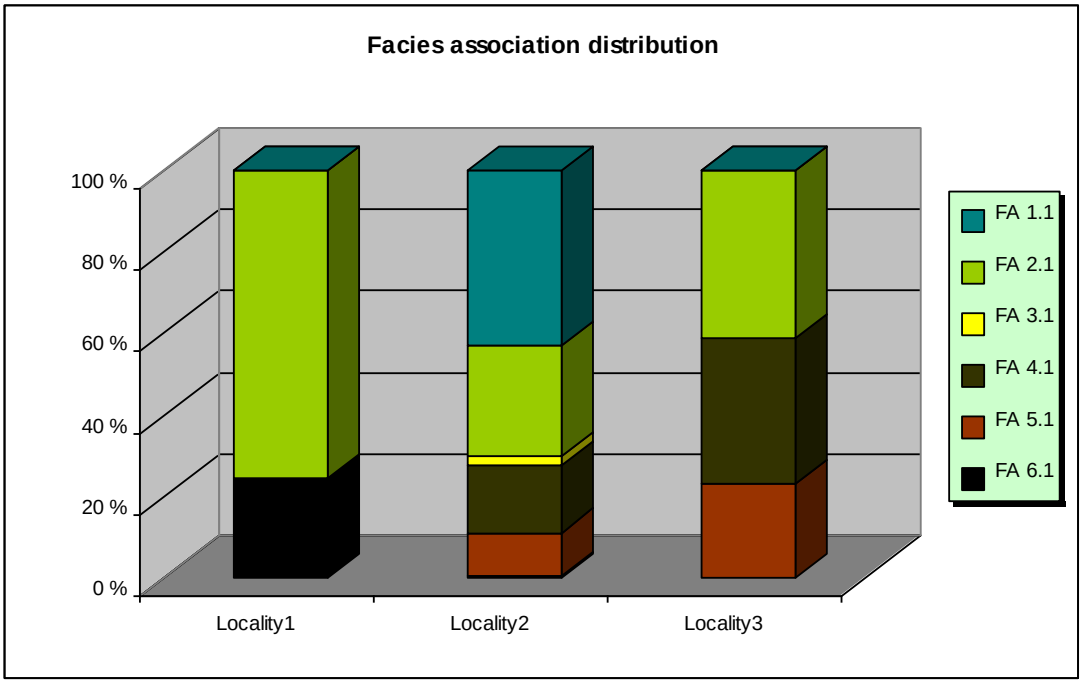

Figure 7.1: representing the percentage facies association distribution in the 3 localities visited. Locality1: FA2.1 (75.4%), and FA7.1 (24.6%). Locality2: FA1.1 (43%), FA2.1 (27%), FA3.1 (2.3%), FA4.1 (17.5%), FA5.1 (10,7%), and FA7.1 (0.5%). Locality3: FA2.1 (41.2%), FA4.1 (35.6%), and

The FA 7.1 units are found episodically in between the FA 2.1 units as high density turbidity current deposits by flow stripping. The facies associations are second order cycles that are part of a hierarchy of cycles defined by Mutti and Normark (1987) as depositional cycles controlled by tectonics or sea-level variations, which is either fining upwards or coarsening upwards (Pickering et al., 1989). The fining upwards units are commonly regarded as channel fill (Mutti and Lucchi, 1975) and the coarsening upwards units as progradational lobes (Mutti,

1977). FA2.1 and FA4.1 are related to each other as overbank deposits in a channel levee system, as described by Walker (1992). These channel-levee systems are formed during a highstand period according to Mutti (1985). During this period there have been fluctuations of the relative sea-level interpreted by fining upward and coarsening upward units of the FA2.1. The facies association distributions from the 3 localities are found in figure 7.1.

Log1 – log4 represents the vertical succession of the Arro sandstonebody (Mutti, 1985), which is overall reflecting a low aspect ratio (net/gross ratio) in the lower part and the upper part of the outcrop, with a higher ratio in between. The Montanana Group is interpreted to contain channel-levee systems by Mutti (1985). One of these systems is recorded (Arro system) in the logs based by the intra-Castissent correlative unconformity (log1 at 93 metres) and the upper boundary in log 15 at 69 metres (base of Santa Liestra Group). A general trend in aspect ratio in mud/sand-dominated systems is decreasing upwards (Richards and Bowman, 1998).

7.2 FA 1: Facies association 1: Basin slope – thin bedded turbidites

Description

The FA1.1 is recorded in log1 and in log5 and comprises 28% of the overall facies associations. The facies present in this facies associations are facies A1 (structureless mudstone), A2 (laminated mudstone), B1 (coarse siltstone), C3 (parallel-laminated sandstone), C5 (structureless sandstone), and C7 (inversely graded sandstone), where A1 is the most abundant facies. Log1 has 14 coarsening upwards units, and 4 finding upwards units. The fining upwards units show more or less the same thickness trends, where the beds are of quiet the same thicknesses. The units are from 1 metre in thickness up to 13 metres in thickness, and the grain size is commonly very fine or fine grained sand, sometimes recorded with tractional structures. Log5 has 3 coarsening upwards units and 1 finding upwards unit. Log1 comprises 2 facies associations. At about 93 metres the FA1.1 is abruptly overlain by

FA5.1 and at 119 metres the FA1.1 is overlaying the FA5.1. The FA1.1 distribution of log1 counts for 79.8% of the total facies associations in the log. In log5 the FA1.1 distribution is covering 100% of the log.

Interpretation

The coarsening upwards and thickening upwards units in log1 are interpreted to be depositional lobes deposited as sand sheets (Shanmugam and Moiola, 1988) on the basin slope. Mutti and Lucchi (1975) referred to these types of deposits as fan fringe facies association. Pickering et al. (1989) gave explanation for fining and thinning upwards units as sea level rise. These sea level rise events are slower events than sea level falls, which are more rapid and erosive. The FA5.1 unit in between the FA1.1 units in log 1 may be an indication of highstand sea level (Pickering et al., 1989).

7.3 FA 2: Facies association 2: Sub-marine canyon floor – low density turbidites and occasionally high density turbidites

Description

This facies association is recorded in all the outcrops and is the most common facies association, comprising 36% of the total facies associations. FA2 consists of 11 different facies; A1 (structureless mudstone), A2 (laminated mudstone), B1 (coarse siltstone), C1 (ripple cross-laminated sandstone), C2 (cross-stratified sandstone), C3 (plane parallel-lamination), C4 (plane parallel-stratified sandstone), C5 (structureless sandstone), C6 (normal graded sandstone), C7 (inversely graded sandstone), and D1 (matrix-supported conglomerate).

The beds in this facies association have generally tractional structures and scour marks as flute marks that are very common. Tractional structures like C1 together with C3 or C4 and mud are the most commonly facies seen in the outcrops. Amalgamated beds are frequently recorded from the outcrops, where the contact zone between the individual beds has either mudclasts or a C1 interval overlain by a C3, C4 or C5 interval (figure 7.2). The configuration of this facies association is 15 units in log3 and log4 of alternating beds of sandstone and mudstone that are both fining and thinning upward and coarsening and thickening upward, most frequently boarded by FA4.1 and one by FA3.1 and FA7.1. The fining and thinning upward trends and coarsening and thickening upward trends, within these units have been described by Mutti and Normark (1987) as a decrease and increase in channel activity, respectively.

Flute marks are frequently observed and soft sediment deformation structures are more rare, but present in both locality1 and locality2. Less frequent are syn-depositional features as syn-faults. These kinds of features are logged in locality 1 in log8 between 18 metres and 24.5 metres. Cut and fill deposits are commonly recorded and logged in all 3 localities. Sand beds of FA2.1 are commonly pinching out in one or more directions (figure 7.3). The palaeo-current directions of the flute marks are seen appendix I.

Figure 7.2: Three amalgamated beds with internal structures given by different notations (C1, C3, and C5), respectively.

Interpretation

This facies association comprises sediments that have been spilled over the confined turbidite channel by the process of flow stripping, after Piper and Normark (1983), {Pickering, 1989 #56; Muttti, 1985 #64}. This diverse facies association has grain size variation from silt to granule that reflects the difference in competency of the flow. Where the C5, C6, C7, and D1 facies are present, the flow had a high competency and caused erosion into the canyon floor sediments and dug small channels. These channel sandstones often contain rip-up clasts.

These deposits represents the Bouma $T_{b\text{-}e}$, but $T_{a\text{-}e}$ are also recorded lacking interval C3 (T_d interval) is commonly seen. The complete Bouma sequence is not recorded. This is in accordance with laboratory experiments, where the complete idealised turbidite bed zonation is developed (Shanmugam 2002). The C1 intervals very often occur separately with thicknesses from 1 centimtre up to 5-6 centimetres and are sometimes undulating, with A1 intervals in between. These beds would be deposited by dilute turbidity currents that have spilled over the turbidite channel as sand sheets. The presence of T_a intervals in this environment give evidence of deposition quiet close to the turbidite channel, where the flow was unconfined and may have lost the compentency (Kane et al., 2007), for example by the mechanism of hydraulic jumping (Russell and Arnott, 2003).

The depositional environment for FA2.1 is the channel margin and adjacent basin or canyon floor. In comparison with the sections described Mutti (1977) from the Hecho Group, these deposits would represent his inter-channel and channel margin facies association (Mutti, 1977) displayed in figure 7.3.

Figure 7.3: inter-channel deposits. A) Cut and fill deposits at 32 metres in log3. B) Low density turbidites in log13. C) Amalgamation of beds and pinch-out in log14. D) Amalgamated beds, low density turbidites, high density turbidites, and slump and slide deposits in log4.

The units that are coarsening upwards seem to be associated with intervals that are characteristic of those units described by Mutti (1977) as channel margin deposits. He described these units as fining upwards. From log3 (between 0.25-3.3 metres) and log7 (between 18-24.5 metres) that are clearly showing coarsening upwards trends. The units may be related to fluctuation sea-level variations (Fernandez-Salas et al., 2003).

The cut and fill deposits recorded in the logged localities have probably formed by erosion of later gravity flows eroding the earlier gravity flow deposits in an unconfined canyon floor setting, due to secondary failure of the channel-levees and subsequently a mounded topography (Galloway, 1998). These scars would by filled in by later gravity flow deposits and background sedimentation.

7.4 FA 3: Facies association 3: Turbidite channel

Description

FA3.1 is only recorded in log4, where it comprises 2.3% of the overall recorded facies asociations. There is registered one unit of this facies association, with a thickness of 7.25 metres. The FA3 consists of the C6 (normal graded sandstone) facies that is amalgamated. The unit is logged in locality2 and comprises 5 normal graded amalgamated beds that are overall fining upwards. The unit has mudclasts in the basal part and in the uppermost 1.5 metres. The grain size ranges from medium sand in the lower part to fine sand in the upper part. In the base of two of the beds there are observed zones that are packed with *nummulites* and oyster fragments. At approximately 33 metres in log4 there is a sandstone clast on top of the lowermost bed and base of the overlaying bed. FA3.1 is boarded by beds of FA4.1 on its lower boundary and FA7.1 on its upper boundary.

Interpretation

The channel fill deposits logged in the outcrop can be compared with Mutti (1985) type III turbidite system, where the channels are thinner than 10 metres and width narrower than 100 metres.

Channel fill is fining upwards beds due to waning of the gravity flow in the turbidite channel. The channel system is confined by channel-levee margins in a basin slope environment. The different beds represent single mass flow deposits stacked on top of the other. The FA3.1 is

boarded on top by FA5.1, which is a 7.3 meter mud flow unit. This may have led to channel switching (avulsion) of the main turbidite channel, and formation of a new depositional lobe at the distal end of the channel, in the way suggested in the deep-marine fan model by (Walker, 1992). The sandstone clast at 33 metres may be a piece of broken off channel margin deposit that have rafted down into the channel, which has been described by (Clark and Pickering, 1996).

Clark and Pickering (1996) made a model composing 3 phases of channel infill, with a phase I erosive and scouring phase and phase II as a coarse grained infilling of the channel and phase III as the channel abandonment phase. The phase III stage may fill the channel with fine grained sediments as silt and mud or some controlling factor acting on the system, which leads to avulsion or channel abandonment. The latter is the case for the recorded deposits in log4, where the overlying unit is a cohesive debris flow unit of the FA4.1.

7.5 FA 4: Facies association 4: Channel-levee – disorganized silt and sand intervals with clasts in mud

Description

The FA4 is recorded in 13 units and shown in 3 logs from locality2 and locality3. The units have a total thickness of approximately 91 metres. This represents 18.9% of the facies associations of locality2, and 35.6% of the facies associations in locality3. The thicknesses of the units range from 0.95 metres up to 22.3 metres, with a mean thickness of 6 metres. FA4.1 consists of facies A1 (structureless mudstone), B1 (coarse siltstone) and E2 (slump structures in mudstone). The units of this facies association are composed of broken up or discontinuous silty/very fine sand beds, mud-balls, and clasts from granule size up to boulders. These units are most frequently boarded by FA2.1 (figure 7.4), only 2 of the units are boarded by FA5.1 and 1 unit with FA3.1.

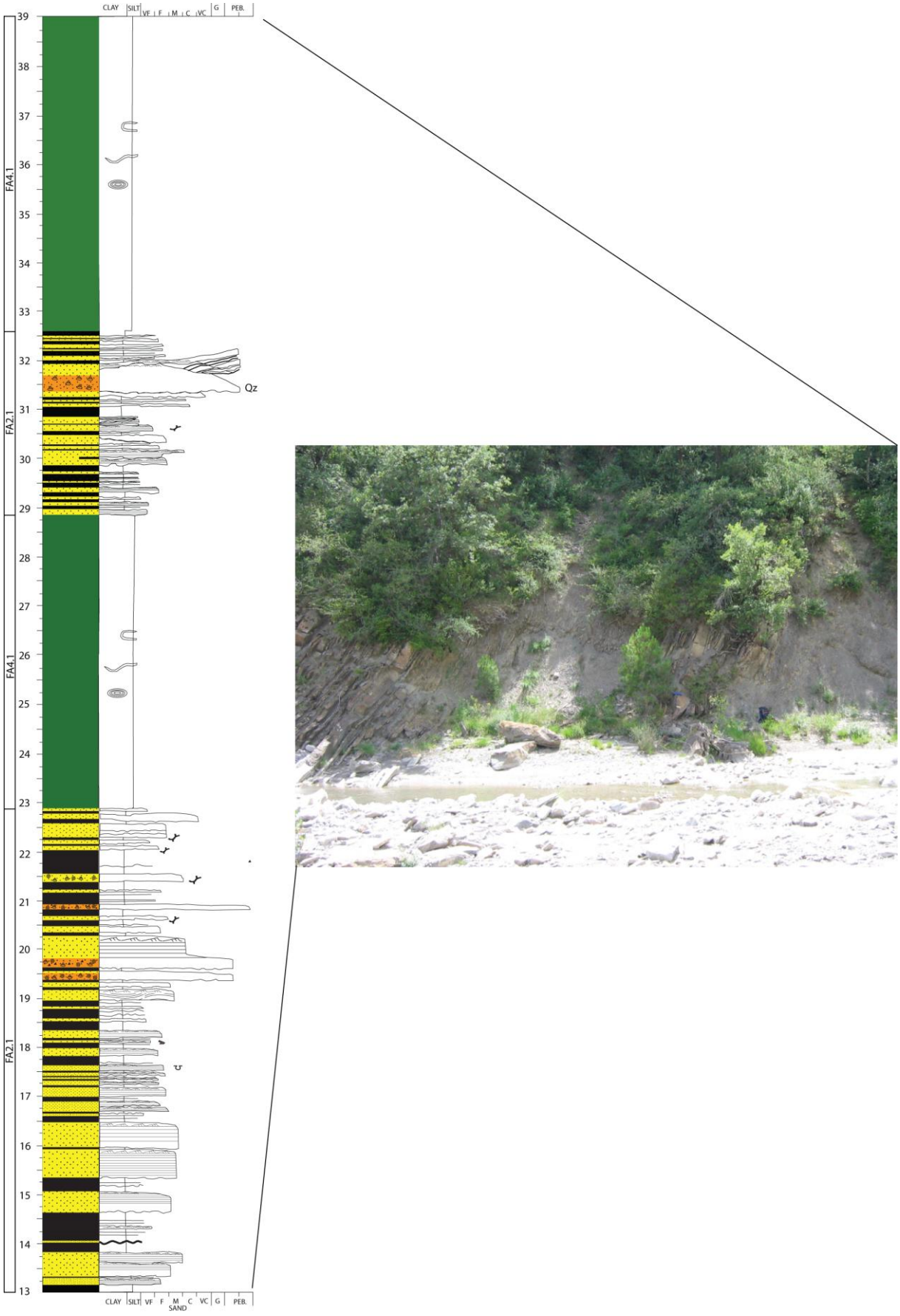

Figure 7.4: facies associations FA2.1 and FA4.1 from log3 by the river *Rio Nata* in locality2.

The overall trend of this facies association is that the units are more frequently recorded in the stratigraphically upper parts of the outcrops in locality 2, and the units become overall thicker upwards.

Interpretation

The FA4.1 units are interpreted as products of slumping and sliding from the turbidite channel levees and cohesive debris flows. The depositional environment is considered the same as that of FA2.1, but the FA4.1 beds have been deposited by other processes than FA2.1. The combination of mud-balls, folded and broken layers together with clasts of various sizes gives evidence for slumping and sliding and debris flows. Seismic activity induced from the thrust system may have triggered the slumping and initiation of debris flows. The slumped levee deposits have been rolling and sliding along the channel slope, and on a later stage been engulfed by debris flows. Galloway (1998) described these deposits as products of secondary failure. The deposits may have been transported down the channel-levees for great distances due to hydroplaning, a processes described by (Mohrig et al., 1998).

The general thickening upward trend of the FA4.1 may be due to a prograding near shore system (Mutti, 1985b) during highstand. The shallow marine and deltaic complex of the Montanana Group sourced the submarine clastic system from the east/southeast and from the north (Nijman, 1998). Log 15 reveals an overall coarsening and thickening trend, which can be related to a prograding system.

7.6 FA 5: Facies association 5: Chaotic mass complex

Description

FA5.1 is logged in locality2 at 93 metres in log1, at 36 metres in log4, and in locality 3 at 69 metres in log 15, which comprises 10.7% of the facies associations in locality2 and 23.1% of the facies associations of locality 3. The unit recorded in log1 is 25.6 metres in thickness consisting of facies A1 (structureless mudstone), D1 (matrix supported conglomerate) and E1

(sedimentary breccia). The unit in log 4 is 7.3 metres thick and contains A1 (structureless mudstone), and the unit in log 15 is 21.3 metres thick and comprises D1 (matrix supported conglomerate). The FA 5.1 unit recorded in log1 has a matrix of mud or very fine sand with slumped blocks with internally folded bedding and lamina, folded and disrupted beds, and clasts ranging in size from granules up to boulders, with cobbles as the main grain size. The clasts are sub-rounded to well-rounded. 12 metres into the chaotic mass complex or mass transport complex (MTC) in log 1 there is a large slump sheet described in chapter 5 having clasts that seems to be pressed under it (figure 7.5). The unit in log 4 would represent a mud flow described by Mulder and Alexander (2001) in chapter 4. The chaotic mass complex seen in log 15 between 69 and 90.2 metres have a sandy matrix with rounded quartz clasts, *nummulites* and pieces of "ripped up" channel-levee deposits.

Figure 7.5: Slump sheet at 105 metres in log1 with wrinkle marks on top of sand beds and clasts that are pressed underneath the sheet.

There is made 5 measurements of the a-axis of clasts in the chaotic mass transport complex in log 1 (appendix II). Some of the clasts, in this unit, contain intra-clasts that have fragments of oysters. The unit is boarded by FA1.1 below and above.

Interpreation

The formation of chaotic mass complexes like the one represented by FA1.1, being composed by slide and slump deposits together with debris flow deposit, can have been triggered by an extreme high energy event like an earth quake, tsunami, or storm activity (Mulder and Cochonat, 1996). The most likely triggering mechanism of the mass complexes are thrusting along the Faradada Fault, which is a left stepping dextral tear fault (Nijman, 1989), or the Mediano Anticline. Mutti et al. (1984) described deposits produced from catastrophic events as seismoturbidites (megaturbidites), which is comparable to these deposits. The problem with classifying these deposits as seismoturbidites is that constrains on the dimensions is needed of the unit {Muttti, 1984 #62}. From the Moscardelli and Wood (2008) classification scheme, these turbidite deposits would be classified as shelf-attached (MTC_1) deposits (MTCs logged in log1 and log15) and slope-attached deposits (MTC_2, log4).

7.7 FA 6: Facies association 6: Debris flow

Description

This facies association is recorded in 3 logs, with units ranging in thickness from 0.1 metres up to 7.7 metres. The units comprises facies D1 (matrix-supported conglomerate), exclusively, and alltogether 4.7% of the overall facies associations. FA 7.1 units are always recorded in conjunction with units of FA2.1 or FA4.1.

The FA 6 units have sandy and muddy matrix, where muddy matrix is the most common. In log 12 there are 2 units of the Arro sequence that show some kind of trend, with normal grading and normal-to-inverse grading (see chapter 6, figure 6.10). Log15 has a unit that is inversely graded. The units logged in locality1 have no general thickening or thinning upwards trends. The non-cohesive debris flows logged in locality2 are pinching out.

There is 1 unit that is 6 meters thick with no observed features recorded in log4 at approximately 53 metres. This unit had fault planes filled with calcite, and the translational displacement of the fault is minimum 4 metre. In addition there may have been some rotational movements; due to some deformed turbidite beds on top of this unit. The beds that were not deformed are logged in log6. More detailed work could be done with this unit.

Interpretation

Subaqueous debris flow deposits can often be distinguished from subariel debris flow deposits by their more organized structures showing grading and imbrication (Nemec and Steel, 1984).

This facies association is related to both non-cohesive and cohesive debris flows (Nemec and Steel, 1984).The non-cohesive debris flows may be interpreted to be high density turbidity currents, where the matrix is sandy and with clasts composing of *nummulites*, oyster fragments, and/or mudclasts dispersed throughout the bed. These deposits represent distal canyon floor deposits in between FA4.1 units. The deposits may be linked to the A1.4 from Pickering et.al. (1989) or be described as deposits from high density turbidity currents by Lowe (1982). The cohesive debris flow deposits are interpreted to be deposited by freezing *en mass* due to decrease in the basin slope gradient (Pickering et al., 1989) and the yield strength of the flow equals the shear strength of the debris flow (Chapter 4). These deposits are similar to the A1.1 of Pickering et al. (1989).

8 Depositional environment

8.1 Introduction

The deposits logged in the Charo and Arro localities represent deep marine turbidite deposits on a submarine ramp. The facies associations are building blocks for interpretation of the environment related to eustatic sea-level changes, tectonics and sediment supply. Some mechanism or combinations of mechanisms triggered instabilities on the ramp and formation of the submarine canyon. This is discussed further below. The canyon funnelled gravity flows from the shallow marine environment into the deep marine environment. These gravity flow deposits have been logged in 3 localities from proximal (locality1) to distal (locality3) part, away from the canyon mouth. The deposits have been transported and deposited by turbidity currents, cohesive and non-cohesive debris flows, slump and slides, which were erosive in nature and scoured into the slope and formed the Charo canyon. The Arro sandstone body (Millington and Clark, 1995) represents the canyon floor fill deposits.

The Arro sandstone body system is fully exposed in locality 2 of the study area (figure 8.4). The sandstone body stretches out from the Charo canyon in the east to north of the Boltaña anticline in the west (Mutti, 1985b). It is considered time equivalent to the Upper Castissent Group (CS2) formed due to initiation of the Mediano anticline (Millington and Clark, 1995). The processes acting in the deep marine realm are discussed in chapter 4.

8.2 Controlling factors

The main control of the depositional environment was controlled by plate tectonics, the convergence of the Iberian and the Eurasian plates in the Late Cretaceous and the subsequent orogenic development of the Pyrenees. During this development the antiformal stacking, the break-back thrusting, and subsequently development of the Mediano and Boltaña anticlines evolved (chapter 3). The change in topographic slope gradients caused by uplift of the axial zone and the resulting erosion may be reflected in the outbuilding of a platform delta, the Montanana delta, that was sourced by a fluvial system, and the axial trending of alluvial fans that prograded southwards (Nijman, 1998). Climatic conditions and subsequently sea-level changes may also have contributed to the depositional control to sedimentation in the deep marine environment (Fernandez-Salas et al., 2003).

The fluvial Castissent sandstones were deposited between 51.7 and 51.3 Ma (Nijman, 1998) (from chronostratigraphic data) during highstand. Nijman proposed that the main control of the depositional system was tectonics that overprinted the effect of sea level highstand. Mutti *et al*. (1988) placed the Castissent sedimentary complex between (time equivalent with the Castissent Formation) 50.5 and 49.5 Ma, where time scale and global unconformities were taken from Haq *et al*. (1987), and with structural control of the unconformities. The FA 5.1 can be compared with Moscardelli and Wood`s (2006) MTC_1 deposit, which is interpreted to represent a shelf-attached system, due to a fluvio-deltaic input, referring to Pickering and Corregidor (2005). The control of the deltaic architectural style would be related to movements along the Faradada fault system and Mediano detachment fold that is seen in the figure from Millington and Clark (1995) (figure 8.5), which is subordinate emplacement of the thrust sheets.

In the Early Eocene there was a peak in global temperature and sea-level due to a higher ocean-crust production and a Late Paleocene – Early Eocene tectonic reorganization. During the last 50 Ma the sea-level has fallen by approximately 70 metres (Miller et al., 2005).

8.3 System classification

Reading and Richards (1994) classified deep-water systems by grain size (mud-rich-, mud/sand-rich-, sand-rich-, and gravel-rich submarine fans) and feeder system (point-source-, multiple-source, and linear-source submarine fans), which resulted in 12 classes of deep-depositional systems. These parameters are used because they are easily identified in the field, in cores, and wireline logs.

The Arro sedimentary system would be classified as a point-source mixed mud/sand system by the Reading and Richards (1994) classification system (Figure 8.1). This system is dominated by channel-levee and down-dip depositional lobes with sandstone contents between 30% and 70%. The Arro system has a sandstone content just above 30% (chapter 6). The Arro deep-marine depositional system is part of the Hecho Group (see chapter 3).

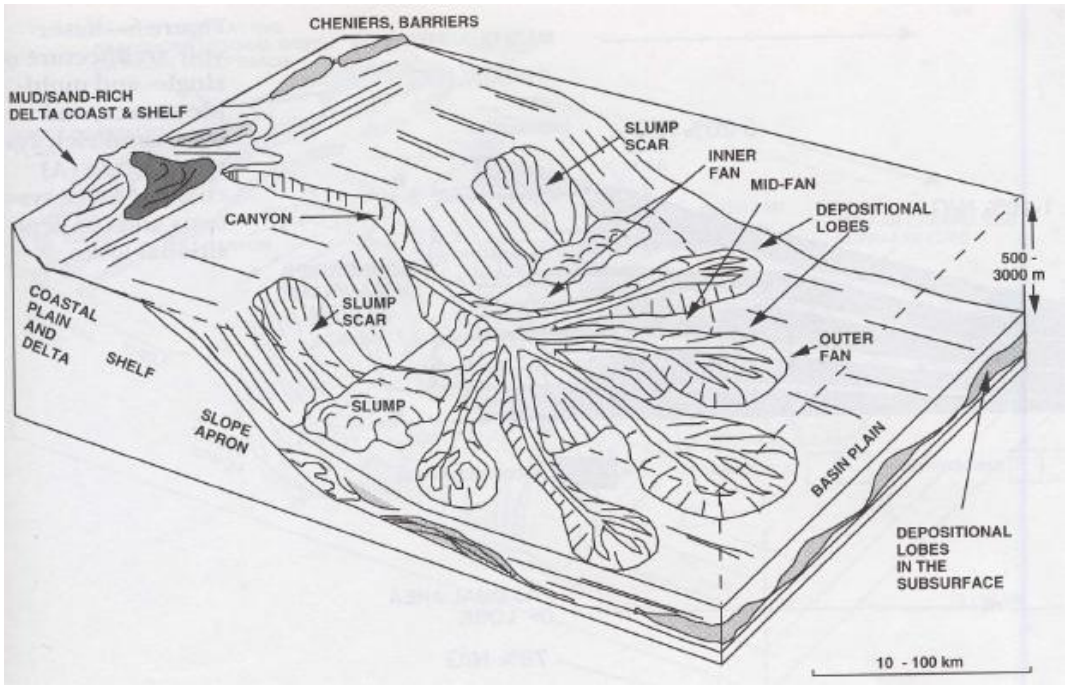

Figure 8.1: A point-source submarine fan system from Reading and Richards (1994). The depositional system is comprising channel- levee in proximal areas and and lobe deposits in the distal areas. The slope mainly consists of sandstone from Bouma (1967) Ta-Te and chaotic deposits.

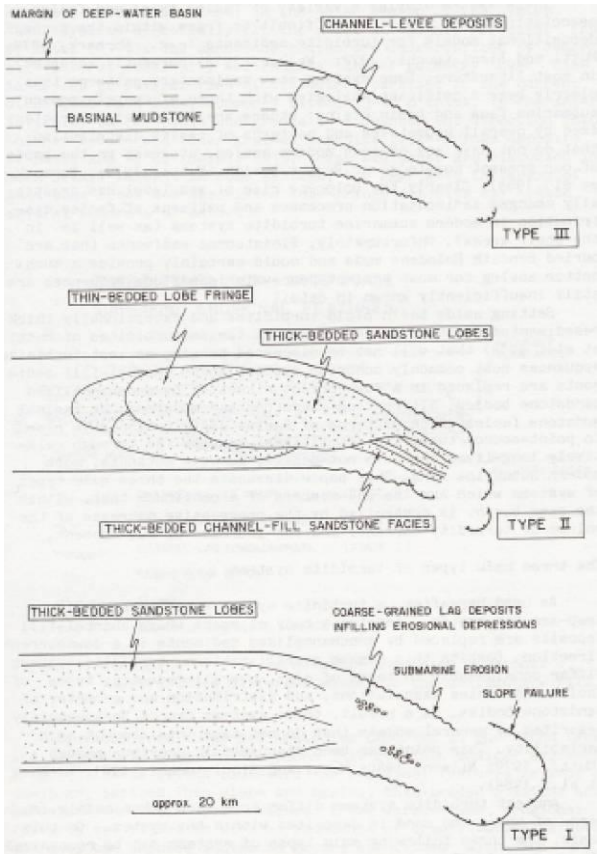

Figure 8.2: Muttis classification system (1985).

Mutti (1985) classified the Hecho Group into 3 types of turbidite depositional systems (type1, type2, and type3) (Figure 8.2). The Arro sandstone body would be perfectly put into this system, with erosion and bypassing of sand and accumulation in lobes further out in the basin (type1) and the overlying inter-channel and turbidite-channel deposits (type 2), with a channel-levee deposition as the main facies association of the last stage (type 3). This system reflects a sea-level cycle from lowstand (type1 and type2) to highstand (type 3) conditions.

Shanmugam and Moiola (1988) classified the Hecho Group as an active margin setting (Pacific type), characterized by comprising elements as large tectonic activity, narrow shelf, short transport of sediment detrius fed by rivers and littoral drift cells, and with high sand/mud ratios. This classification regards the whole deep marine Ainsa Basin, but the Arro system alone would not reflect that classification system.

Mutti and Normark (1987) classified deep-marine turbidite deposits based on size, mobility of the crust, effects of syn-depositional tectonic activity and volume of sediments available in the source areas. This would give rise to 1st, 2nd, 3rd, 4th, and 5th order of sequences (figure 8.3).

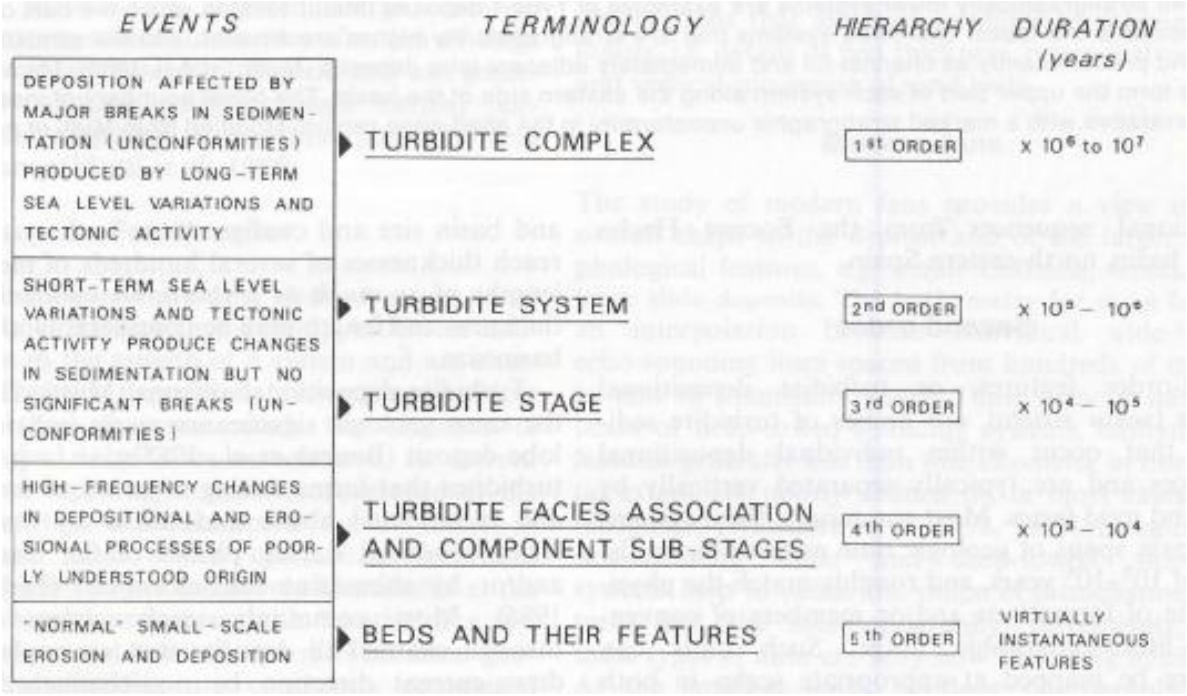

Figure 8.3: Classification scheme form Mutti and Normark (1987).

Mass transport complexes (MTCs) are integrated elements of many deep-water gravity flow deposits and can be applied for classfying these types of sedimentary systems. Moscardelli and Wood (2008) made a classification of MTCs based on seismic data. They divided the MTCs into attached and detached MTCs by using the length/width (L/W) ratio and the volume of the deposits. For detached MTCs the volume is less than 10 km³ and the L/W ratio < 4. The study of Moscardelli and Wood (2008) is based on interpretation of seismic geometries; the weakness in their classification system lays in that the deposits are not visible and available for inspection. In outcrops, constrains on dimensions of depositional units can be directly obtained.

8.4 Depositional style of the eastern part of the Ainsa Basin

Mutti and Normark (1987) put the 5th order events as instantaneous features (cut and fill, graded beds, syn-faulting), the 4th order as high frequency changes in depositional and erosional processes (channel fill and lobe fringe), the 3rd order facies associations together into systems (systems tracts) of 2nd order cycles (Arro sandstone body system), which are influenced by short-term sea-level change and tectonic activity and are separated vertically by highstand mud facies. These deposits were again subordinate the 1st order control of the deep marine turbidite environment, as the turbidite complexes (Figols Group, Montanana Group, Santa Liestra Group, and Campodarbe Group) that gave rise to the unconformities (Figure 3.5B), which were controlled predominantly by tectonism and subordinate long-term sea-level variations (Nijman, 1998).

The Ainsa Basin was initially a deep marine piggy-back basin (see chapter 3), which means that the basin moved and changed configuration over time. The eastern part of the basin was structurally controlled by the Faradada tear fault and the Mediano anticline; a structural control that have made changes in the depositional style due to sediment supply and change of base level over time. The western part of the basin was bounded by the Boltaña anticline that separates the Ainsa and the Jaca basins. These structures were not active at the same time. This is reflected in the stratigraphic architecture with younger turbidite deposits onlapping older turbidite deposits within the deep marine Ainsa Basin (Millington and Clark, 1995; Mutti, 1985b; Mutti, 1985a; Mutti et al., 1988). The deep marine realm is linked to the clastic source area by a shallow marine carbonate platform or ramp. The issue of how the shallow marine deposits were deposited on this platform have been addressed by (Woyessa, 2008), who postulated that the environment of the shallow marine eastern part of the Ainsa Basin was a land-attached carbonate platform environment.

The 1st order control of the depositional style of the eastern part of the basin was controlled by movements of the Mediano detachment fold and the Faradada tear fault system, which gave rise to unconformities (figure 3.5). Mutti *et al*. (1988) recorded 7 unconformities (correlative

unconformities) within the deep marine deposits in the basin. They described the lowermost part of the time equivalent Castissent Group (CS1) as a prograding lowstand complex, but Nijman (1998) disagreed on that due to the sheet sandstones are sandwiched between two of the largest marine onlaps in the area. He interpreted the complex as a prograding highstand complex. His interpretation would reflect the recorded overall progradational nature of the Arro sandstone succession, represented by the lowermost 93 metres in log1 in locality2. The unconformity between the Montanana complex and the Santa Liestra complex may be related to the largest Eocene drop in sea-level (Nijman, 1998). Miller *et al*. (2005) stated a fall in sea-level at this time, as well.

The Charo canyon may have formed when the sediment supply to the platform was low, but with availability of gravity potential and other sources of marine energy (cf. Galloway, (1998)). The initiation of the canyon formation can be related to localized instability on the ramp triggered by movement of the initial movement of the Mediano anticline.

8.4.1 The Arro system

In locality 2 the 2nd order Arro sandstone body is logged from its base to its top. The Arro sandstone can be separated into 4 units (figure 8.4), which is based by a (1) chaotic mass complex (FA 5.1), and overlain by an (2) inter-channel facies associations (FA 6.1, FA 4.1, and FA 2.1) represented in logs 2, 3, 6, and log 4 from base of log and up to 28.75 metres, and from 43.6 metres to 111.15 metres. (3) A FA 3.1 channel system (between 28.75 metres and 36 metres in log 4) is overlaying the lowermost inter-channel units. The FA 3.1 unit is overlain by a mud flow unit (FA 5.1), which may have been triggered by a catastrophic event like a storm or an earthquake on the upper slope. Stratigraphically above the mud flow unit, (4) channel-levee (FA 4.1) units are more frequently recorded than in the lower part, with thin units of FA 2.1 in between (figure 8.4), seen in log 4. Mass transport complexes, as the mud flow unit, have been recorded to destroy or modified channel systems from other areas during highstand (Wynn et al., 2007).

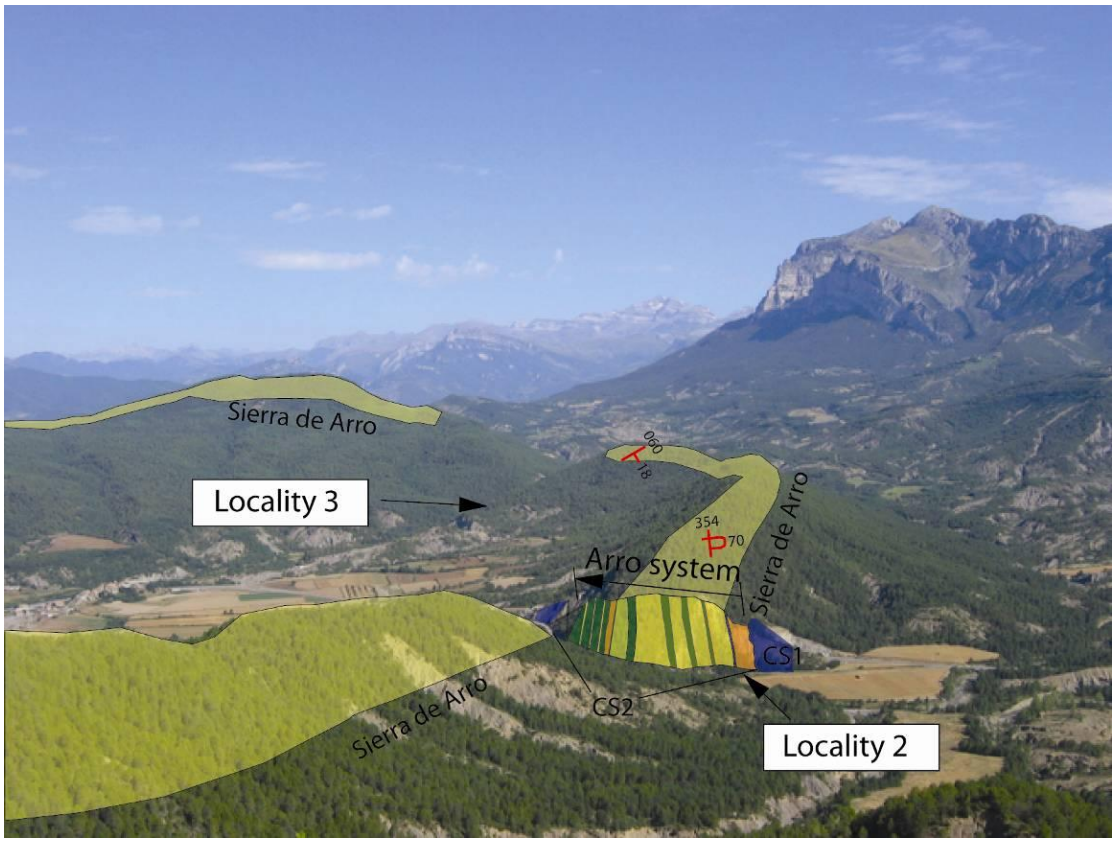

Figure 8.4: The Arro sandstone body viewed towards northwest. The colours in the Nata River gorge are representing the different facies associations of the Arro system. Blue clour is FA 1.1, organge is FA 5.1 and FA 6.1, green colour is FA 4.1, yellow is FA 2.1, and the light yellow colour is FA 3.1 (see chapter 7 for more details). The drawing is not to scale.

The Arro system would be described as a destructional slope system in the classification system of Galloway (1998). These systems are based by a slump/slide plane, canyon-cut erosion surface, or compound mass-wasting surface. The middle part of a succession would contain debris flows and turbidites, generated by secondary failure and erosion. These deposits would be ponded between the irregular blocks, mounds and tongues of slide and slump debris (FA 4.1 or FA 5.1) (cf. Galloway, 1998).

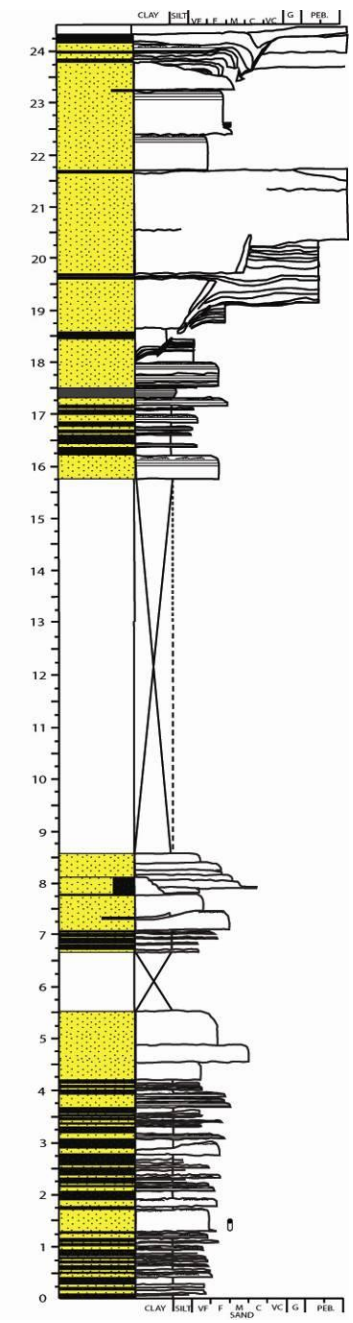

Figure 8.5: Log 7 in locality 1

Millington and Clark (1995) made a model (figure 8.6) of the sedimentary environment that is covering the locality1 and the locality 2. They placed the Charo canyon mouth between the Faradada tear fault and the Mediano anticline, which resulted in a hydraulic jump at the canyon mouth due to slope angel variations. Heiniö and Davies (2007) did studies on fold growth and subsequent knickpoint migration in submarine channels in western Niger Delta. They proposed that this process play a significant role in controlling the depositional style of the Niger delta channel-levee complexes. The uplift of an anticline across a channel make the local gradient lower on the upstream side of the fold axis, where the thalweg is back cutting into earlier deposited sediments. On the downstream side of the fold axis the gradient is increasing due to the fold growth. The diagram proposed by Millington and Clark (1995) may fit the study done by Heiniö and Davies (2007) and the data collected for this study at locality 1. The beds are frequently amalgamated, thinning and thickening laterally, cut and fill features are observed and syn-depositional features are common in the southern part of the locality 1 (figure 8.5). The cut and fill deposits are also logged in locality 2 and 3, but here they may be related to change in path for the gravity flows due to slumping and sliding on the canyon floor. This will deflect the gravity flows and erode the older deposits.

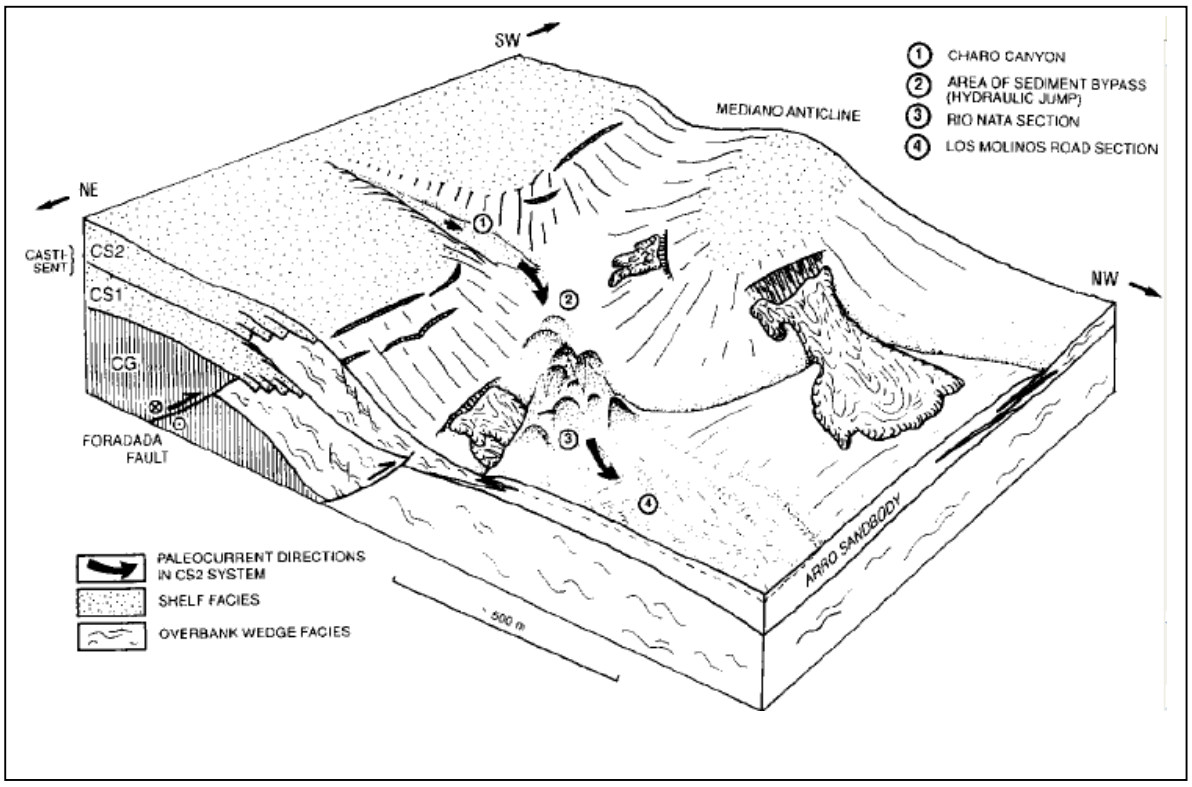

Figure 8.6: A modell from Millington and Clark (1995) of the Arro system.

The locality3 deposits represent distal facies association of FA 2.1 and FA 4.1 and a chaotic mass complex (FA 5.1) as the uppermost unit. The FA 2.1 deposits comprise 4th order fining upward inter-channel units in the basal 28.8 metres of the succession that grade into a more channel-levee (FA 4.1) dominated part from 28.8 metres to 69 metres. The basal 69 metres of log 15 may be related to log 4, genetically. The uppermost unit (69-90 metres) is interpreted to be a chaotic mass complex (FA 5.1) and the basal part of the overlying Santa Liestra complex (Banastõn system).

The successions in upper part of the locality 2 logs have a lower aspect ratio (see chapter 6) compared to the lower part, and predominantly comprise thick units of FA 4.1 with occasionally FA 2.1 units and FA 6.1 units in between. Sample RF4 contains detrial glauconite from a Ta interval at about 89.5 metres in log4. Detrial glauconite was also

observed in the chaotic mass complex at 69 metres in log 15 (sample RF12). These beds would have been deposited penecontemporaneously.

A candidate type 2 sequence boundary may separate the Lower Castissent Group from the Upper Castissent FA 5.1 in log1. A likely cause of a sequence boundary at this position is thought to be initiation of the thrusting of the Cotiella nappe and subsequent movement of the Mediano detachment fold and incision of the ramp to create the Charo canyon (Mutti et al., 1988). The canyon is most likely formed by back-cutting of the platform. The basal fill of the time equivalent Upper Castissent Group is described as a mass transport complex, which can be compared with Pickering and Corregidor (2005) MTC I, with a slumped sheet of shelfal origin. The large slumped sheet block (log 1) has travelled at least 2 km before it ceased to stop. The flow may have been a Bingham flow (Elverhøi et al., 1997) or plug flow, where the basal shear of the flow is within the water that was pressed underneath the sheet (see chapter 4) and caused hydroplaning down the slope (cf. Mohrig, 1998). Elverhøi *et al*. (1997) have recorded Bingham flows with mid-slope gradients of 0.5 degrees to flow up to 200 kilometres.

The locality1 logs show a proximal to distal channel trend laterally from south towards north. The southernmost logs (log7-log9) recorded represent the proximal deposits with syn-depositional features and with some vertical and horizontal bioturbation. The FA 6.1 units are mostly mud dominated without shear features, and clasts are commonly found in different zones. The a(p)b(i) data (appendix II) indicate a more east-west trend, which is different from the northwest direction of the flute marks. The clasts in the FA 6.1 units indicate a shallow marine origin, with intra-clasts of oyster fragments, *nummulites*, and they are sub-rounded to well-rounded clasts that have the same features as the clasts observed in locality 2 and locality 3, in general. These clasts have been reworked by river currents and/or shallow marine processes. The palaeo-canyon funnelled the gravity flows from the San Esteban fandelta (Nijman, 1998) that was prograding southwards forced tectonically the fandelta/fluvial system further southwards (Nijman, 1998), and sourced the canyon with muddy debris flows consisting of grains from pebbles to boulders in size. The debris flows are more muddy stratigraphically upward in log11 and less and smaller clasts. The triggering of these FA 6.1

units may be due to outbuilding of the delta from the southeast and the fandelta from the north, or tectonics related to movement along the Faradada tear fault system or movement of the Mediano anticline. The FA 6.1 units, only recorded in the northern part of locality1, may have settled not far from the canyon wall due to change in gradient from the steep wall to the canyon floor. The lithology of the clasts in these units has the same appearance as the clasts seen in locality 2 and 3 in the FA 4.1 and FA 5.1 units, which indicate the same source area.

Millington and Clark (1995) claimed that the northern part of locality 1 (logs 10-14) is bounded by an unconformity, which corresponds to the unconformity between the upper Castissent Group and the overlying Santa Liestra complex (Mutti et al., 1988). The clasts in the conglomerates in this locality have the same features as the conglomerates recorded in locality2 and locality 3. Travé *et al*. (1998) documented thrusting in the locality 1 area, where splay thrusts from the Cotiella thrust (see figure 3.6) are recorded in the studied area. One of these thrusts (Samper thrust) may be related to the unconformity recorded by Mutti *et al*. (1988).

The FA 2.1 unit between 62.5 metres and 69 metres has a cut and fill and shallow marine and fluvial imprints (See chapter 6 page 8 and chapter 7 page 5). Confined tectonically active basins tend to be shaped by basin topography and syndepositional tectonic movement (Reading and Richards, 1994). The topography in the basin would deflect turbidity currents around MTC deposits and channel-levee deposits, which would be acting as mounds in the gully environment. This may indicate that the deep marine slope system of the basin was connected to the Montanana delta at this time, which has prograded to the canyon entrance due to high sedimentation rates by gradient change in the hinterland or/and lowering of the eustatic sea-level.

8.4.2 The channel system of the Arro sandstone body

Galloway (1998) described sediment slope aprons fed from distributary mouths along the front of active delta lobes, with focusing of submarine channels around active mouth bars.

The upper slope and prodelta deposits are subjected to mass wasting or remobilization by storms. This scenario would fit with a feeder canyon that funnelled sediments to the deep marine realm, as for the Arro system (figure 8.7).

The flutecast measurements recorded in all the localities show the same overall palaeo-current direction from the lowermost deposits to the uppermost deposits. The mean direction of the flutecasts is approximately 330° (north-northwest). In locality2 the lowermost inter-channel sandstones indicate an approximate northward direction of the flute marks. Whereas, the uppermost inter-channel flute marks indicate a more northwest direction, with a spread from 250° to 027°. The flute marks recorded in locality 1 in the lowermost part of the succession indicate a west to northwest palaeo-current direction, while the uppermost part indicates a north to northwest directional trend, with a smaller spread from 282° to 336°. The

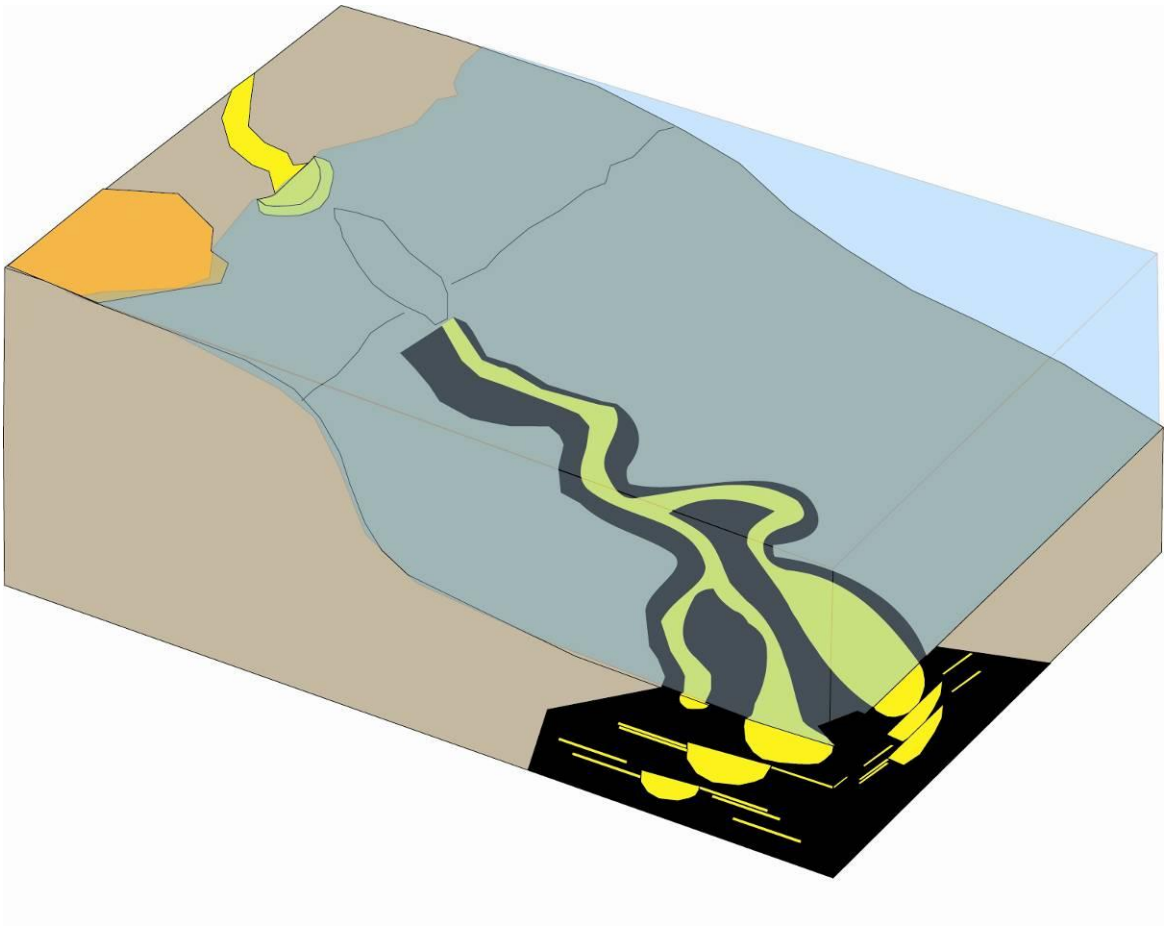

Figure 8.7: A principal model for the depositional systems (locking towards southeast).

measurements from locality3 are only taken from one single bed, with a flute mark spread from 271° to 323°. These data may indicate that the channel system has a more meandering character from locaity1 to locality2. This may be due to MTC deposits that deflect the channel position and/or difference in slope gradients. Clark *et al*. (1992) recognized from their studies that sinuosity of submarine channels are linked to gradient of the slope in the basins. A decrease in gradient is giving rise to higher sinuosity of the submarine channels. The meander depth of the turbidite channel is 7.25 meters in locality2, and the width could not be measured in the locality. According to Mutti (1985) the width/depth ratio is no more than 100/10 in the Hecho Group. The ratio describes the cross-sectional geometry, channel symmetry, and the channel overbank slope (Keevil et al., 2007).

Channel migration is proposed to evolve only laterally on the outer bends of the channels, and not longitudinally (Peakall et al., 2000; Wynn et al., 2007) as for fluvial systems. Straub *et al*. (2007) did laboratory study on the topography in aggrading sinuous submarine channels, where the experiment showed that channel fill and levee aggradation decrease down stream along with a decrease in grain size. The cross section of the channel shows an asymmetric channel-levee configuration, with a highly aggradational outer bend. The asymmetric geometry is described as a result of difference in current velocity from outer to inner bend.

Modification by a MTC may be the case for the FA 5.1 unit in log4 at 36 metres, above the turbidite channel (FA 3.1). The unit may represent a slope-attached MTC according to the Moscardelli and Wood (2008) classification scheme. The MTC may have plugged the channel, which Peakall *et al*. (2000) described as the last process of a three-stage model of submarine channel architecture. Stage 1 represents lateral bend growth and point bar development, stage 2 is an aggradational phase of the channel, and stage 3 a channel abandonment phase (plugged by debris flow or draped by hemipelagic mud). The channel may have changed direction (avulse) due to the mound of mud plugging the channel, or the channel system is “switched off” due to changes in sediment supply or sea-level fluctuation.

Galloway (1998) described this by channels that commonly shift from an erosional character to depositional character in response to change in the sediment load/discharge ratio or to changing boundary conditions of grade and base level.

The locality2 deposits have the quiet same characteristics as deposits of locality1, but the locality2 deposits are deposited further down-slope in a confined canyon floor slope environment. The locality2 deposits are more erosive in nature, by the presence of rip-up clasts in many of the high density turbidites. The inter-channel turbidite deposits are deposited by flow stripping and will rapidly settle proximally to the turbidite channel (Peakall et al., 2000) and give rise to Ta or Ta-Tb intervals close to the channel and Tb-Td more distal from the channel axis, due to the lost momentum (hydraulic jump) from confined channel to unconfined outer channel area. Proximal to distal relationships in a turbidite system were recorded by Kane *et al*. (2007) from the Rosario Formation in Baja California, Mexico. They used bioturbation traces to document the proximal to distal reslationship (vertical/horizontal), which decreased away from the channel-levee proximal part. This kind of relationship has not been observed in the dataset of this study, but the large vertical bioturbation traces (*Thalassinoides and Skolithos*) are most often seen in the proximal T_a beds. The medial beds would have traces of *Thalassinoides and Planolites* as the most common. *Nereites* is only observed in one bed of medial to distal turbidite deposits.

Thin high-density turbidite overbank deposits composed of *nummulites* and oyster fragments are probably a result of runup of turbidity currents along the outer bends of channels (Straub et al., 2008). These deposits are interpreted to be deposited by non-cohesive debris flows (FA 6.1), with marine imprints and wood/plant debris (RF3 table 4.1).

The fining and thinning upwards- and coarsening and thickening upwards units recorded in the FA 2.1 may be due to 4^{th} order response of climatic fluctuations as recorded in the Holocene epoch (Fernandez-Salas et al., 2003). This led to delta lobe switching and a change in river gradient.

9 Reservoir characterization

9.1 Introduction

Reservoir characterization is the act of building reservoir models incorporating the characteristics of a reservoir and thus simulating and predicting the behaviour of fluids within the reservoir. Petroleum companies are therefore interested in the reservoir properties (porosity and permeability) of reservoir rocks and barriers to fluid flow, such as sealed faults and heterogeneties, in order to extract as much petroleum out of the ground as possible. The need for good sedimentological and geophysical data and subsequent interpretations are crucial when making a model of a reservoir. A brief reservoir characterization of the Arro sandstone body is given here on two different scales; (i) reservoir properties related to the inter-pore connectivity in the sandstones (microscopical features) and (ii) barriers to fluid-flow (macroscopical features) (figure 9.1).

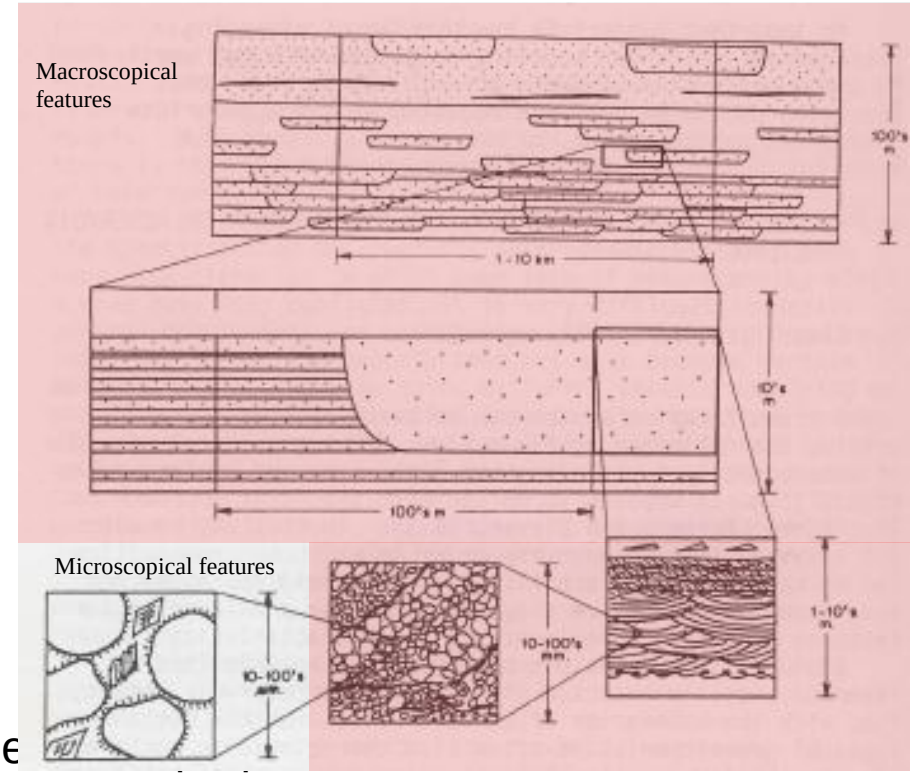

Figure 9.1: Different scales of heterogeneity affecting fluid-flow in reservoirs modified after Weber (1986).

9.2 Re

Porosity and permeability in a reservoir is a function of the depositional porosity/permeability and diagenesis. Textural parameters, such as grain-size, sorting and angularity of grains, and

clay content are important factors controlling the depositional porosity/permeability (cf. Giles(1997)). The depositional properties of the rock will then be altered by diagenetic processes. Diagenesis will depend on composition as well as texture, but other factors as fluid (Bjørlykke, 1994), temperature-history and effective stress (cf. Chuhan et al., (2002), Bjørlykke and Egeberg, (1993)) are critical.

The Arro sandstones are rich in calcareous grains (19-36%). Petrographic observations show that the sandstones are completely carbonate cemented. This is probably because the Arro sandstones contained large amounts of biogenic carbonate derived from nearby platform areas that has recrystallized into carbonate cement. Due to this the Arro sandstones themselves are useless as potential reservoirs. Despite this the macroscopical characteristics of the Arro sandstones may be used as analogues to similar, siliciclastic turbidite systems that have good reservoir properties.

9.3 Barriers to fluid flow

Macroscopical heterogeneities can be recognized on several levels (figure 9.1). In addition faults observed in the Arro/Charo region are filled with calcite, and will act as fluid barriers within the deep marine systems of the Ainsa Basin.

The upper Montana Group and the lower Santa Liesatra Group contains several turbidite systems, which are linked to the Charo feeder canyon. One of these systems is the Arro sandstone body. The net/gross ratio (aspect ratio) of the sandstone body is just above 30 % (see chapter 6), which according to Reading & Richards (1994) may indicate that the logged deposits are close to the turbidite channel axis (figure 9.2).

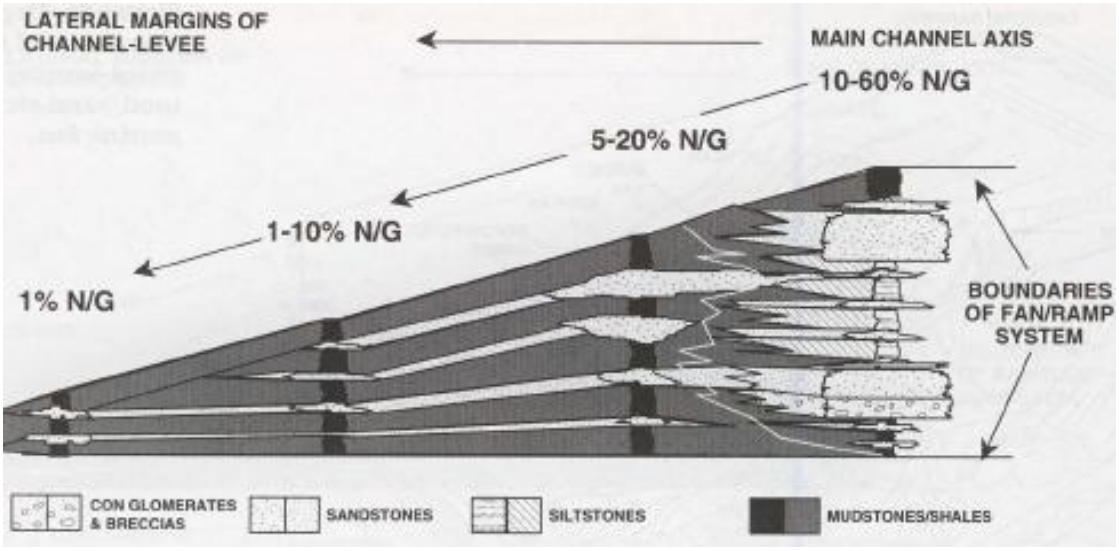

Figure 9.2: Reservoir arcitecture of channel and inter-channel system from Reading and Richards (1994).

The turbidite channel unit (FA 3.1) and the inter-channel sandstones (FA 2.1) would act as good reservoir sands. The inter-channel beds are often amalgamated, erosive in nature, and frequently pinching out laterally (see chapter 6). They are separated by muddy channel-levee (FA 4.1) units. These units may act as barriers for fluid flow, locally. The turbidite channel unit may act as an excellent reservoir sandstone with good connectivity. This sandstone body probably stretches out from the canyon down into the deepest part of the basin, where it may be connected to the fan lobes (stage 2 deposits, Mutti, 1985).

The mass transport complexes and the channel-levee mounds act as barriers for the turbidity currents in the gully, which will result in turbidite beds being ponded onto these features, or that the flow is deflected around the mounds. This may lead to two different reservoir heterogeneities, with isolated sand bodies or connected sand bodies.

Laminated and cross-bedded zones in sandstones are zones with decreased fluid flow, even between bedsets and the intervening lamina. According to Emmett *et al*. (1971) permeability parallel to the cross-stratified laminae is about 4 times higher than perpendicular to the laminae. This has implications for the lateral flow of fluids, where dependence lies on the

permeability contrast of the cross-beds and the associated bottom-set (Weber, 1986). These properties are valid in low density turbidites in the inter-channel sandstones. Some of the inter-channel sandstone beds may be isolated by mud thus hindering petroleum migration into these potential reservoir rocks. This may be the case for the beds recorded in log 4 from 68 metres up to 111.15 metres.

The Arro sandstone body would act as a highly heterogeneous reservoir that may have isolated inter-channel sand bodies and/or connected inter-channel sand bodies. The turbidite channel sand body would be an excellent reservoir with connectivity from upper slope down to the basin lobes.

The Arro sandstone body is a stratigraphically significant reservoir with the overlying basin slope sediments (FA 1.1) logged in log 5 as a seal. The architecture and the geometry of the sandstones may be used as analogues for other slope/ramp apron reservoirs. The Arro sandstone body may not be a good analogue to the rift basin architecture of the turbidite deposits described by Ranvås and Steel (1998), but the processes behind deposition are the same. This may not be sufficient enough for using the Arro sandstone body or the Ainsa Basin as an analogue for the deep marine Viking Graben sediments of the North Sea, or other rift basin deep marine deposits, but analogue for other deep marine foreland basin deposits.

10 Conclusion

The Eocene Ainsa Basin was formed due to thrusting and folding by movements of the Montsec and the Cotiella thrust sheets to form the Mediano anticline that controlled the eastern part of the deep marine basin. The Boltaña anticline evolved at a later stage due to movement of the Serres Marginales thrust sheet to form the western boundary of the basin. In between these structures is the Buil syncline, which comprises the Ainsa Basin. The movement of the Mediano detachment fold controlled the sedimentation into the basin along with the Faradada tear fault system. These movements created the unconformities in the basin.

The Arro system is deposited in a canyon floor related environment, composed of gravity flow deposits fed from the Montanana delta in the eastern part of the basin and secondary gravity flow deposits within the scoured canyon floor environment. The Arro sandstone body is based by the mass transport complex in log1, which is a candidate type 2 sequence boundary (Exxon group) for the system. The mass transport complex represents the initial erosion and development of the Charo canyon. The depositional style in the different localities are of different character, due to the different gradients in locality 1 compared to locality 2. Locality 1 has a lot of high and low density turbidite deposits, together with non-hydroplaning debris flows. These deposits are containing ersional structures and syn-faulting, due to change in the flow regime. Locality 2 deposits are characterized by channel-levee slumping and high and low turbidite deposits. The locality 3 deposits have a more channel distal character than the 2 other localities.

The reservoir quality in the turbidite channel sandstones are regarded along with the inter-channel sandstones, where the turbidite channel would act as the primary reservoir target and the inter-channel as the secondary taregt.

References

2008, Google Earth.

Aksu, A.E. and Hiscott, R., 1992, Shingled quaternary debris flows bases on the north-east Newfoundland slope. Sedimentology, 39: 193-206.

Amorosi, A., 1997, Detecting compositional, spatial, and temporal attributes of glaucony: a tool for provenance research. Sedimentary Geology, 109: 135-153.

Bagnold, R.A., 1956, The flow of cohesionless grains in fluids. Philosophical Transactions of the Royal Society of London Series a-Mathematical and Physical Sciences, 249: 235-297.

Beavington-Penney, S.J. and Racey, A., 2004, Ecology of extant nummulitids and other large foraminifera: applications in palaeoenvironment alanalysis. Earth-Science Reviews, 67: 219-265.

Bjørlykke, K., Nedkvitne, T., Ramm, M. and Saigal, G.C., 1992, Diagenetic processes in the Brent Group (Middle Jurassic) reservior of the North Sea: an overview. Geological Society of London, special publications, 61: 263-287.

Bjørlykke, K. and Egeberg, P.K., 1993, Quartz cementation in sedimentary basins. The American Association of Petroleum Geologists Bulletin, 77: 1538-1548.

Bjørlykke, K., 1994, Fluid-flow processes and diagenesis in sedimentary basins. Geological Society of London, special publications, 78: 127-140.

Bouma, A.H., 1962, Sedimentology of some Flysch deposits: a graphic approach to facies interpretation. Elsevier, Amsterdam XII, 168 s. p.

Carter, R.M., 1975, A Discussion and Classification of Subaqueous Mass-Transport with Particular Apllication to Grain-Flow, Slurry-Flow, and Fluxoturbidites. Earth-Science Reviews, 11: 145-177.

Caus, E., Teixell, A. and Bernaus, J.M., 1997, Depositional model of a Cenomanian-Turonian extensional basin (Sopeira Basin, NE Spain): Interplay between tectonics, eustasy and biological productivity. Palaeogeography Palaeoclimatology Palaeoecology, 129: 23-36.

Chuhan, F.A., Kjeldstad, A., Bjørlykke, K. and Høeg, K., 2002, Porosity loss in sand by grain crushing - experimental evidence and relevance to reservoir quality. Marine and Petroleum Geology, 19: 39-53.

Clark, J.D. and Pickering, K.T., 1996, Architectural elements and growth patterns of submarine channels: Application to hydrocarbon exploration. Aapg Bulletin-American Association of Petroleum Geologists, 80: 194-221.

Collinson, J.D. and Thompson, D.B., 1989, Sedimentary structures. Unwin Hyman Ltd, London 208 p.

Coussot, P. and Meunier, M., 1996, Recognition, classification and mechanical description of debris flows. Earth-Science Reviews, 40: 209-227.

Cronin, B., Owen, D., Hartley, A. and Kneller, B., 1998, Slumps, debris flows and sandy deep-water channel systems; implications for the application of sequence stratigraphy to deep water clastic sediments. [Serial] Journal of the Geological Society of London, 155: 429-432.

Dasgupta, P., 2003, Sediment gravity flow - the conceptual problems. Earth-Science Reviews, 62: 265-281.

Dinares, J., McClelland, E. and Santanach, P., 1992, Contrasting rotation within thrust sheets and kinematics of the thrust tectonics as derived from palaeomagnetic data: an example from the Southern Pyrenees. In: MacClay, K.R. (ed.), Thrust tectonics. Chapman and Hall, London265-275.

Elverhøi, A., Norem, H., Andersen, E.S., Dowdswell, J.A., Fossen, I., Haflidason, H., Kenyon, N.H., Laberg, J.S., King, E.L., Sejrup, H.P., Solheim, A. and Vorren, T.O., 1997, On the origin and flow behavior of submarine slides on deep-sea fans along the Norwegian-Barents Sea continental margin. Geo-Marine Letters, 17: 119-125.

Embley, R.W., 1982, Anatomy of some Atlantic margin sediment slides and some comments on ages and mechanisms. In: Saxsoy, S. and Nieuwenhuis, J.K. (eds.), Marine slides and other mass movments, New York. Plenum Press, 189-213.

Emmet, W.R., Beaver, K.W. and MaCleb, J.A., 1971, Little Buffalo Basin Tensleep Heterogeneity - Its influence on infill Drilling and secondary Recovery. Petr. Techn.: 161-168.

Fernandez-Salas, L.M., Lobo, F.J., Hernandez-Molina, F.J., Somoza, L., Rodero, J. and Diaz del Rio, V., 2003, High resolution architecture of late Holocene highstand prodeltaic deposits from southern Spain: the imprint of high-frequency climatic and relative sea-level changes. Continental shelf research, 23: 1037-1054.

Fernandez, O., Munoz, J.A., Arbues, P., Falivene, O. and Marzo, M., 2004, Three-dimensional reconstruction of geological surfaces: An example of growth strata and turbidite systems from the Ainsa basin (Pyrenees, Spain). American Association of Petroleum Geology Bulletin, 88: 1049-1068.

Ford, D. and Golonka, J., 2003, Phanerozoic paleogeography, paleoenvironment and lithofacies maps of the circum-Atlantic margins. Marine and Petroleum Geology, 20: 249-285.

Galloway, W.E., 1998, Siliciclastic slope and base-of-slope depositional systems: component facies, stratigraphic architecture, and classification. American Association of Petroleum Geology, 82: 569-595.

Gee, M.J.R., Gawthorpe, R.L. and Friedmann, J.S., 2005, Giant striations at the base of a submarine landslide. Marine Geology, 214: p. 287-294.

Giles, M.R., 1997, Diagenesis: a quantitative perspective. Kluwer Academic Publishers

Gjelle, E. and Sigmond, E.M.O., 1995, Bergartsklassifikasjoner og kartfremstilling. 1-77.

Haq, B.U., Hardenbol, J. and Vail, P.R., 1987, Chronology of fluctuating sea levels since the Triassic. Science, 235: 1156-1167.

Harms, J.C., Southard, J.B., Spearing, D.R. and Walker, R.G., 1975, Depositional environments as interperpreted from primary sedimentary structures and stratification sequences. Society of Economic Paleontologists and Mineralogists, 161 p.

Humphreys, B., Smith, S.A. and Strong, G.A., 1989, Authigenic chlorite in late Triassic sandstones from the central graben North Sea. Clay minerals, 24: 427-444.

Ilstad, T., Elverhøi, A., Issler, D. and Marr, J.G., 2004, Subaqueous debris flow behaviour and its dependence on the sand/clay ratio: a laboratory study using partical tracking. Marine Geology, 213: p. 415-438.

Johnson, A.M., 1970, Physical processes in geology: a method for interpretation of natural phenomena - intrusions in igneous rocks, fractures and folds, flow of debris and ice. Freeman, San Fransisco, Calif. xiii, 577 s. p.

Jorry, S.J., Hasler, C.A. and Davaud, E., 2005, Hydrodynamic behavior of Nummelites: implication of depostional models Facies, 52: 221.235.

Kane, I.A., Kneller, B.C., Dykstra, M., Kassem, A. and McCaffrey, W.D., 2007, Anatomy of a submarine channel-levee: An example from Upper Cretaceous slope sediments, Rosario Formation, Baja California, Mexico. Marine and Petroleum Geology, 24: 540-563.

Keevil, G.M., Peakall, J. and Best, J.L., 2007, The influence of scale, slope and channel geometry on the flow dynamics of submarine channels. Marine and Petroleum Geology, 24: 487-503.

Klein, C., 2002, Mineral science. John Wiley & sons, inc. 641 p.

Kneller, B. and Buckee, C., 2000, The structure and fluid mechanics of turbidity currents: a review of some recent studies and their geological implications. Sedimentology, 47: 62-94.

Kuenen, P.H., 1966, Experimental turbidite laminationin a circular flume. Geology, 74: 523-545.

Laberg, J.S. and Vorren, T.O., 1995, LateWeichselian submarine debris flow deposits on the Bear-island-trough-mouth-fan. Marine Geology, 127: 45-72.

Le Roux, J.P., 2003, Can dispersive pressure cause inverse grading in grain flows? Discussion. Journal of Sedimentary Research, 73: 333-334.

Legros, F., 2002, Can dispersive pressure cause inverse grading in gran flows. Journal of Sedimentary Research, 72: 166-170.

Leigh, N.S. and Hartley, A., 1992, Mega-debris flow deposits from Oligo-Miocene Pindos foreland basin, western mainland Greece: implications for transport mechanisms in ancient deep marine basins. Sedimentology, 39: 1003-1012.

Lowe, D.R., 1979, Sediment gravity flows: their classification and some problems of application to natural flows and deposits. The Society of Economic Paleontologists and Mineralogists, 27: 75-82.

Lowe, D.R., 1982, Sediment gravity flows: II. Depositional models with special reference to the deposits of high-density turbidity currents. Journal of Sedimentary Petrology, 52: 279-298.

Maliva, R.G. and Siever, R., 1989, Nodular chert formation in carbonate rocks. Journal of geology, 97: 421-433.

Masson, D.G., Huggett, Q.J. and Brunsden, D., 1993, The surface texture of the Saharan Debris Flow and some speculations on submarine debris flows. Sedimentology, 40: 583-598.

Middleton, G.V., 1967, Experiments on density and turbidity currents, III. Earth-Science Reviews, 4: 475-505.

Middleton, G.V., 1970, Experimental studies related to problems of flysch sedimentation. In: Lajoie, J. (ed.), Flysch sedimentology in North America. Geol. Assoc. Cananda Spec. paper253-272.

Middleton, G.V. and Hampton, M.A., 1973, Sediment gravity flows: mechanics of flow and depostion. In: Middleton, G.V. and Bouma, A.H. (eds.), Turbidities and Deep Water Sedimentation. The Society of Economical and Paleontological Mineralogists1-38.

Miller, K.G., Kominz, M.A., Browning, J.V., Wrigth, J.D., Mountain, G.S., Katz, M.E., Sugarman, P.J., Cramer, B.S., Chrisitie-Blick, N. and Pekar, S.F., 2005, The Phanerozoic recodr of global sea-level change. Science, 310: 1293-1298.

Millington, J.J. and Clark, J.D., 1995, The Charo/Arro canyon-mouth sheet system, south-central Pyrenees, Spain: a structurally influenced zone of sediment dispersal. Journal of Sedimentary Research, B65: 443-454.

Mohrig, D., Whipple, K.X., Hondzo, M., Ellis, C. and Parker, G., 1998, Hydroplaning of subaqueous debris flows. Geological Society of America Bulletin, 110: 387-394.
Mulder, T. and Cochonat, P., 1996, Classification of offshore mass movements. Journal of Sedimentary Research, 66: 43-57.
Mulder, T. and Alexander, J., 2001, The physical character of subaqueous sedimentary density flows and their deposits. Sedimentology, 48: 269-299.
Muñoz, J.A., 1992, Evolution of a continental collision belt: ECORS-Pyrenees crustal balanced cross-section. In: McClay, K.R. (ed.), Thrust tectonics. Chapman & Hall235-246.
Mutti, E. and Lucchi, F.R., 1975, Examples of turbidite facies and facies associations from selected formations of the northern Apennines. Consiglio Nazionale Ricerche, Nice.
Mutti, E., 1977, Distinctive thin-bedded turbidite facies and related depositional environments in the Eocene Hecho Group (South-central Pyrenees, Spain). Sedimentology, 24: 107-131.
Mutti, E., 1983/1984, The Hecho Eocene submarine fan system, south-central Pyrenees, Spain. Geo-Marine Letters, 3: 199-202.
Mutti, E., 1985a, Turbidite systems and their relations to depositional sequences. In: Zuffa, G.G. (ed.), Provenance of Arenites. D.Reidel Publishing Company, 65-94.
Mutti, E., 1985b, Hecho turbidite system, Spain. In: Bouma, A.H., Normark, W.R. and Barnes, N.E. (eds.), Submarine fans and related turbidite systems. Springer-Verlag, 205-209.
Mutti, E., Seguret, M. and Sgavetti, M., Year, Sedimentation and deformation in the Teritary sequences of the southern Pyrenees. AAPG Mediterranean basins conference, 1-155.
Nardin, T.R., Hein, F.J., Gorsline, D.S. and Edwards, B.D., 1979, A Review of mass movement processes, sediment and acoustic characteristic, and contrasts in slope and base-of-slope systems versus canyon-fan-basin floor fan. The Society of Economic Paleontologists and Mineralogists, 27: 61-73.
Nemec, W. and Steel, R.J., 1984, Alluvial and coastal conglomerates: their significant features and some components on gravelly mass-flow deposits. In: Koster, E.H. and Steel, R.J. (eds.), Sedimentology of Gravels and Conglomorates. The Canadian Society of Petroleum Geology, 1-31.
Nichols, G., 1999, Sedimentology and stratigraphy. Blackwell science Ltd, 355 p.
Nijman, W., 1989, Thrust sheet rotation? The South Pyrenean Teriary basin configuation reconsidered. Geodinamica Acta, 3: 17-42.
Nijman, W., 1998, Cyclicity and basin axis shift in a piggyback basin: towards modelling of the Eocene Tremp-Ager Basin, South Pyrenees, Spain. Geological Society of London, special publications, 134: 135-162.
Peakall, J., McCaffrey, W.D., Kneller, B., Stelting, C.E., McHargue, T.R. and Schweller, W.J., 2000, A process model for the evolution of submarine fan channels: implications for sedimentary architecture. In: Bouma, A.H. and Stone, C.G. (eds.), Fine-grained turbidite systems. AAPG memoir73-88.
Pemberton, S.G., MacEachern, J.A. and Frey, R.W., 1992, Trace fossil models: environmental anf allostratigrapich significance. In: Walker, R.G. and James, N.P. (eds.), Facies models: Response to sea level change. Geological Assocation of Canada, St. Johns Newfoundland, 47-72.
Pickering, K.T., Hiscott, R.N. and Hein, F.J., 1989, Deep-marine environments: clastic sedimentation and tectonics. Unwin Hyman Ltd 416 p.

Pickering, K.T. and Corregidor, J., 2005, Mass-transport complexes (MTCs) and tectonic control on the basin-floor submarine fans, Middle Eocene, South Spanish Pyrenees. Journal of Sedimentary Research, 75: 761-783.

Poblet, J., Munoz, J.A., Trave, A. and Serra-Kiel, J., 1998, Quantifying the kinematics of detachment folds using three-dimensional geometry: Application to the Mediano anticline (Pyrenees, Spain). Geological Society of America Bulletin, 110: 111-125.

Postma, G., 1986, Classification for sediment gravity-flow deposits based on flow conditions during sedimentation. Geology, 14: 291-294.

Puigdefabregas, C. and Souquet, P., 1986, Tecto-sedimentary cycles and depositional sequences of the Mesozoic and Tertiary from the Pyrenees. Tectonophysics, 129: 173-203.

Puigdefabregas, C., Muñoz, J.A. and Vergés, J., 1992, Thrusting and foreland evolution in the Southern Pyrenees. In: MacClay (ed.), Thrust tectonics. Chapman and Hall, 247-254.

Ravnås, R. and Steel, R.J., 1998, Architecture of marine rift.basin successions. American Association of Petroleum Geology Bulletin, 82: 110-145.

Reading, H.G. and Richards, M., 1994, Turbidite systems in deep-water basin margins classified by grain size and feeder systems. American Association of Petroleum Geology, 78: 792-822.

Richards, M. and Bowman, M., 1998, Submarine fans and related depositional systems II: variability in reservoir architecture and wireline log character. Marine and Petroleum Geology, 15: 821-839.

Rickards, D., 1997, Kinetics of pyrite formation by the H_2S oxidation of iron(II) monosulfide in aqueous solutions between 25 and 125^0C: The rate equation. Geochimica et Acta, 61: 115-134.

Robert, A., 2003, River processes: An introduction to fluvial dynamics. Arnold publishers:London 214 p.

Russell, H.A.J. and Arnott, R.W.C., 2003, Hydraulic-jump and hyperconcentrated-flow deposits of a glacigenic subaqueous fan: Oak Ridges Moraine, southern Ontario, Canada. Journal of Sedimentary Research, 73: 887-905.

Sanders, J.E., 1965, Primary sedimentary structures formed by turbidity currents and related resedimentation mechanisms. In: Middleton, G.V. (ed.), Primary sedimentary structures and their hydrodynamic interpretation. The Society of Economic Paleontology and Mineralogy 192-219.

Shanmugam, G., 1997, The Bouma Sequence and the turbidite mind set. Earth-Science Reviews, 42: 201-229.

Shanmugam, G., 2000a, 50 years of the turbidite paradigm (1950s-1990s): deep-water/processes and facies models- acrtitical perspective. Marine and Petroleum Geology, 17: 285-342.

Shanmugam, G., 2006, Deep-water processes and facies models: implications for sandstone petroleum reservoirs. Elsevier 475 p.

Shor, A.N. and Piper, D.J.W., 1989, A large late Pleistocene blocky debris flow on the central Scotian slope. Geomarine Letters, 9: 153-160.

Sohn, Y.K., 1997, On traction-carpet sedimentation. Journal of Sedimentary Research, 67: 502-509.

Southard, J.B., 1971, Representation of bed configurations in depth-velocity-size diagrams. In: Middleton, G.V. (ed.), Sedimentary processes: Hydraulic interpretation of primary sedimentary structures. Society of Economic Paleontologists and Mineralogists.

Stow, D.A.V., Reading, H.G. and Collinson, J.D., 1996, Deep seas. In: Reading, H.G. (ed.), Sedimentary Environments: Processes, Facies and Stratigraphy, 1-688.
Stow, D.A.V., Faugeres, J.C., Viana, A. and Gonthier, E., 1998, Fossil contourites: a critical review. Sedimentary Geology, 115: 3-31.
Straub, K.M., Mohrig, D., McElroy, B., Buttles, J. and Pirmez, C., 2008, Interactions between turbidity currents and topography in aggrading sinuous submarine channels; a laboratory study. Geological Society of America Bulletin, 120: 368-385.
Teixell, A., 1996, The Anso transect of the southern Pyrenees: basement and cover thrust geometries. Journalof the Geological Society of London, 153: 301-310.
Trave, A., Labaume, P., Calvet, F., Soler, A., Tritlla, J., Buatier, M., Potdevin, J.-L., Seguret, M., Raynaud, S. and Briqueu, L., 1998, Fluid migration during Eocene thrust emplacement in the south Pyrenean foreland basin (Spain): an integrated structual, mineralogical and geomechanical and geochemical approach. In: Mascle, A., Puigdefabregas, C., Luterbacher, H.P. and Fernandez, M. (eds.), Cenozoic Foreland Basins of Western Europe. Geological Society163-188.
Vergés, J., munoz, J.A. and Martinez, A., 1992, South Pyrenean fold and thrust belt: The role of foreland evaporitic levels in thrust geometry. In: MacClay, K.R. (ed.), Thrust tectonics. Chapman and Hall255-264.
Walker, R.G., 1967, Turbidite sedimentary structures and their relationship to proximal and distal depositional environments. Society of Economic Paleontologists and Mineralogists
Walker, R.G., 1992, Turbidites and submarine fans. In: Walker, R.G. and James, N.P. (eds.), Facies models: response to sea level change. Geological Association of Canada239-264.
Weber, K.J., 1986, How heterogeneity affects oil recovery. In: Lake, L.W. and Caroll Jr., H.B. (eds.), Reservoir characterization. Academic press, inc.487-544.
Woyessa, A.T., 2008,
Depositional environment, sequence stratigraphy and reservoir properties of an Eocene mixed carbonate-siliciclastic succession in the Ainsa Basin, Southern Pyrenees, University of Oslo, Oslo
Wynn, R.B., Cronin, B.T. and Peakall, J., 2007, Sinous deep-water channels: Genesis, geometry and architecture. Marine and Petroleum Geology, 24: 341-387.
Young, H.D., Freedman, R.A., Sears, F.W. and Zemansky, M.W., 2004, Sears and Zemansky's University physics. Pearson/Addison-Wesley, San Fransisco, Calif. XXI, 1714 p.

Appendix

Appendix I

	Flute mark measurements							
Log 3 FA 2.1	0 meters:	360 20 32 40 26 14 18	356 24 350 27 8 16 18	14 25 33 352 8 355 358	35 10 15 20 27 25 350			
	3,25 meters	5						
	7,74 meters	352						
	8,75 meters	67						
	F.C.1:	1 349 358						
	F.C.2:	17 21 11 12						
	F.C.3:	5 21 19						
	F.C.4:	1 352 343 357 26	20 20 27 25					
	F.C.5:	23 16 12	14 10 25	6 20				
	F.C.6:	21						
	F.C.7:	29						
	F.C.8:	31 31 33	65 47					
	F.C.9:	32 42 21						

Log 4 FA 2.1	F.C.10:	26 19 36	59 55					
	F.C.11	13 20 31						
	F.C.12	31 26 31 17 33 31						
	F.C.13	358 2 2 3						
	F.C.14	346 344 358 355						
Log 4 FA 2.1	F.C.15	317 332 332	346 331 343	349 320 346	334			
	F.C.16	287 310 301						
	F.C.17	331 315 326	317 332 325					
	F.C.18	308 304	295 297					
	F.C.19	338 354 328	332 332 334	349 335				
	F.C.20	292 297 289	251 262 274					
	F.C.21	295 333 327	323					

Log 4 FA 2.1	F.C.22	209 226						
Log 7 FA 2.1	F.C.23	288						
	F.C.24	297 336						
	F.C.25	267						
	F.C.26	312 385 307						
	F.C.27	284 291 293	300 318 313	311 313 284	289 296 305	299 308 306	294 290 302	299 303
	F.C.28	293 283 290	282 280					
	F.C.29	294 301 306	309 283 291	285				
	F.C.30	289 286 287	279 277 295	302 306 289	284			
	F.C.31	321 312 316	320 311					
	F.C.32	299 316 307	302 316					
	F.C.33	310 278 311	307 304 310	299 308 321	314 322 310	314 304 317	322 319 322	316 303
	F.C.34	287 289 297	290 283 299	294 320 320	283 285 277			
Log 8 FA 2.1	F.C.35	289 321 309	303 308 303	322 314				
	F.C.36	334 338 332	340 339 347					
	F.C.37	334 347 308	345 333 347	353 348				

Log 8 FA 2.1	F.C.38	329 336 357	323 339 329				
Log 9 FA 2.1	F.C.39	360 351 357	7 337 351	346			
	F.C.40:	311 313 309	304 298 309	301 308 309	304 310 291	295 289 282	299
	F.C.41	304 297 311	301 290 301				
	F.C.42	308 316 312	311 299 303	297 295 305			
	F.C.43	349 352 355	358 360 347	342 355			
Log 11 FA 2.1	F.C.44	299					
Log 12 FA 2.1	F.C45	313 309 306					
	F.C.46	338 335 330	337 315				
Log 13 FA 2.1	F.C.47	352 346 334	348 331 347	344 341			
	F.C.48	328 327 318	328 315 332	338 321 345	323		
Log 14 FA 2.1	F.C.49	329 328 323	336 325				
	F.C.50	315 311 331	323 323 321				

Log 14 FA 2.1	F.C.51	354 348 339	336 341 347					
	F.C.52	344 348 349	346 353 350	325 337 343	324			
	F.C.53	327 326 325	327 336 322					
	F.C.54	339 342 353	335					
	F.C.55	311 317 317	312 309 303	309 314				
	F.C.56	336						
	F.C.57	271 262 283	285 274 323					

Appendix II

	A-axis paleocurrent directions a(p)b(i)				
log 4 FA 4.1	Aa1:	275-095 317-132	273-093 242-062		
	Aa2:	342-161 258-078			
Log 11 FA 6.1	Aa3:	097-277 073-253 065-245	095-275 145-325 116-296	036-216 947-227 024-204	011-191
	Aa4:	032-212 005-185 029-209	031-211 026-206 335-155		
	Aa5:	040-220 043-223 043-223	051-231 067-247 032-212	019-199 015-195 032-212	
	Aa6:	344-164 340-160			
Log 12 FA 6.1	Aa7:	110-290 119-299 094-274	084-264 107-287		
Log 14 FA 4.1	Aa8:	316-136 328-148 325-145	319-139 331-151 340-160		
Log 15 FA 4.1	Aa9:	105-285 062-242 156-336	085-265 091-271 099-279		
Log 1 FA 5.1	Aa10:	338-158 027-207 309-129	345-165 344-164		

Appendix III

Legend

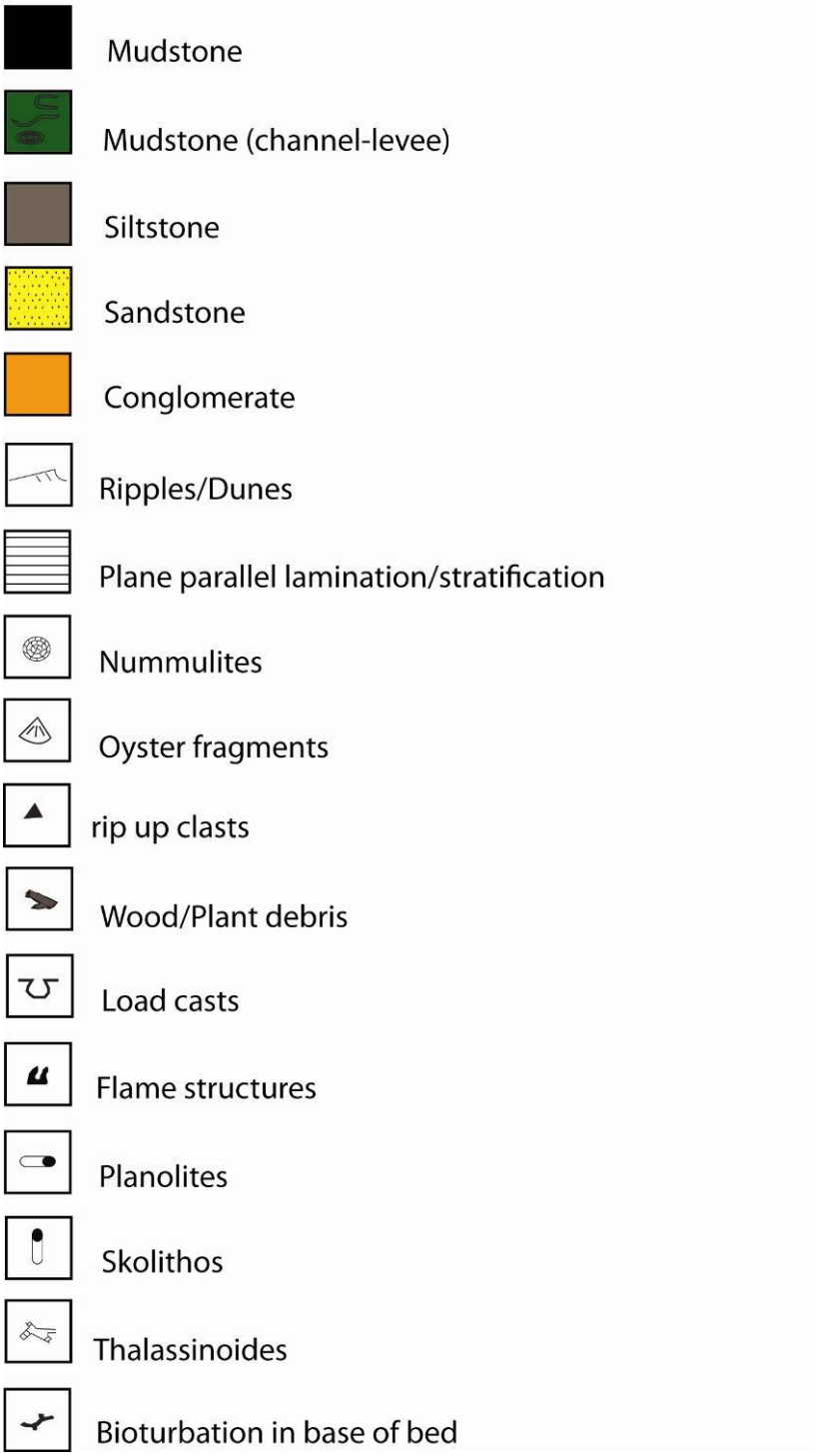
Mudstone
Mudstone (channel-levee)
Siltstone
Sandstone
Conglomerate
Ripples/Dunes
Plane parallel lamination/stratification
Nummulites
Oyster fragments
rip up clasts
Wood/Plant debris
Load casts
Flame structures
Planolites
Skolithos
Thalassinoides
Bioturbation in base of bed

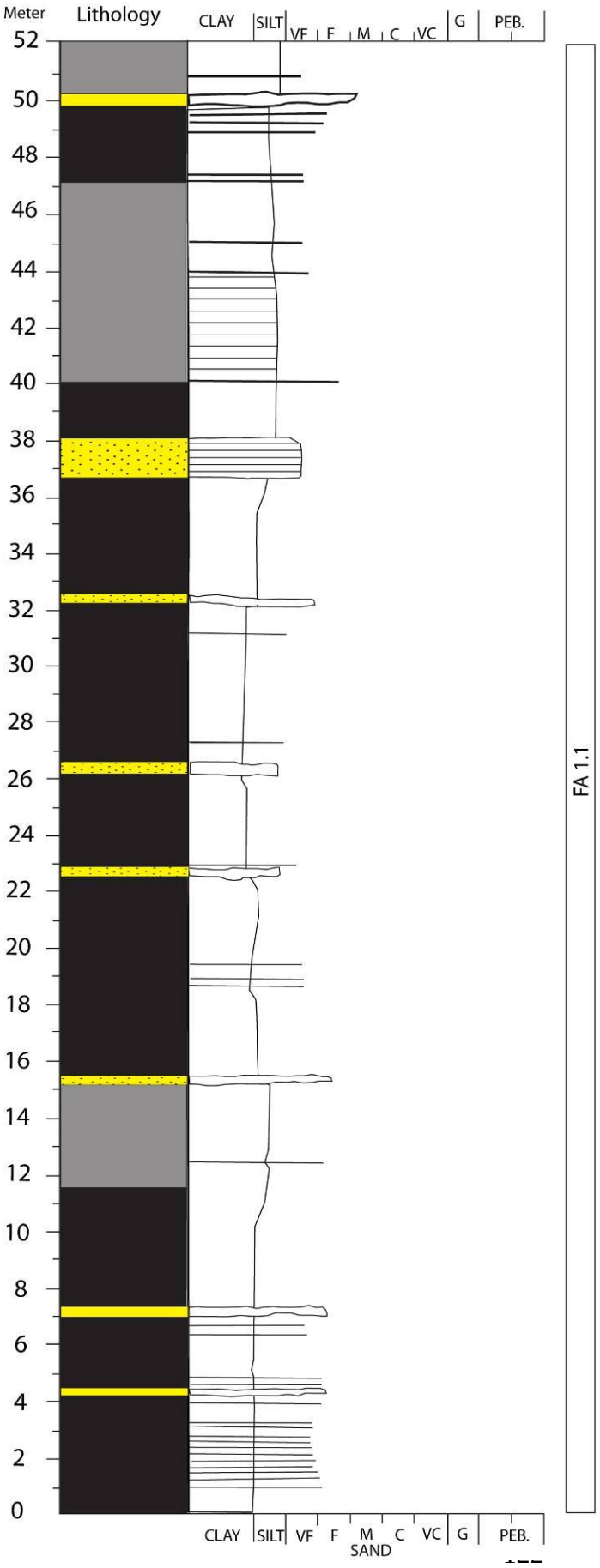

Log 1: 1/3
Locality 2
Scale: 1/200
UTM: 0272956 - 4698948

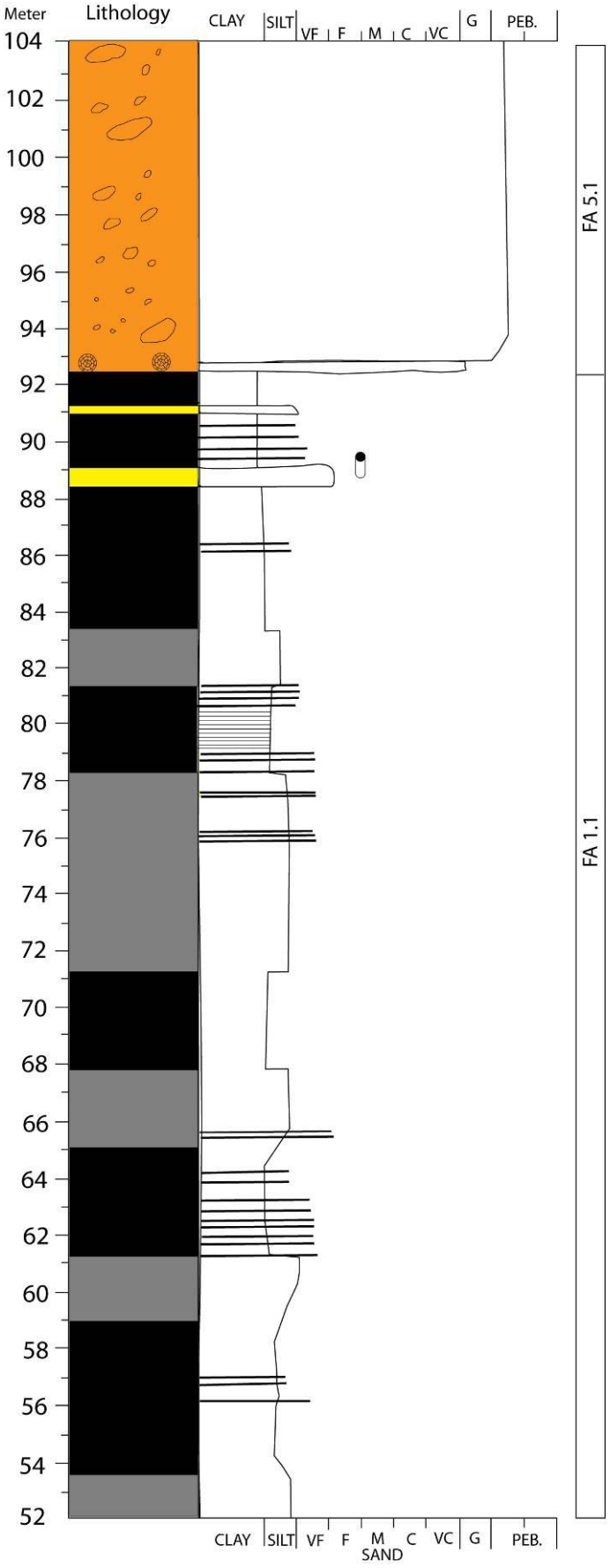

Log 1: 2/3
locality 2
Scale: 1:200

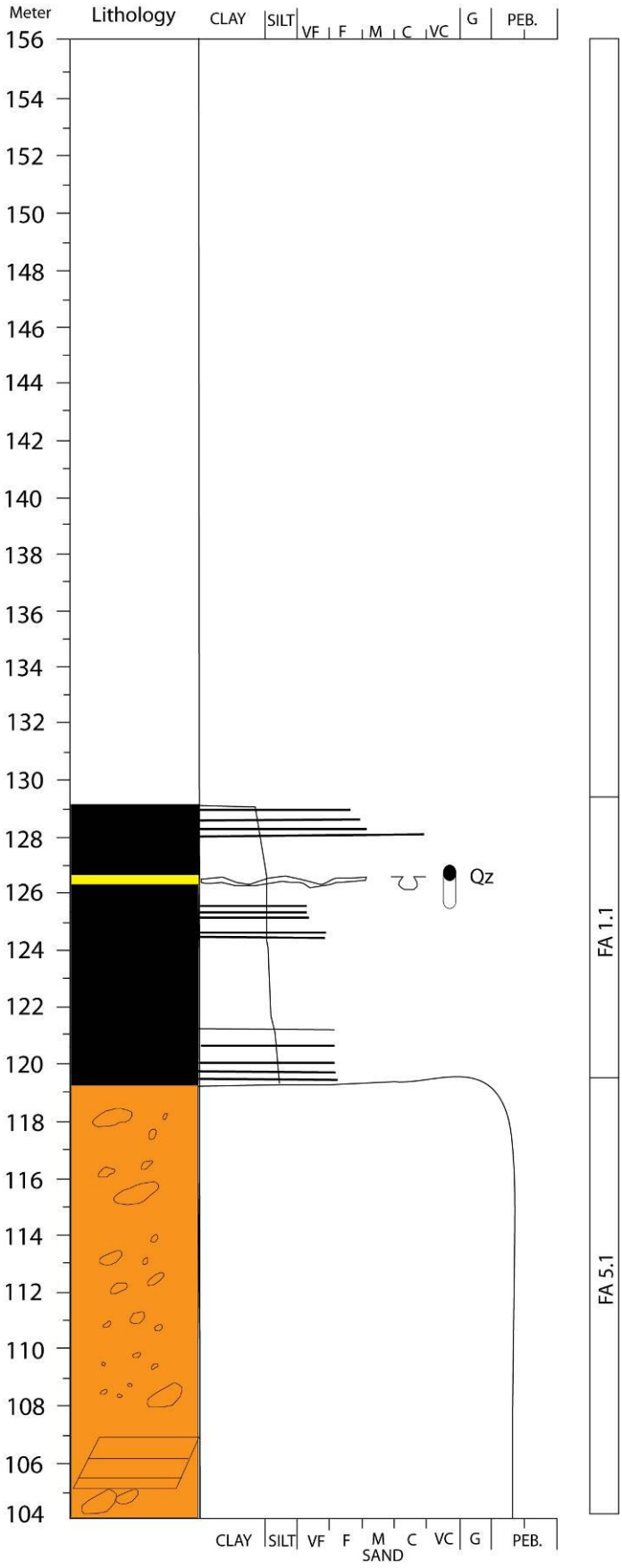

Log1: 3/3
Locality 2
Scale: 1:200
UTM: 0272824 - 4698969

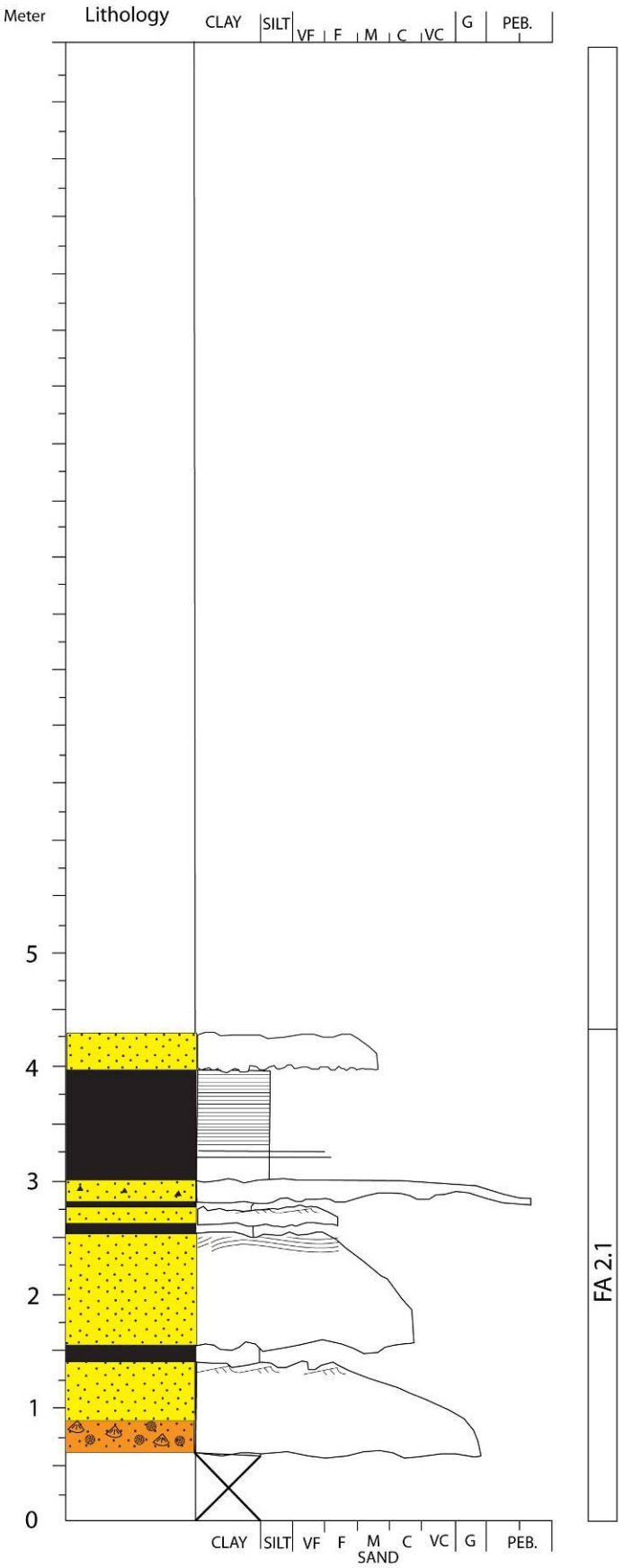

Log 2: 1/1
Locality 2
Scale: 1:50
UTM: UTM: 0272858 - 4698839

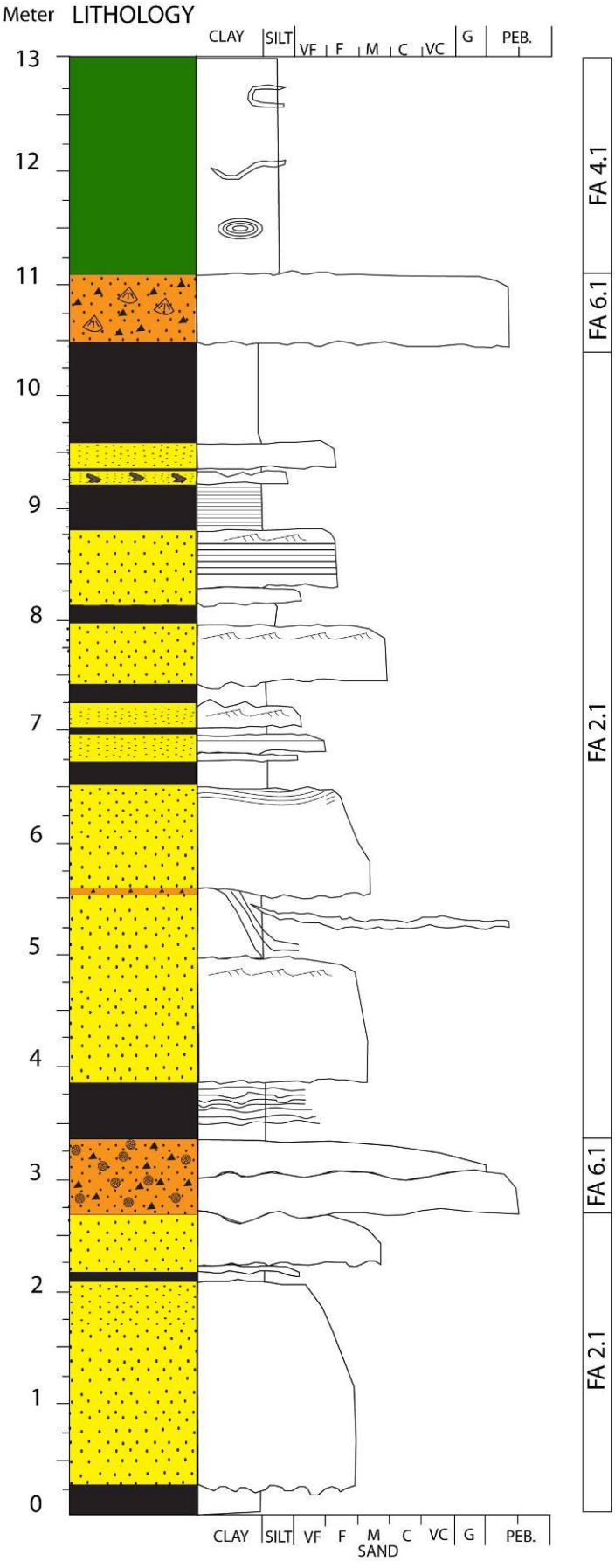

Log 3: 1/4
Locality 2
Scale: 1:50
UTM: 0272873 - 4698647

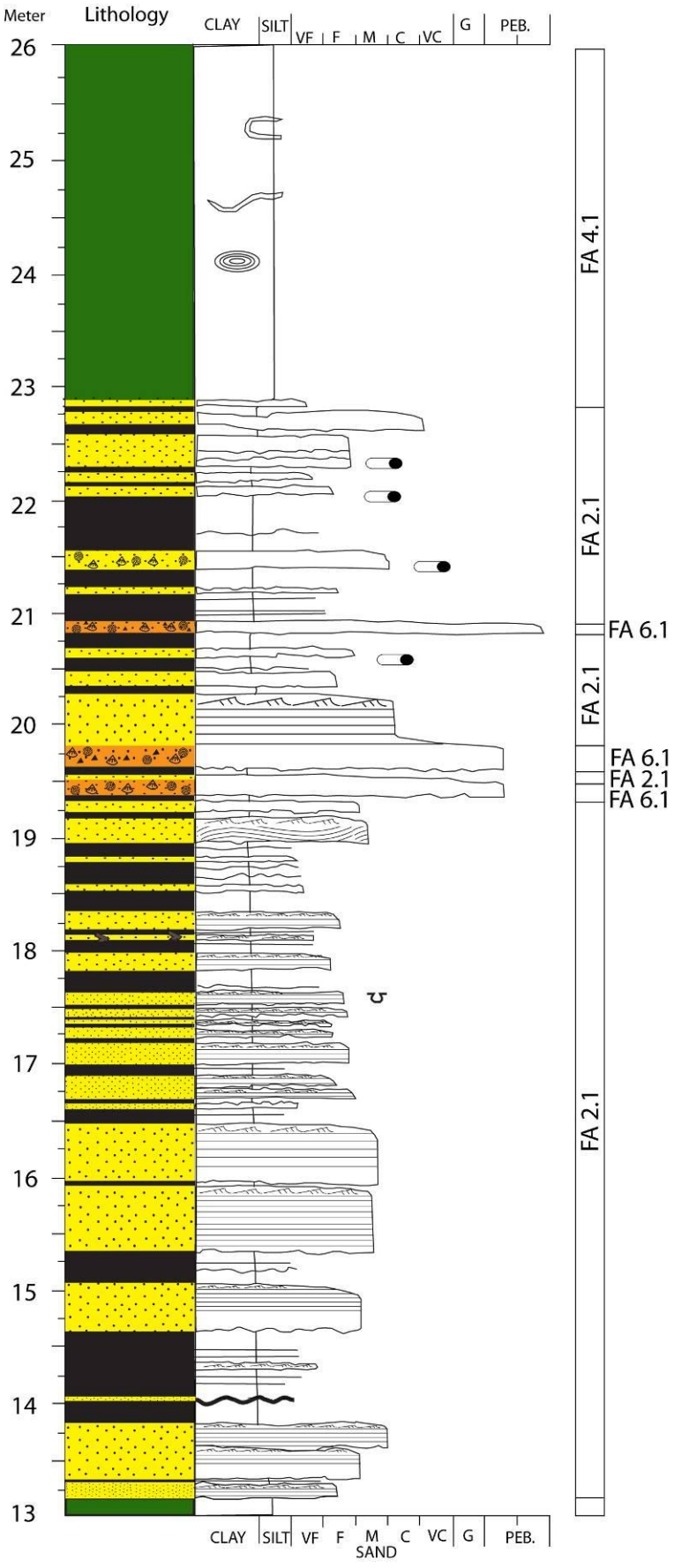

Log 3: 2/4
Locality 2
Scale: 1:50

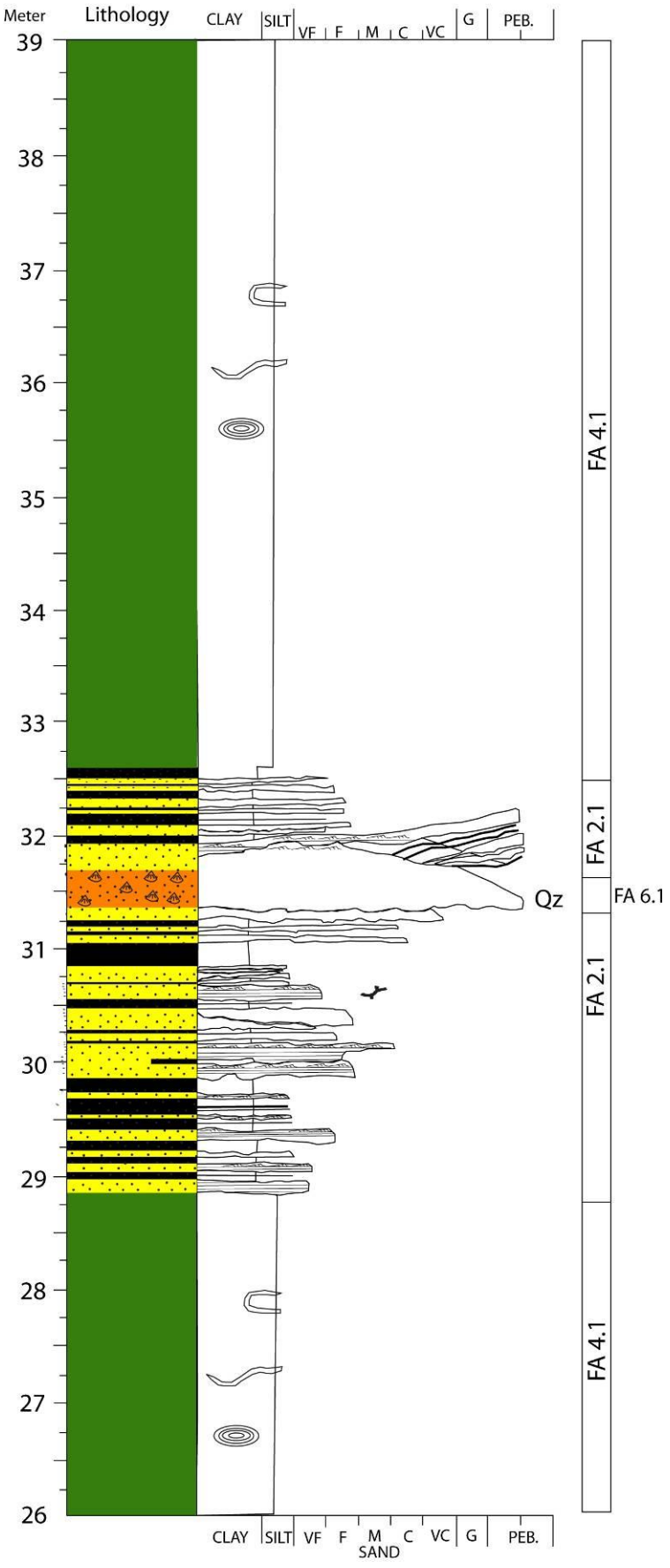

Log 3: 3/4
Locality 2
Scale: 1:50

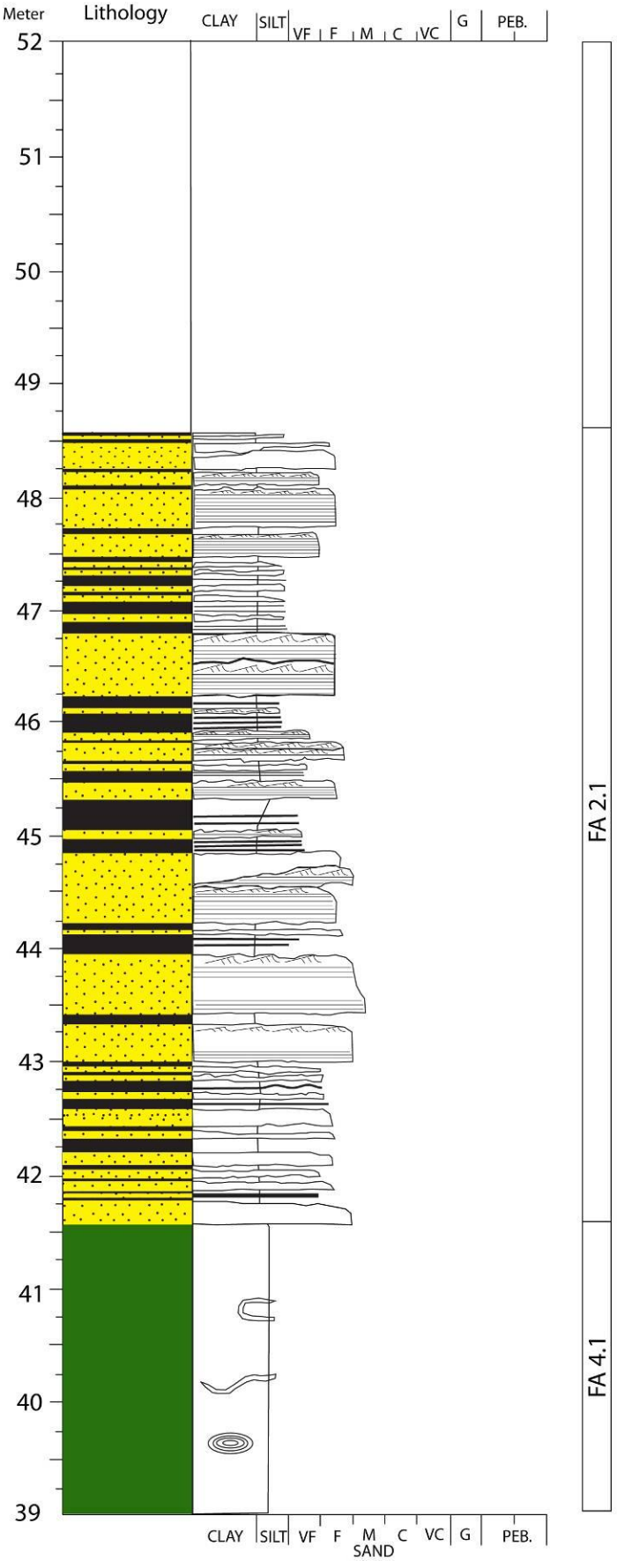

Log 3
Locality 2
Scale: 1:50

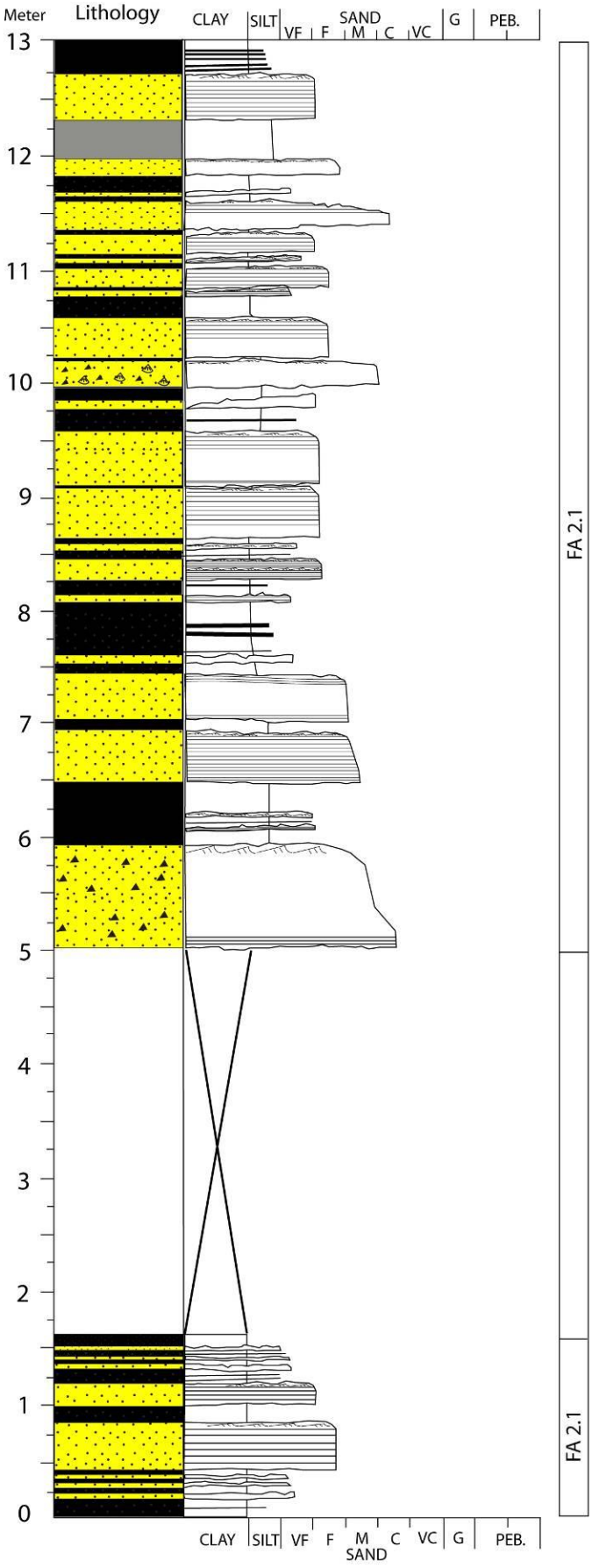

Log 4 1/9
Locality 2
Scale: 1:50
UTM: 0272814 - 469874

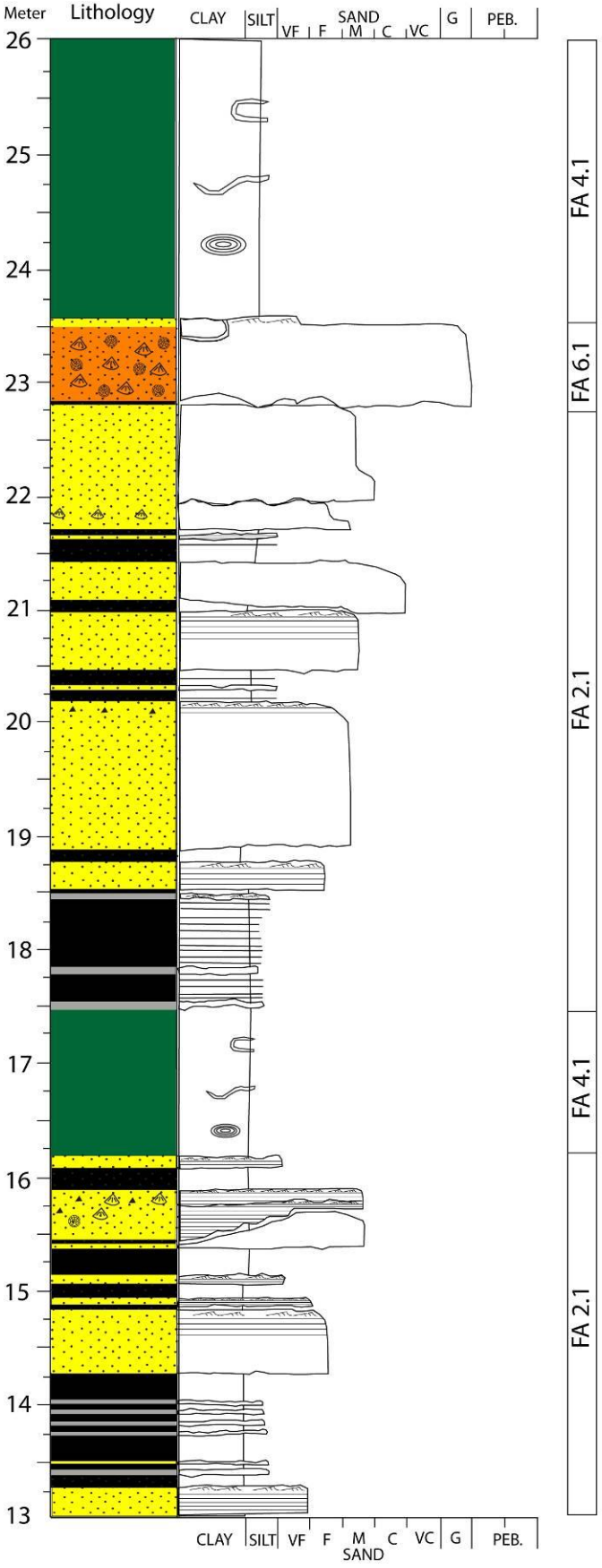

Log 4: 2/9
Locality 2
Scale: 1:50

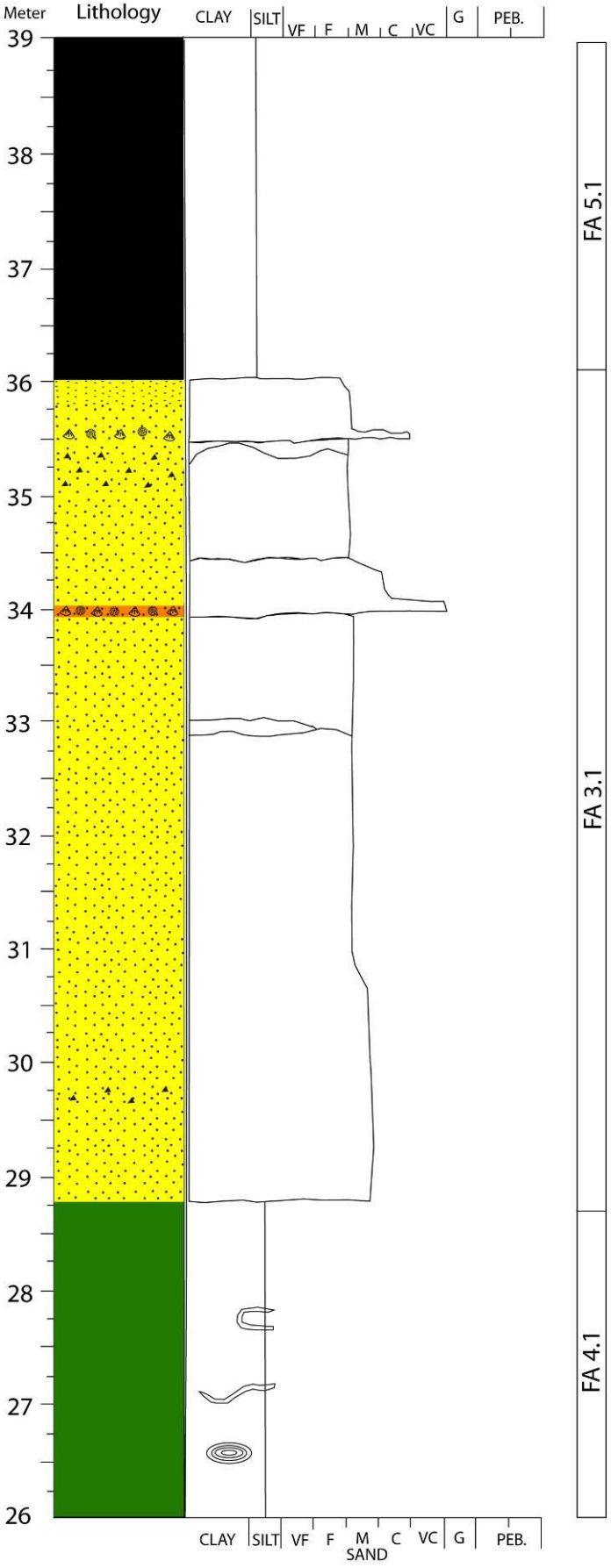

Log 4: 3/9
Locality 2
Scale: 1:50

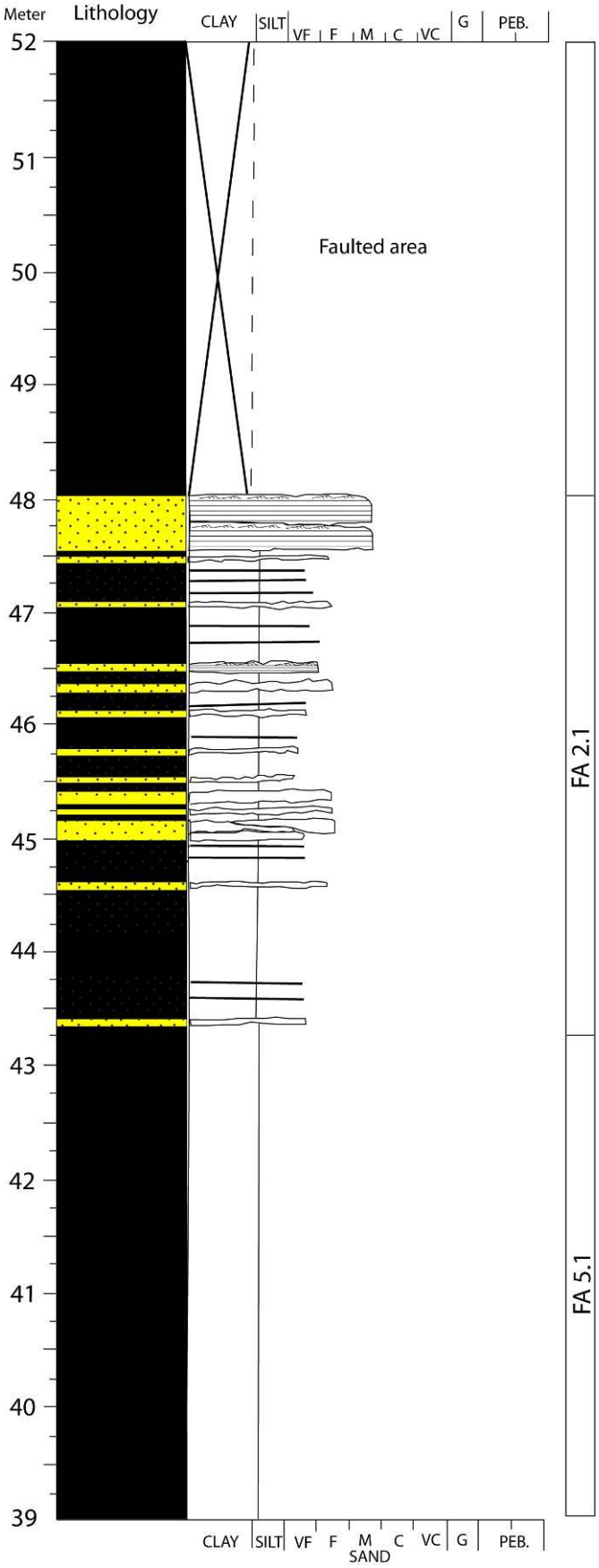

Log 4: 4/9
Locality 2
Scale: 1:50

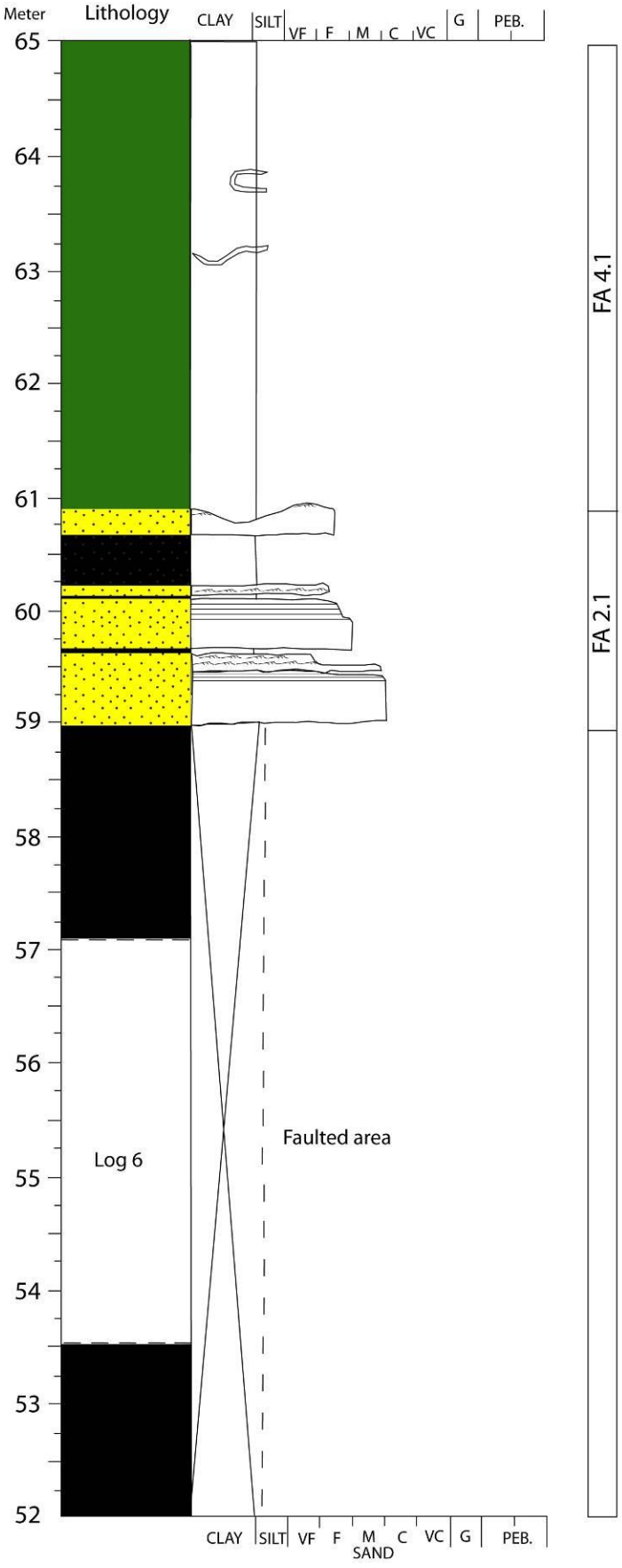

Log 4: 5/9
Locality 2
Scale: 1:50

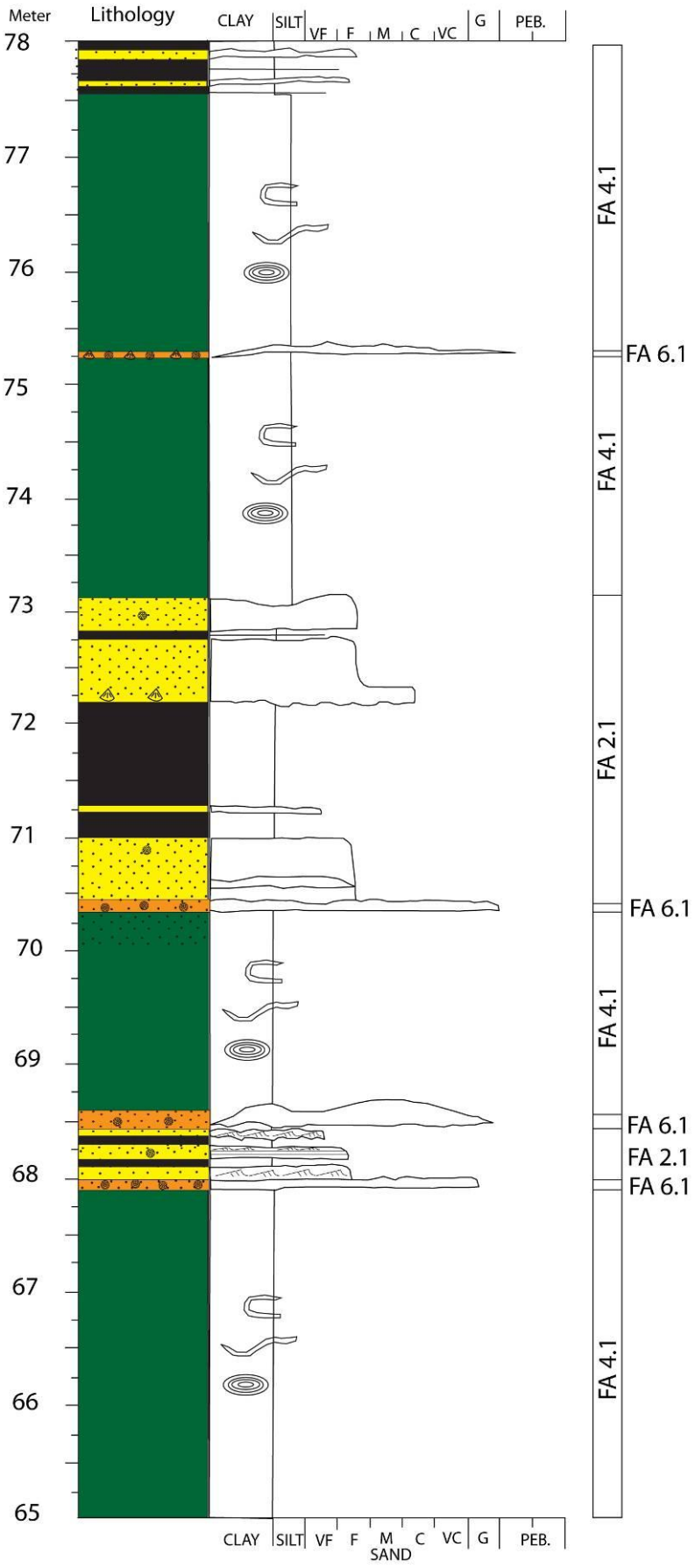

Log 4: 6/9
Locality 2
Scale: 1:50

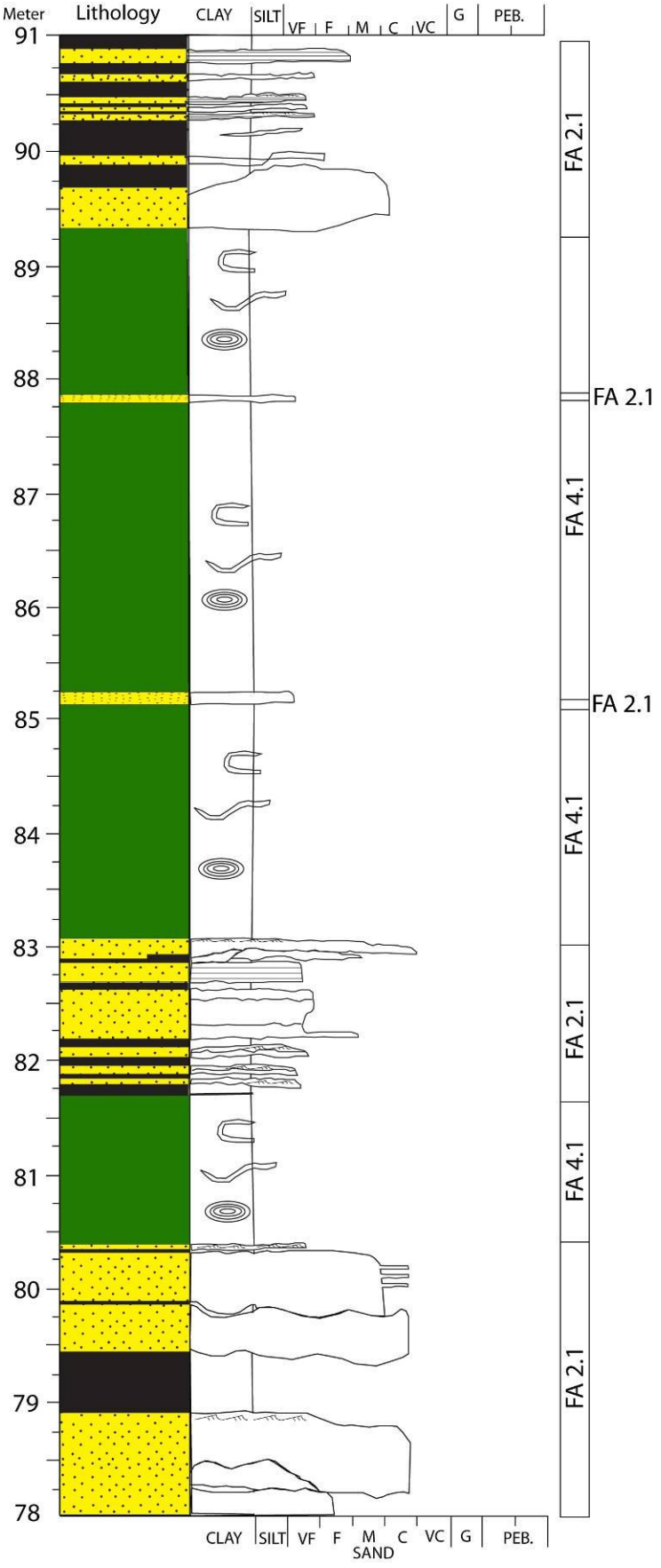

Log 4: 7/9
Locality 2
Scale: 1:50

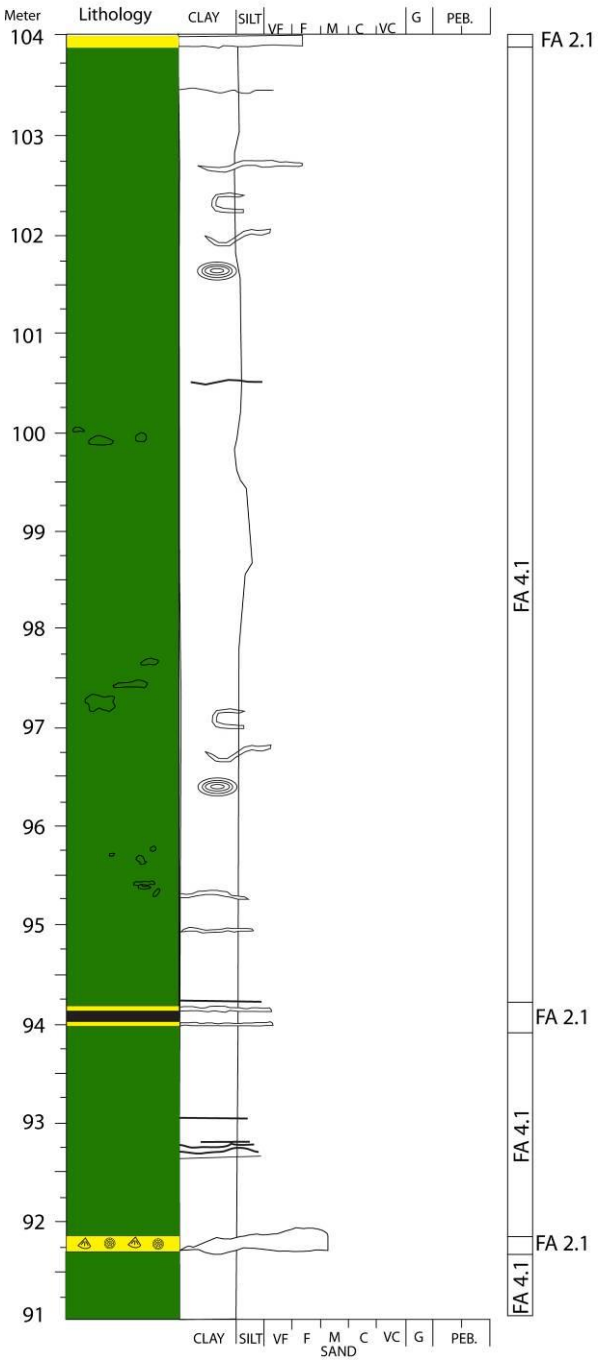

Log 4: 8/9
Locality 2
Scale: 1:50

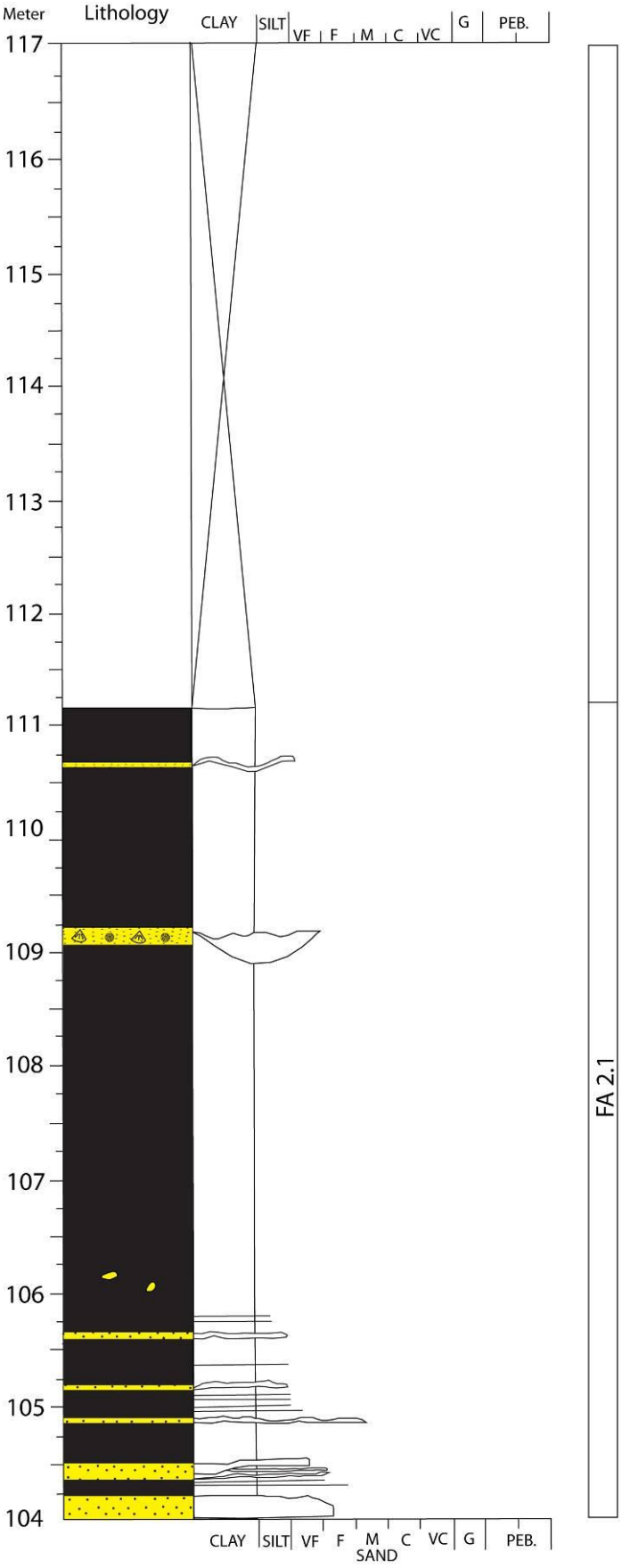

Log 4: 9/9
Locality 2
Scale: 1:50
UTM: 0272670 - 4698847

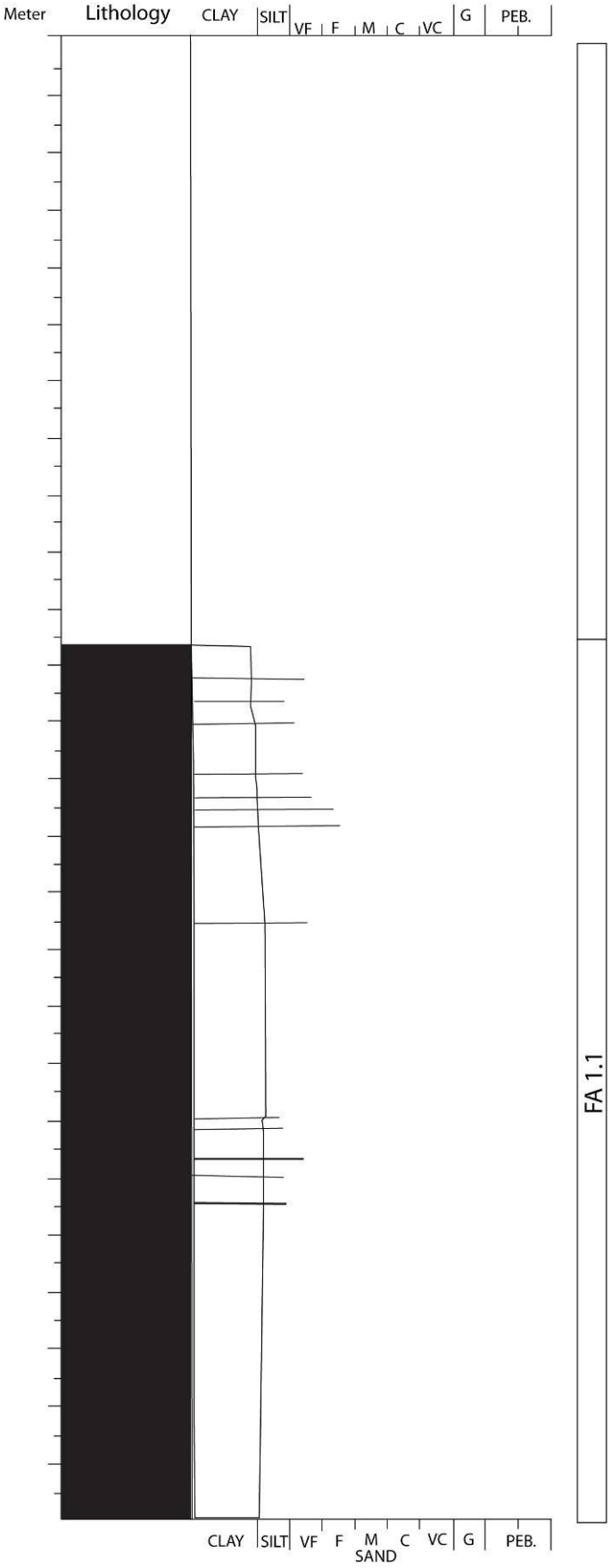

Log 5: 1/1
Locality 2
Scale: 1:200
UTM: 0272561 - 469906

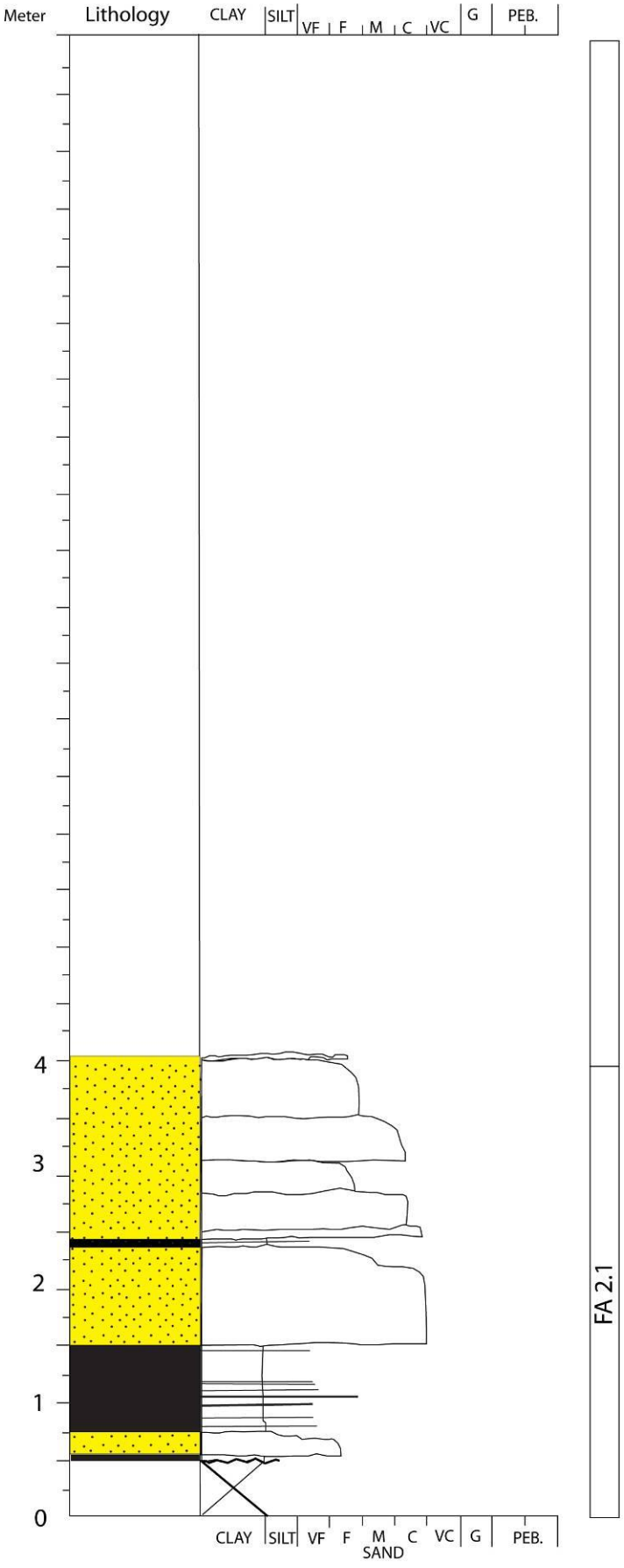

Log 6: 1/1
Locality 2
Scale: 1:50

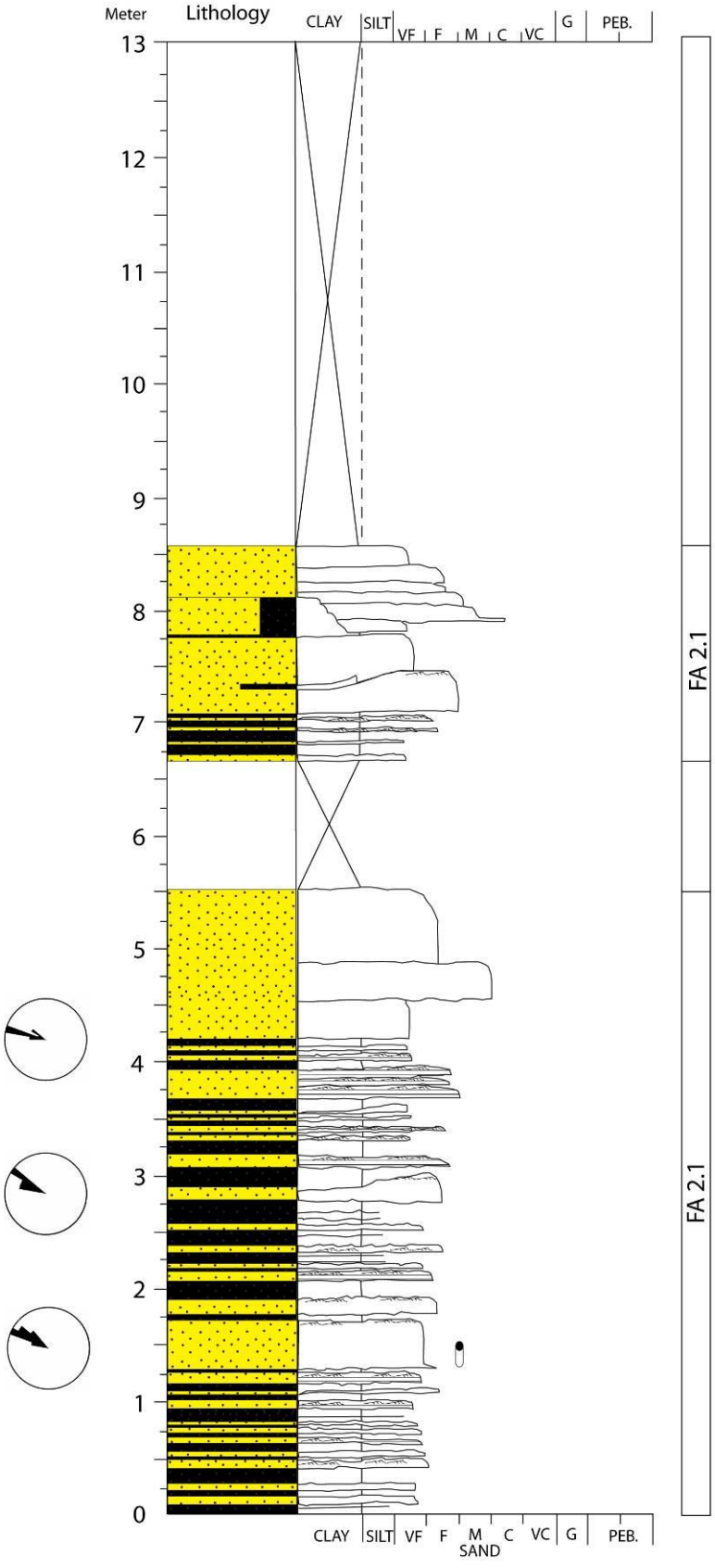

Log 7: 1/2
Locality 1
Scale: 1:50
UTM: 0273713 - 4697086

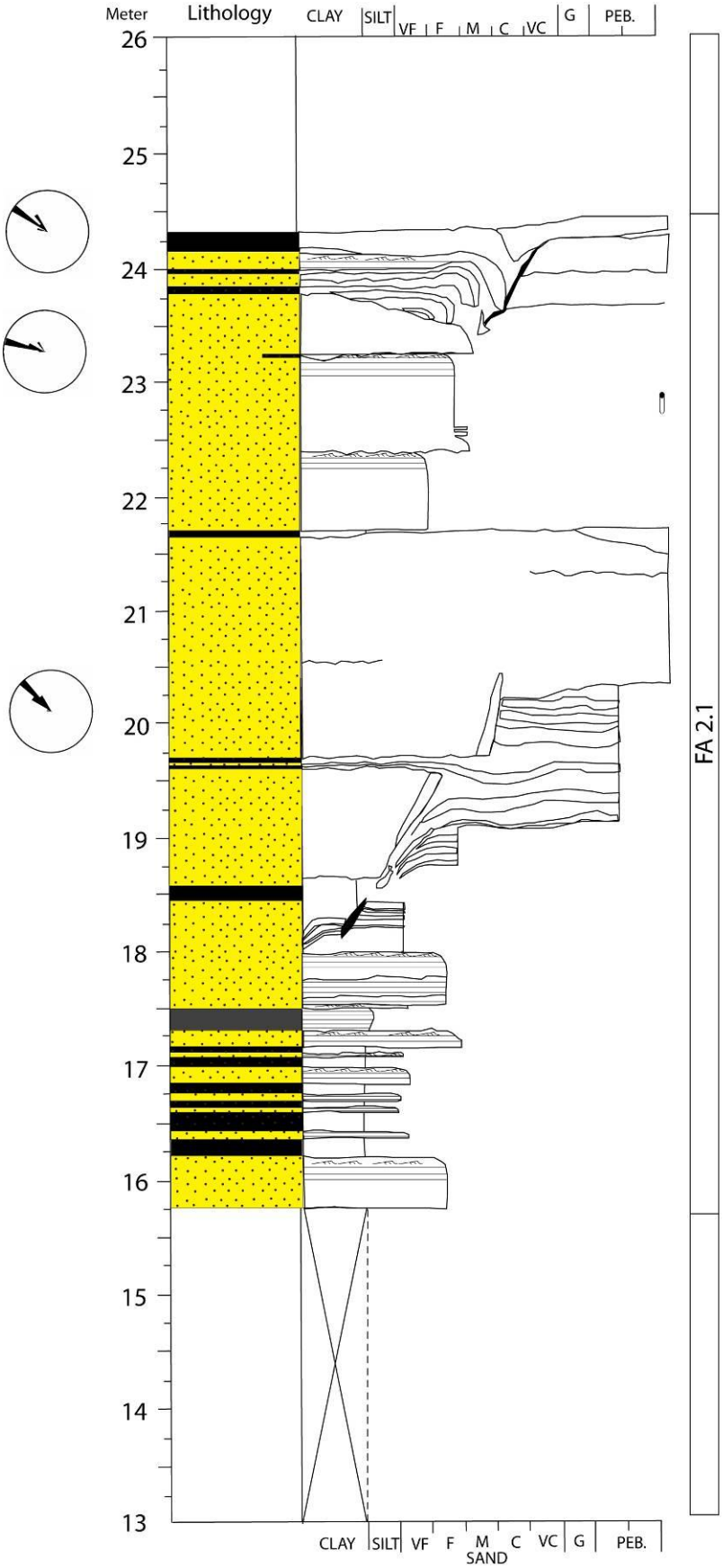

Log 7: 2/2
Locality 1
Scale: 1:50
UTM: 0273732 - 4697085

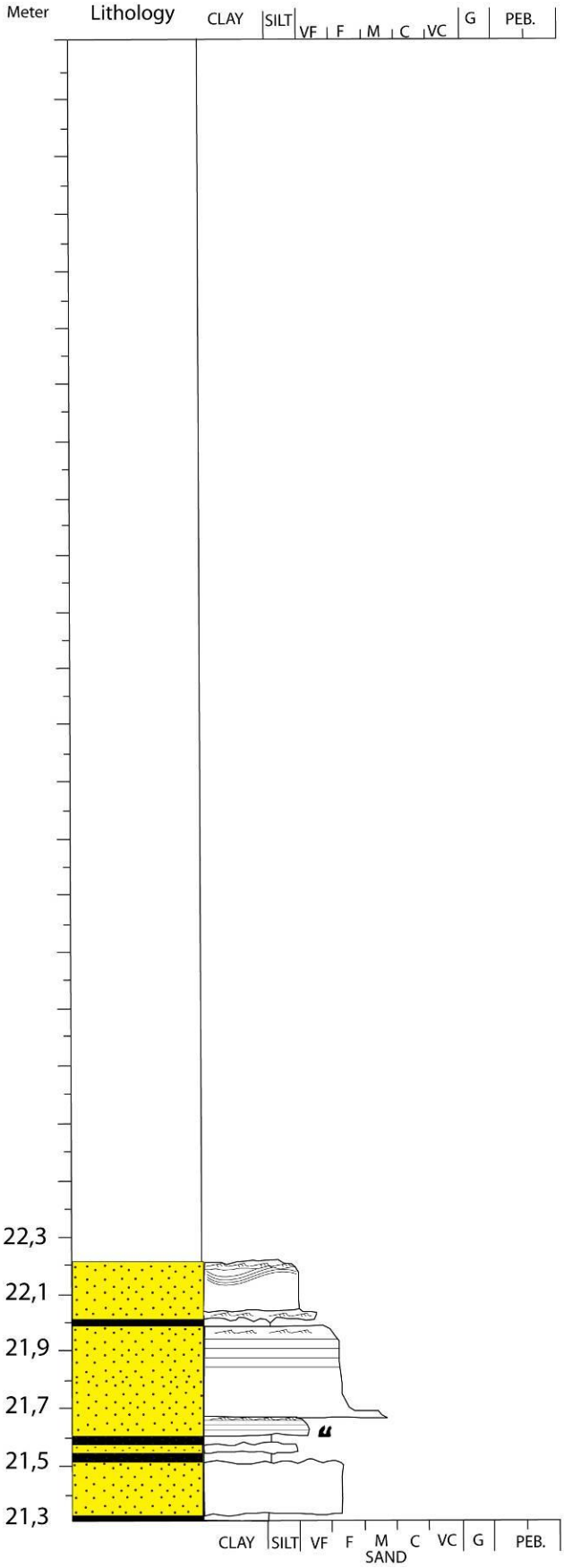

Log 7(2): 1/1
Locality 1
Scale: 1:20

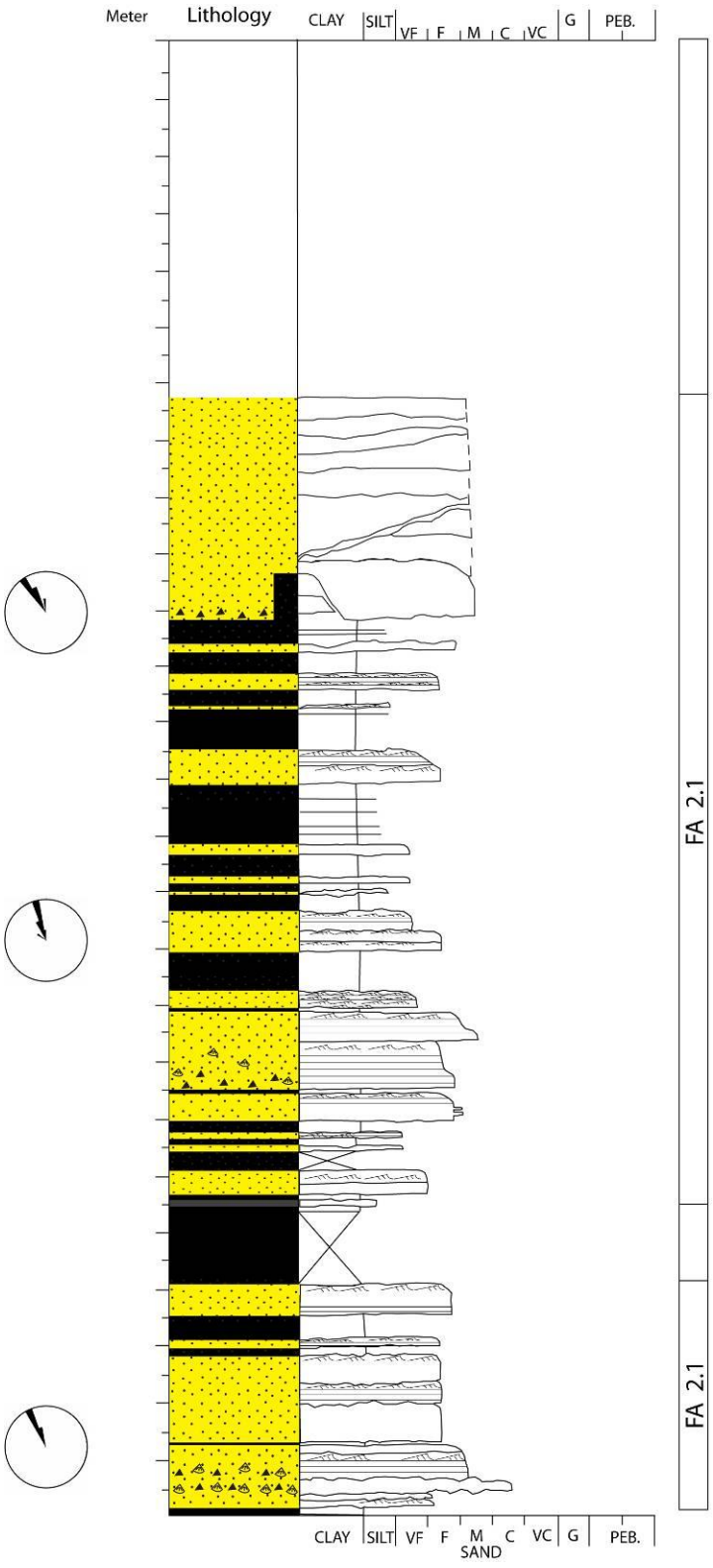

Log 8: 1/1
Lokality 1
Scale: 1:50
UTM: 0273755 - 4697110
UTM: 0273773 - 4697123

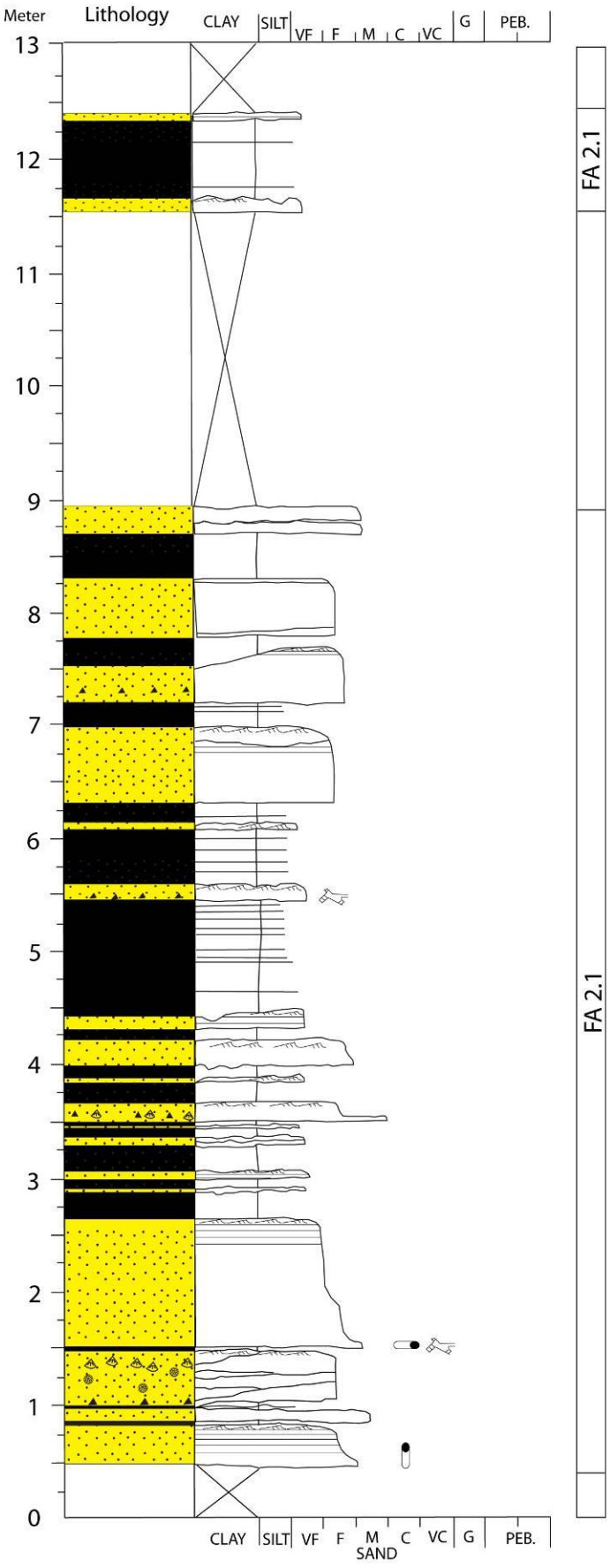

Log 9: 1/2
Locality 1
Scale: 1:50
UTM: 0273798 -4697137

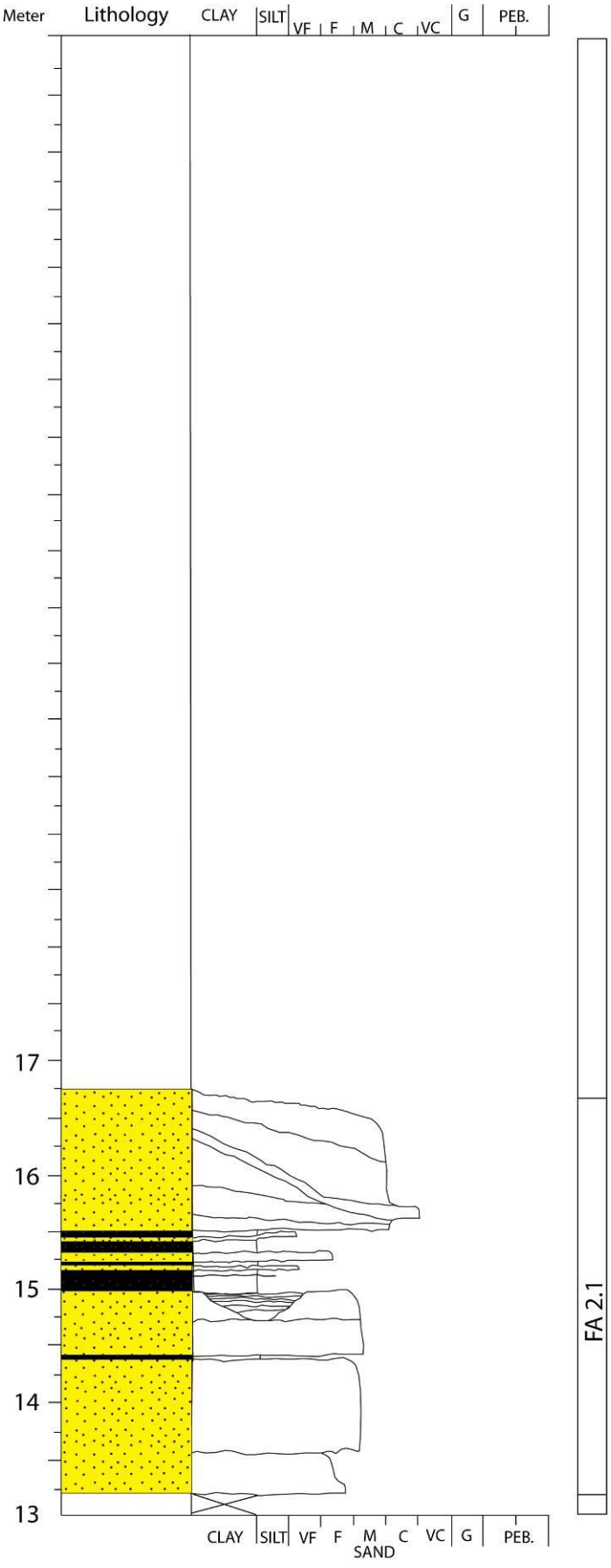

Log 9: 2/2
Locality 1
Scale: 1:50
UTM: 0273820 - 4697144

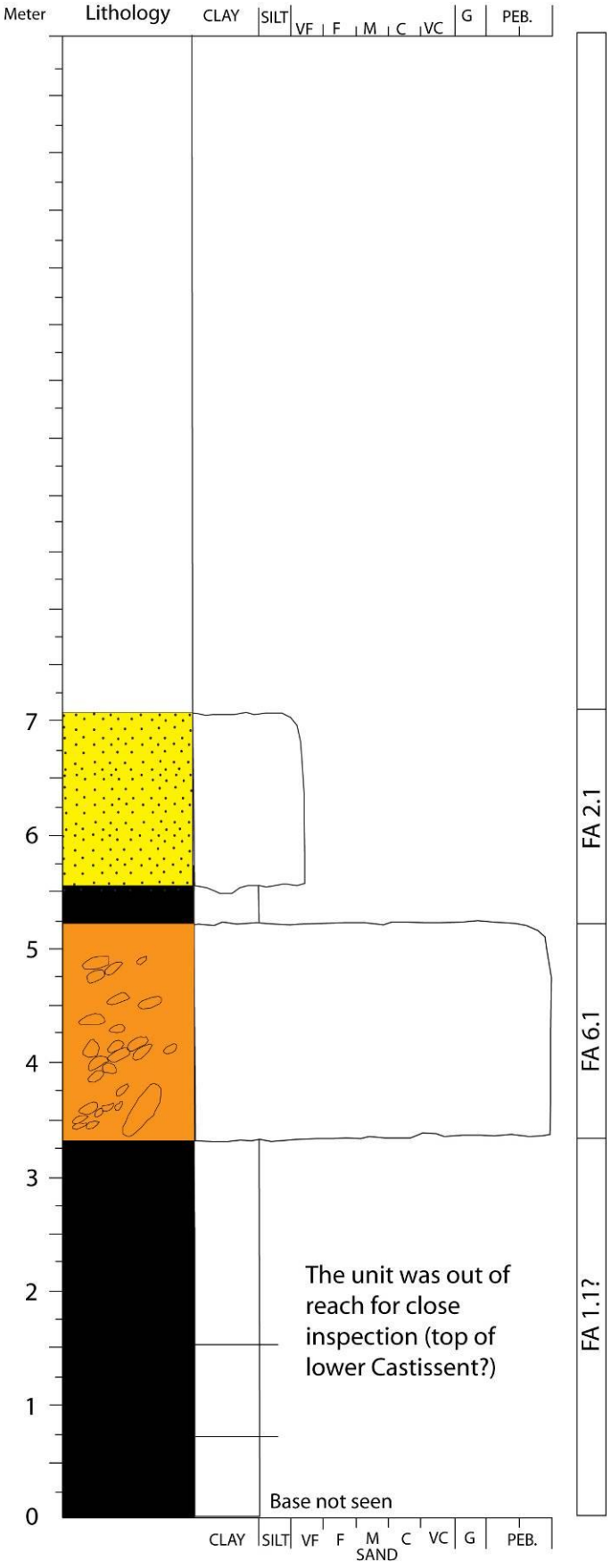

Log 10: 1/1
Locality 1
Scale: 1:50
UTM: 0274053 - 4697271

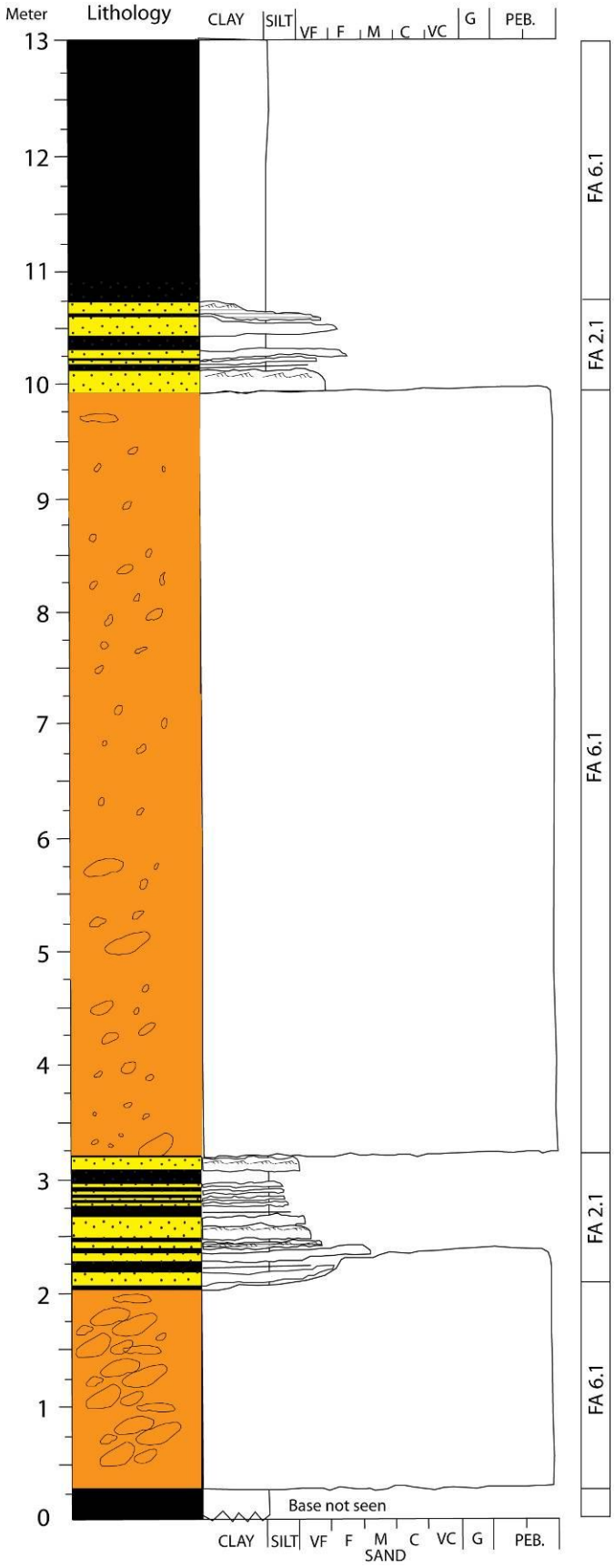

Log 11: 1/2
Locality 1
UTM: 0274000 - 4697096

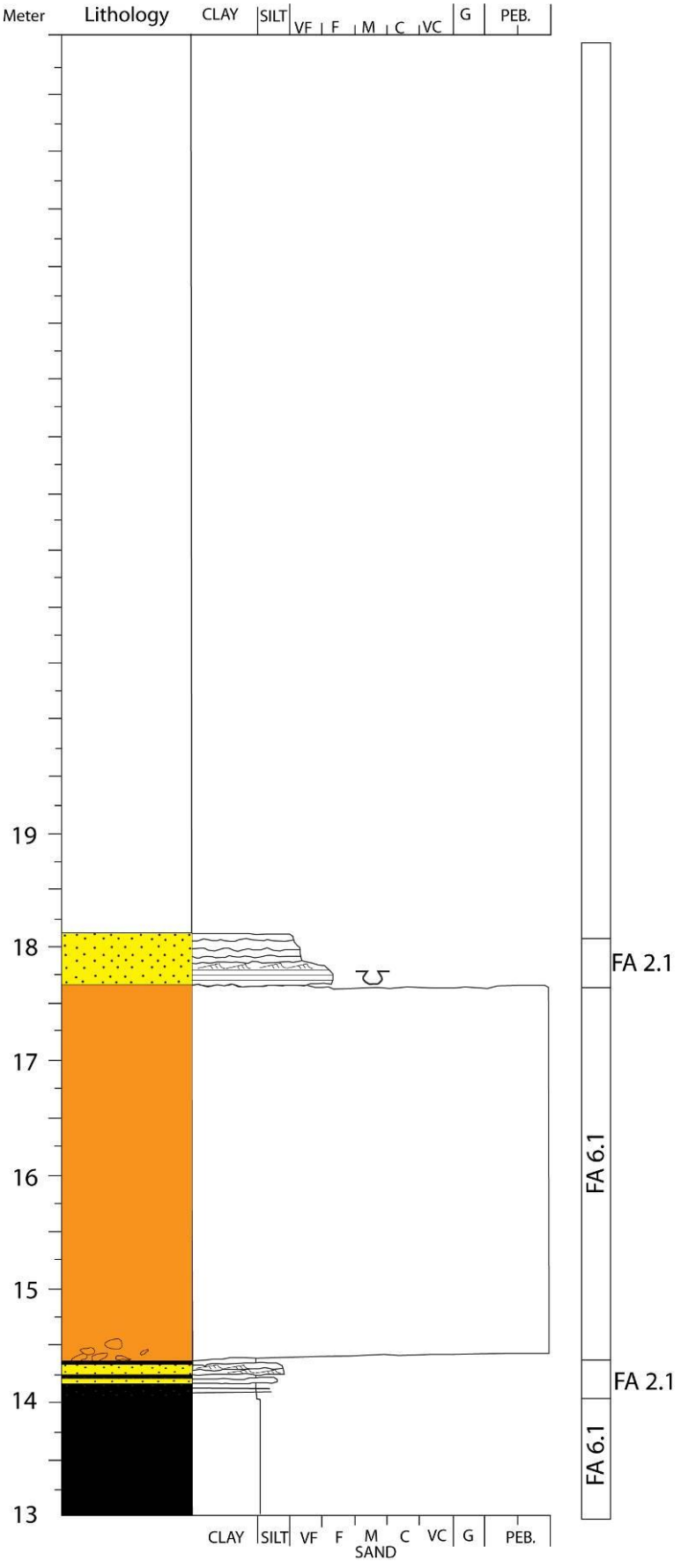

Log 11: 2/2
Locality 1
Scale: 1:50
UTM: 0274049 - 4697006

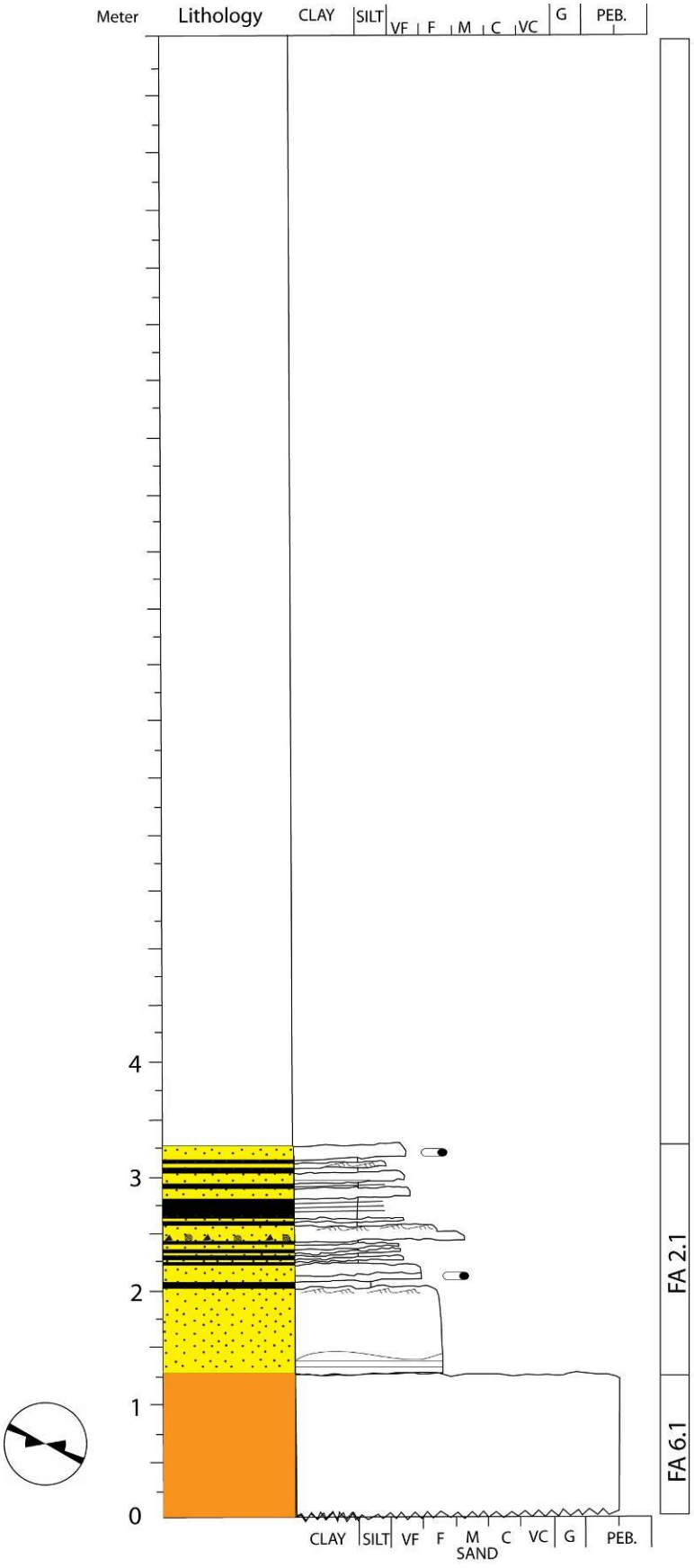

Log 12: 1/1
Locality 1
Scale: 1:50
UTM: 0274014 - 4697101

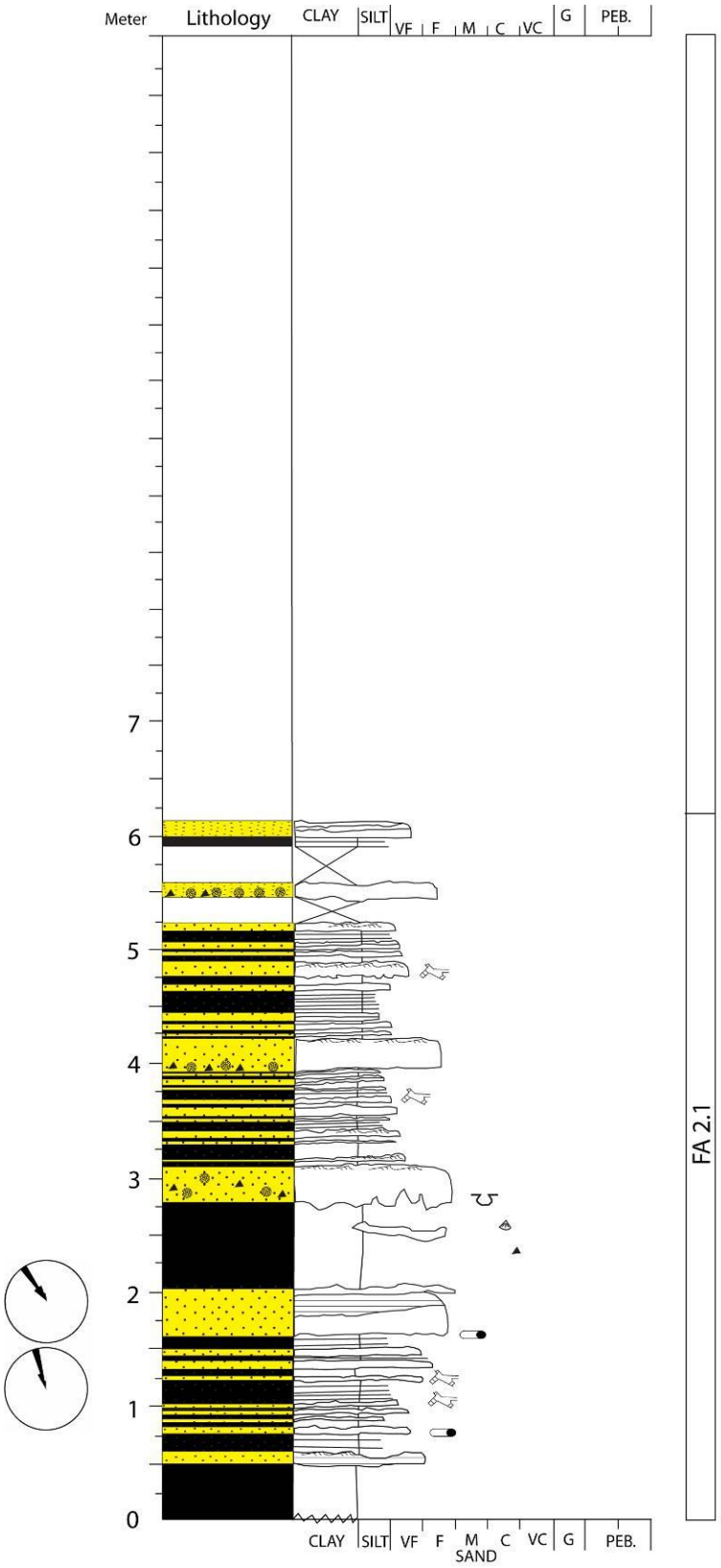

Log 13: 1/1
Locality 1
Scale: 1:50
UTM: 0274042 - 4697140

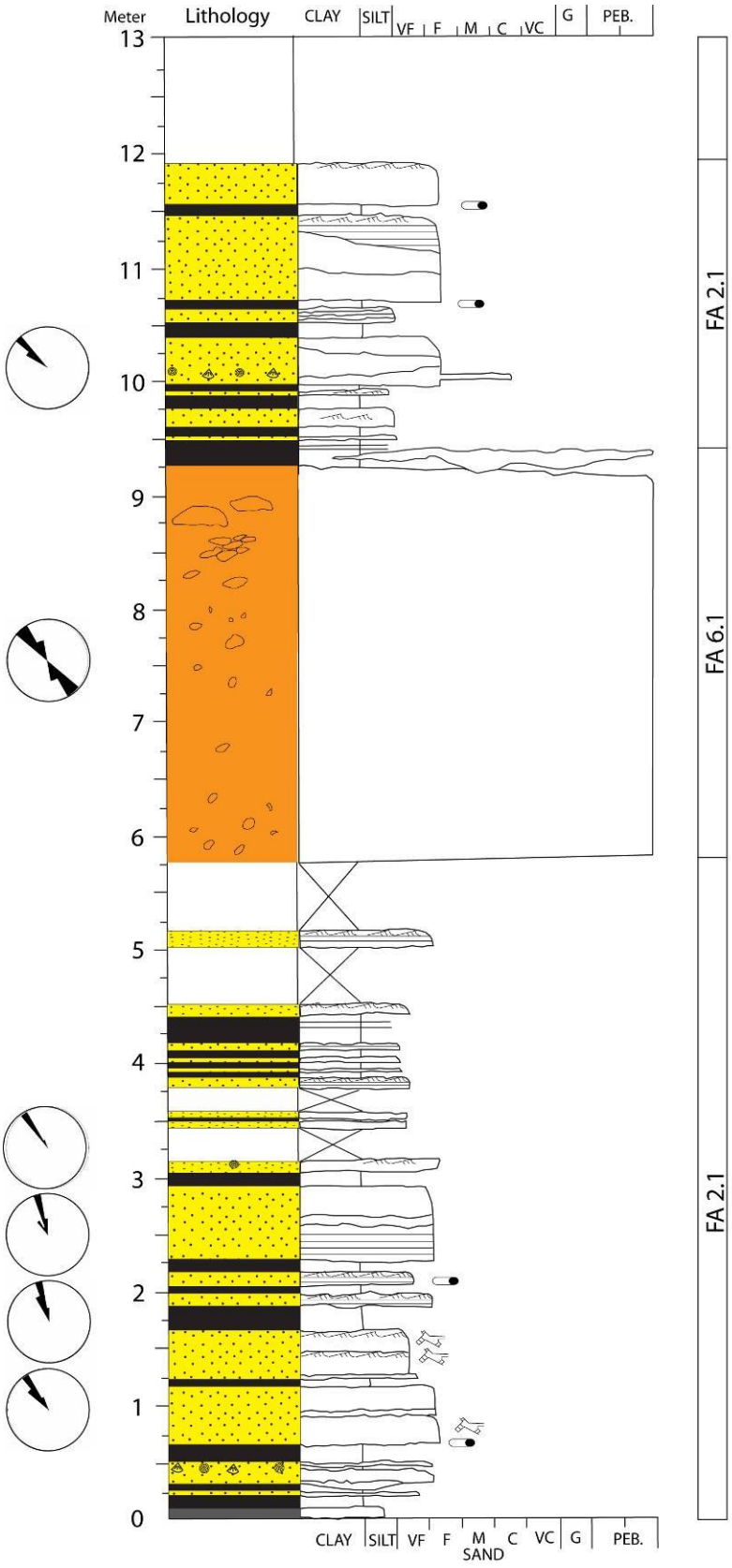

Log 14: 1/1
Locality 1
Scale: 1:50
UTM: 0274073 - 4697191
UTM: 0274082 - 4697195

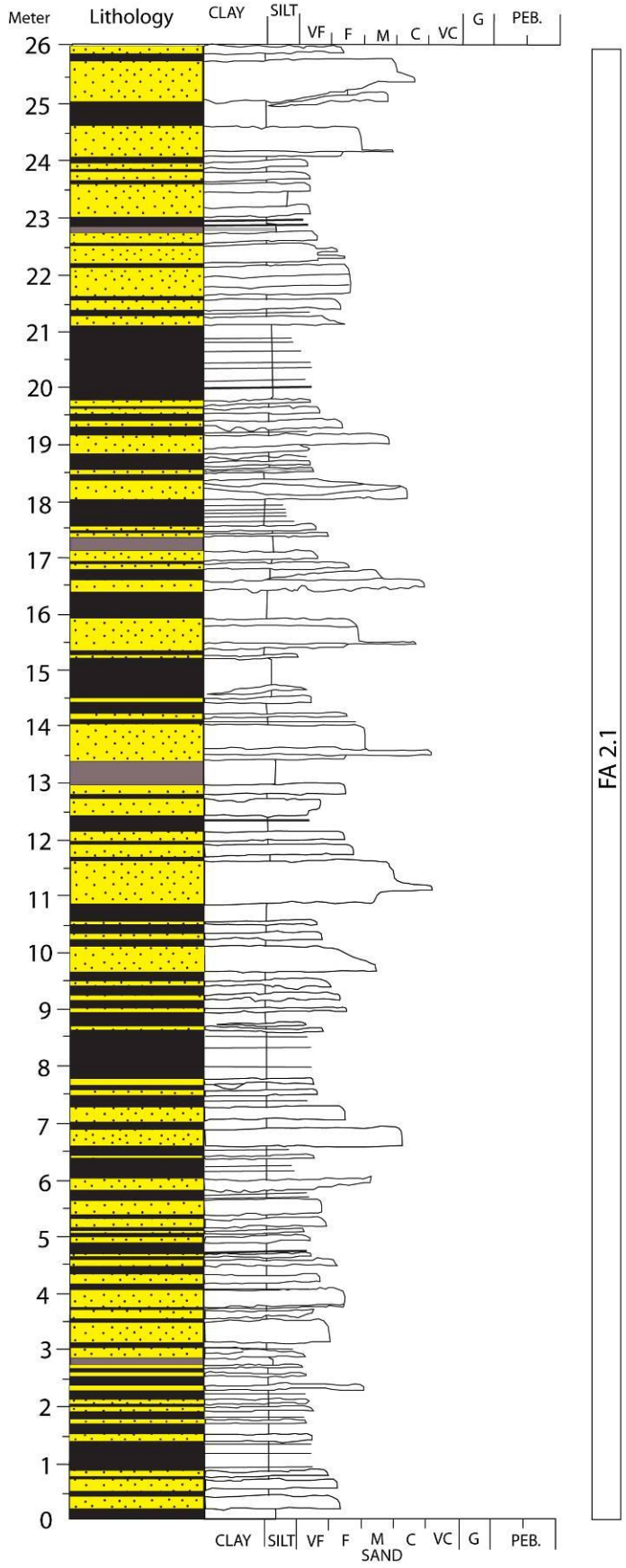

Log 15: 1/4
Locality 3
Scale: 1:100
UTM: 02715140 - 4700761

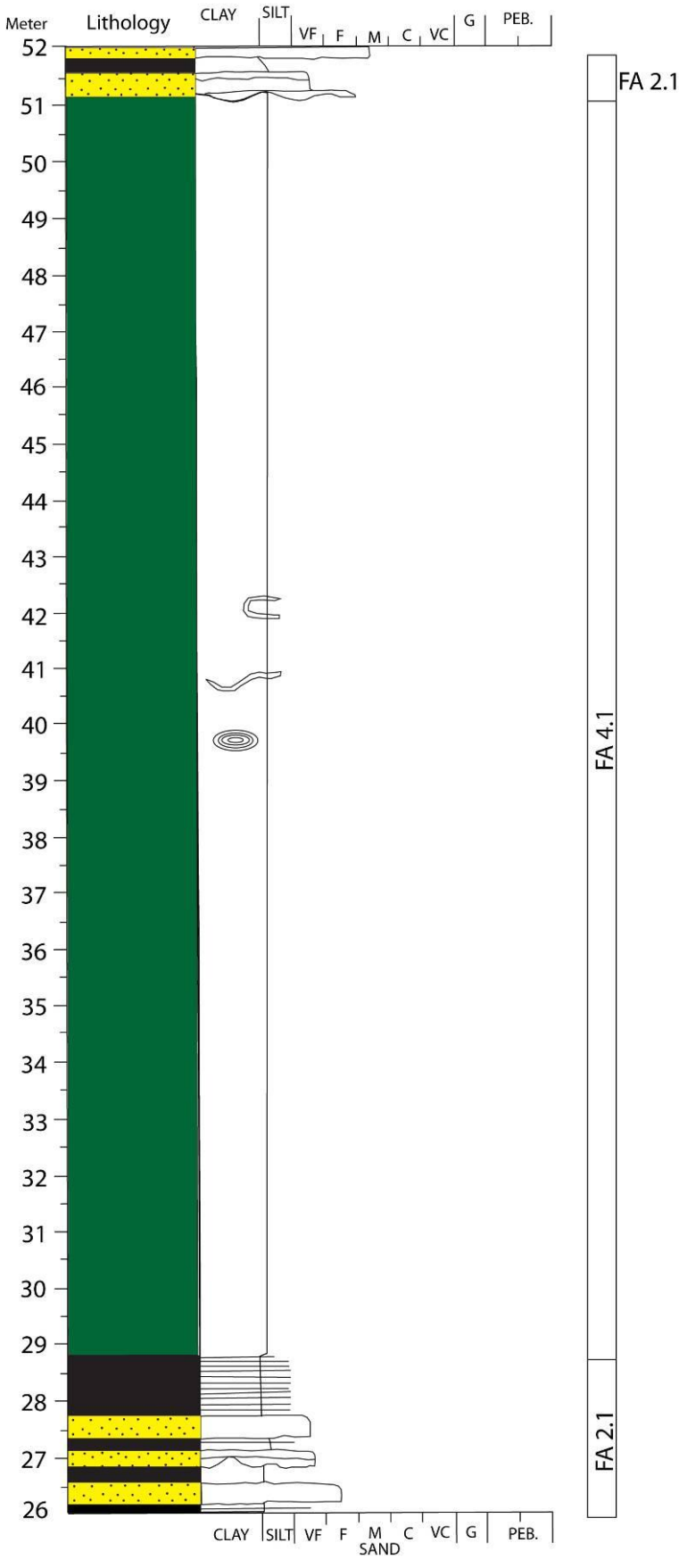

Log 15: 2/4
Locality 3
Scale: 1:100

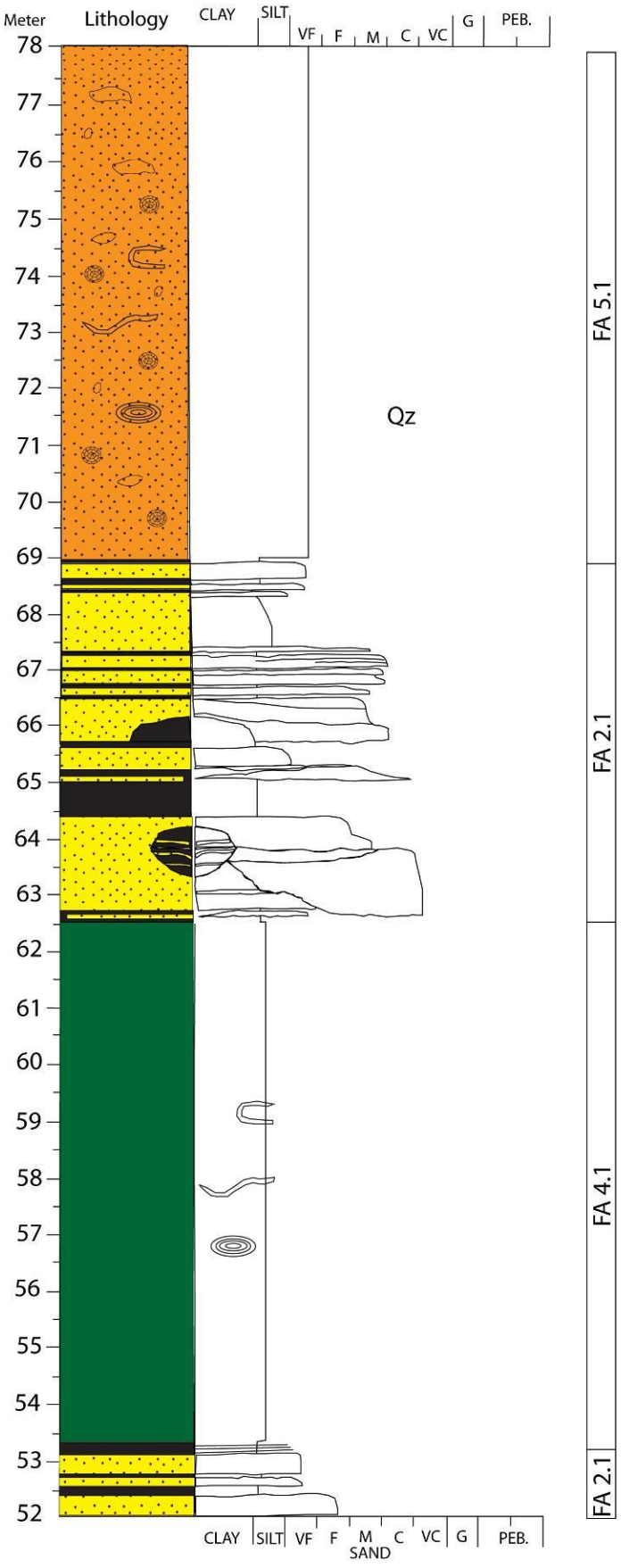

Log 15: 3/4
Locality 3
Scale: 1/100

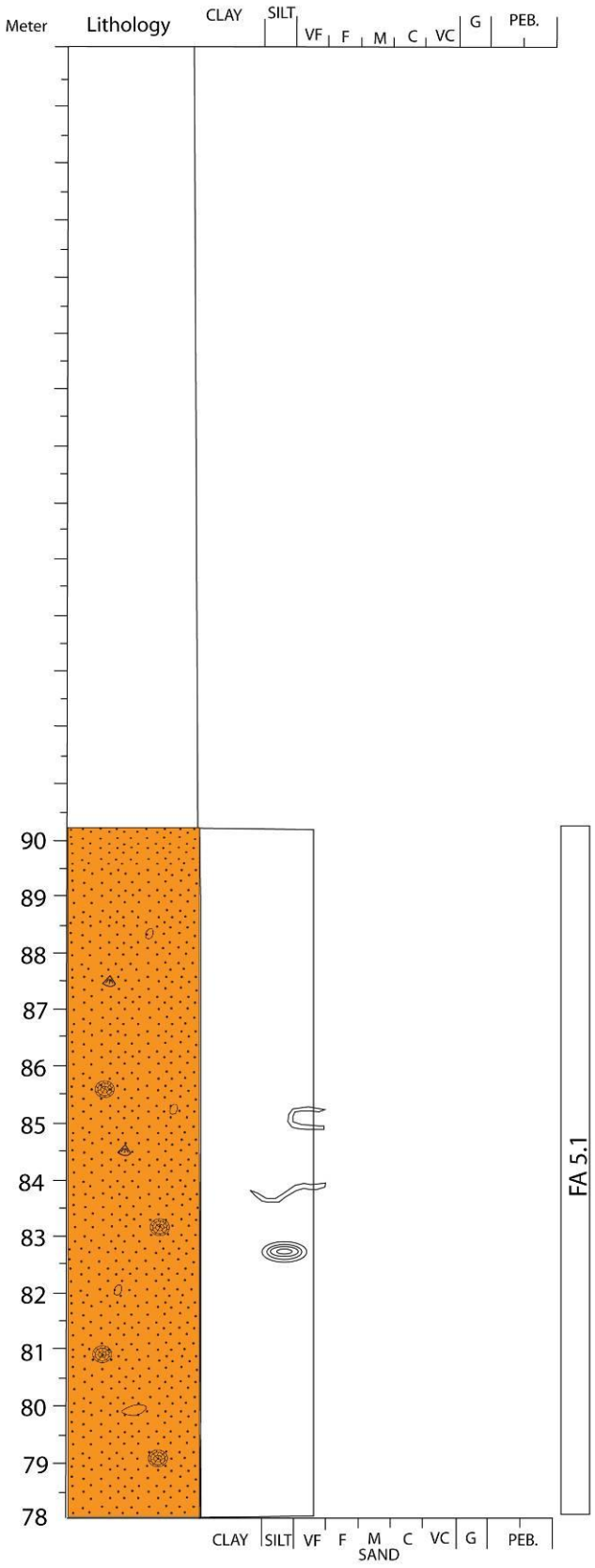

Log 15: 4/4
Locality 3
Scale: 1:100

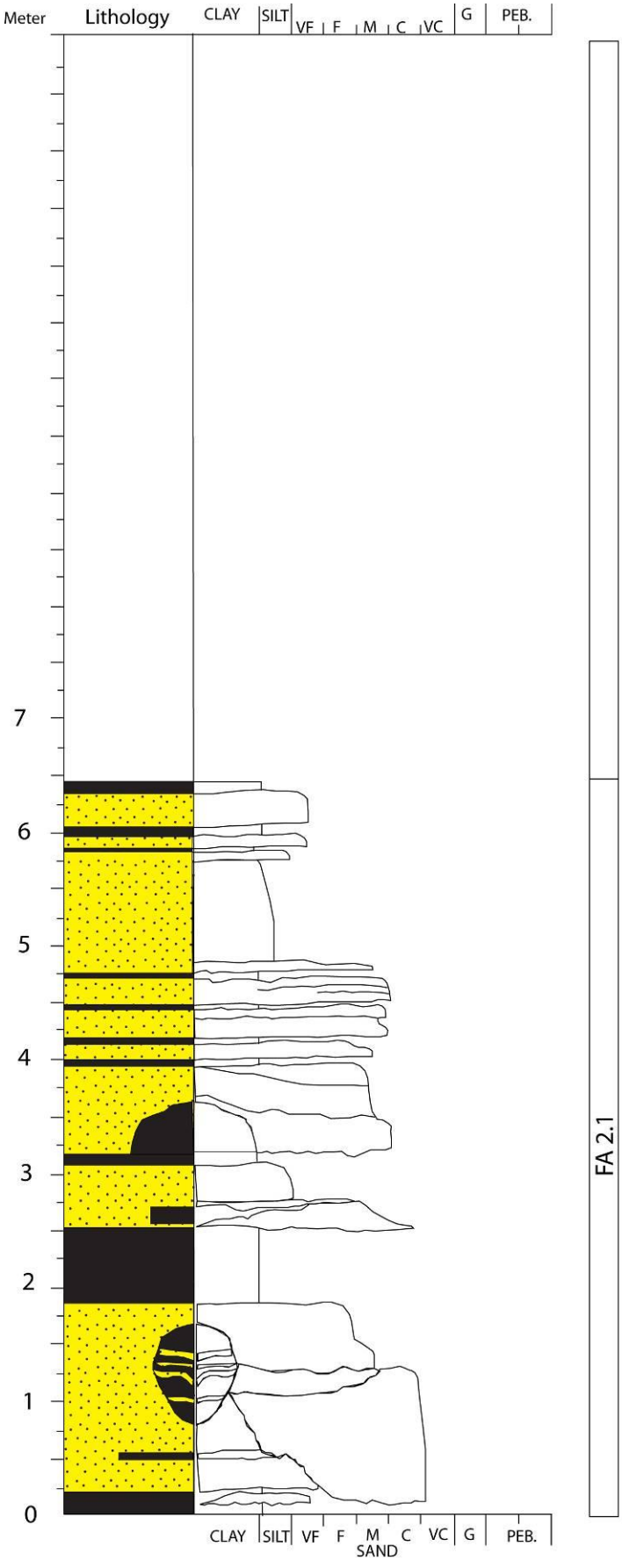

Log 16: 1/1
Locality 3
Scale: 1:50